

ERBIUM AND MWCNT-MODIFIED TITANIUM DIOXIDE NANOCOMPOSITES FOR THE PHOTOCATALYTIC DEGRADATION OF AZO DYES

Report

to the Water Research Commission

by

D. Boikanyo, SB Mishra, EN Nxumalo

SD Mhlanga and AK Mishra

Nanotechnology and Water Sustainability Research Unit,

University of South Africa

WRC Report No. 2583/1/19

ISBN 978-0-6392-0065-1

July 2019



Obtainable from:

Water Research Commission
Private Bag X03
Gezina, 0031

orders@wrc.org.za or download from www.wrc.org.za

DISCLAIMER

This report has been reviewed by the Water Research Commission (WRC) and approved for publication. Approval does not signify that the contents necessarily reflect the views and policies of the WRC, nor does mention of trade names or commercial products constitute endorsement or recommendation for use.

EXECUTIVE SUMMARY

The textile industry is a water-intensive industry. Water is used in large volumes for textile processing, which involves the dissolution and application of chemicals onto textiles and product washing, plant and equipment washing and maintenance, cooling systems and steam generation, air conditioning and consumption by personnel. Textile dyeing and finishing has inherent inefficiencies where the dyes and other chemicals, such as detergents, lubricants, acids, bases and stabilisers, are discharged unspent into the wastewater. These substances make textile wastewater highly variable in terms of its physical and chemical characteristics, such as pH, temperature, salinity, chemical oxygen demand (COD), biological oxygen demand (BOD) and concentration. Both industrial and municipal wastewater treatment works (WWTW) treat water in three steps, which involve the use of biological, chemical and physical techniques. Dye wastewater is complex as it contains highly coloured pigments, along with various organic and inorganic substances that have been used to improve the performance of the dye. In many instances, primary and secondary wastewater treatment methods are inadequate for the removal of the dye and the concomitant organic pollutants in the wastewater.

Of the tertiary treatment methods used to treat textile dye wastewater, advanced oxidation processes that involve the generation of highly oxidising free radicals have proven more effective than the singular use of ultraviolet (UV) radiation or oxidising agents, or other techniques such as membrane technology, adsorption and ion exchange. Photochemical processes can degrade recalcitrant organic pollutants, rather than transfer them to another phase that causes secondary pollution. As an advanced oxidation process, the use of titania-mediated heterogeneous photocatalysis for the decolourisation of textile dye wastewater presents a viable solution. Titania has limitations as far as industrial applications are concerned. It is only UV-light active, which requires powering UV-light sources, and it has a high electron-hole recombination rate that compromises its quantum efficiency. In this project, erbium (Er) and multi-walled carbon nanotube (MWCNT)-modified titanium dioxide (TiO₂) nanocomposites immobilised on a biopolymer were proposed as a candidate solution applied to the photodegradation of a model textile azo dye (Reactive Red 120).

The aim of the project was to develop smart bio-nanocomposites for organic dye remediation, which involved a visible light-driven photocatalyst based on rare earth metal-modified TiO₂ nanoparticles grafted onto MWCNTs and immobilised on a cellulose acetate (CA) and polycaprolactone (PCL) biopolymer blend matrix. This photocatalyst was evaluated for the degradation of azo dyes typically used in the textile industry. Multi-walled carbon nanotubes were synthesised via the decomposition of acetylene over a bimetallic iron-cobalt catalyst. The MWCNT-modified TiO₂ nanocomposite was synthesised via a sol-gel technique and modified with erbium cations (Er³⁺) via a wet impregnation process. The nanocomposites were characterised by transmission electron microscopy (TEM), scanning electron microscopy (SEM), Brunauer, Emmett and Teller (BET) nitrogen (N₂) adsorption-desorption, energy dispersive X-ray spectroscopy (EDS), X-ray diffraction (XRD) and UV-visible (UV-Vis) spectroscopy. The photocatalytic dye degradation efficiency of the nanocomposites was evaluated under simulated solar radiation using diazo dye CI Reactive Red 120 as a model textile dye. The nanocomposite that showed the highest percentage colour-removal efficiency was immobilised on a cellulose acetate-polycaprolactone film and the colour-removal efficiency evaluated.

The SEM analysis showed that the TiO₂ and Er-modified TiO₂ (Er:TiO₂) was brittle and the surface exhibited a porous microstructure with diameters of around 1-2 µm. Modification of TiO₂ with Er and MWCNTs decreased the particle sizes. The TEM analysis of the MWCNTs, Er:TiO₂ and Er:TiO₂@MWCNT showed that the carbon nanotubes were multi-walled and randomly oriented. The MWCNTs showed catalyst particles in the nanotube walls, but with low metal residue inside the tube cavities, implying that the MWCNTs formed via a basal growth mechanism.

The acid treatment successfully removed the catalyst particles and the support. The uniform inorganic particles of the Er:TiO₂ that were grafted onto the MWCNTs adhered to it well in clusters. The EDS chemical analysis mapping results confirmed the successful synthesis of all TiO₂ particles modified with MWCNTs (1:5 m/m %) and Er-modified nanocomposites with a 1% (wt %) presence of Er as calculated during synthesis. Optical absorption measurements showed that the nano-photocatalysts absorb at higher wavelengths than TiO₂. All samples showed characteristic absorption resulting from the excitation of electrons from the valence band (VB) to the conduction band (CB) in anatase TiO₂ (390 nm). The TiO₂ modified with MWCNTs showed absorption over the entire UV-Vis spectrum as a

result of the MWCNT's broad spectrum absorption. The Er:TiO₂ absorption edge showed a red shift due to the charge transfer between the TiO₂ and Er³⁺ intra 4f electrons. There were intense absorption peaks in all the Er-modified composites. This can be ascribed to the transition from the ⁴I_{15/2} ground state to the Er ions' excited states. The XRD showed a pure anatase phase of TiO₂ without a rutile phase and Er was not detected as a result of the low Er³⁺ dopant content. The Er and MWCNT co-modified TiO₂ composites (Er:TiO₂@MWCNT) were highly crystalline with no peaks corresponding to the MWCNTs due to overlapping by the main peak of anatase at ~25.3° with the MWCNT (200) reflections. The Er³⁺ and MWCNTs caused a reduction in the crystallite sizes of the TiO₂.

Furthermore, XRD showed successful blending of amorphous CA and semi-crystalline PCL as seen by the weak, broadened diffuse halo of the CA-PCL. The N₂ adsorption-desorption measurements were performed to evaluate the effect of Er³⁺ and MWCNTs on the surface area of TiO₂. The nanocomposites had type IV and type V adsorption isotherms with H1 and H3 hysteresis loops with two types of pores: narrow and open-ended mesopores. Furthermore, BET analysis indicated that all composites exhibited mesoporosity through type IV adsorption isotherm. The surface areas ranged from 67.9 to 100.6 m²/g, with the highest BET surface area observed for Er:TiO₂@MWCNT. The Er³⁺ and MWCNT increased the TiO₂-based composite's BET surface area compared to pure TiO₂ nanoparticles and the increased surface area enhanced the adsorption ability of photocatalysts. Thus, this study revealed that the best-performing photocatalyst showed the highest dye adsorption due to the large surface area.

The photocatalytic degradation studies showed that TiO₂ achieved about 35% colour-removal efficiency within 90 minutes, while Er:TiO₂@MWCNT showed about 80% colour-removal efficiency within 90 minutes and a consistently higher colour removal over the entire reaction time. The photodegradation reactions occurred as first-order reactions and followed the Langmuir-Hinshelwood (L-H) kinetic model. The Er³⁺ and MWCNT-modified photocatalyst had the highest rate of reaction (18.43 x 10⁻³ min⁻¹) that was ~3.5 times greater than that of TiO₂ (5.59 x 10⁻³ min⁻¹). A mechanism was proposed where a synergy exists between the erbium oxide (Er₂O₃), MWCNTs and TiO₂, and the Er³⁺ function as a photosensitiser. When irradiated with visible light, the 4f-4f electrons are injected to the CB of TiO₂. The Er₂O₃/Er³⁺ forms sub-band gap energy levels below the CB of TiO₂, allowing for the electronic transitions of TiO₂ VB electrons to these (empty) sub-band gap energy levels of Er³⁺. Since

these transitions require less energy than the TiO₂ VB-to-CB (3.2 eV) transition, they can be induced by visible light. The MWCNTs have a broad spectrum absorptivity and act as photosensitisers that transfer excited electrons to the CB of TiO₂ upon visible light illumination in the Er:TiO₂@MWCNT. The MWCNTs also introduced trace carbon doping into the TiO₂ lattice, which resulted in defects such as oxygen vacancies and trivalent titanium that increased the shallow trap states leading to substantially enhanced optical absorption in the visible light region; while these defects induce disorder that facilitates the separation and transfer of photo-formed charge carriers, thus effectively delaying the recombination of electrons and holes. Additionally, the MWCNTs improved the textural properties and thus the visible light sensitisation because of their large surface area, pore volume and pore sizes that improve interfacial charge transfer and enhance visible light absorption.

The inclusion of Er and MWCNTs into TiO₂ markedly improved the visible light activity and photocatalytic efficiency in the decomposition of azo dyes. The photocatalysts displayed great potential for environmental remediation applications such as the decontamination of textile industrial wastewater. It is recommended that the Er:TiO₂@MWCNT-CAPCL composite be explored further because of its demonstrated photocatalytic efficacy. However, different varieties and combinations of biodegradable polymer, such as starch, cellulose and its derivatives, and other natural polymers, can be applied in various combinations and tested for the immobilisation of the photocatalyst.

ACKNOWLEDGEMENTS

The financial support of the Water Research Commission (WRC) and the contributions of the members of the Reference Group are highly acknowledged. The Reference Group responsible for the project comprised the following members:

Member	Affiliation
Dr N Kalebaila	Water Research Commission
Prof V Fester	Cape Peninsula University of Technology
Dr H Madhav	Eskom
Mr J Nathoo	NuWater Global
Project Management	
Prof AK Mishra	University of South Africa
Prof SB Mishra	University of South Africa
Prof SD Mhlanga	University of South Africa
Prof EN Nxumalo	University of South Africa
Ms D Boikanyo	University of South Africa
Ms R Muthivi	University of South Africa
Mr KS Mabape	University of South Africa
Others	
Prof A Maity	Council for Scientific and Industrial Research
Prof H Tutu	University of the Witwatersrand
Dr P Matabola	Mintek
Dr NP Gule	Stellenbosch University

CONTENTS

EXECUTIVE SUMMARY	i
ACKNOWLEDGEMENTS.....	v
CONTENTS	vi
LIST OF FIGURES	x
LIST OF TABLES.....	xii
ACRONYMS AND ABBREVIATIONS	xiii
CHAPTER 1: INTRODUCTION.....	1
1.1 BACKGROUND.....	1
1.2 AIM AND OBJECTIVES.....	6
1.3 SCOPE AND LIMITATIONS.....	6
CHAPTER 2: LITERATURE REVIEW	7
2.1 THE CLOTHING, TEXTILE, FOOTWEAR AND LEATHER INDUSTRY IN SOUTH AFRICA ...	7
2.1.1 Introduction and definition of the clothing, textile, footwear and leather industry in South Africa	7
2.1.2 Profile of the KwaZulu-Natal Textile Cluster	8
2.2 WATER USE AND WASTEWATER MANAGEMENT IN THE TEXTILE INDUSTRY	11
2.2.1 Water use in the textile industry	11
2.2.2 Wastewater generation and management in the textile industry	13
2.2.2.1 Azo dyes	16
2.2.2.2 Aromatic amines	18
2.3 TEXTILE WASTEWATER TREATMENT TECHNOLOGIES	19
2.3.1 Overview.....	19
2.3.2 Biological methods	20

2.3.3	Physical methods	23
2.3.3.1	Adsorption	24
2.3.3.2	Filtration	25
2.3.4	Chemical methods.....	26
2.3.4.1	Coagulation-flocculation.....	26
2.3.4.2	Chemical oxidation.....	27
2.4	DECOLOURISATION OF DYE AND TEXTILE EFFLUENT USING ADVANCED OXIDATION PROCESSES	28
2.4.1	Overview.....	28
2.4.2	Semiconductor-mediated photocatalysts	29
2.4.3	Improving the photocatalytic activity of TiO ₂ using carbonaceous nanomaterials	32
2.4.4	The use of rare earth metals to improve the photocatalytic activity of TiO ₂	34
2.4.5	Biopolymers as photocatalyst supports.....	36
2.4.5.1	Definition of terms	36
2.4.5.2	Immobilisation of photocatalysts on supports	37
2.4.5.3	Features of an immobilising support.....	38
2.4.5.4	Approaches used for the immobilisation of the photocatalyst	39
2.4.5.5	Cellulose acetate and polycaprolactone as immobilisation support	40
2.5	SUMMARY	43
	CHAPTER 4: EXPERIMENTAL WORK.....	46
4.1	REAGENTS.....	46
4.2	SYNTHESIS METHODS	46
4.2.1	Synthesis of Fe-Co catalyst.....	46
4.2.2	Carbon nanotube synthesis.....	47
4.2.3	Synthesis of TiO ₂	47
4.2.4	Synthesis of Er-modified TiO ₂	47

4.2.5	Synthesis of Er-modified TiO ₂ grafted onto MWCNT	47
4.2.6	Synthesis of Er-modified TiO ₂ grafted onto MWCNTs and embedded onto PCL and CA blended.....	48
4.3	CHARACTERISATION.....	49
4.3.1	Microscopy analyses	49
4.3.2	UV-Vis spectroscopy	49
4.3.3	X-ray diffraction measurements	49
4.3.4	Surface area analysis.....	50
4.4	EVALUATION OF PHOTOCATALYTIC ACTIVITY.....	50
CHAPTER 5: RESULTS AND DISCUSSION		52
5.1	CHARACTERISATION OF NANOCOMPOSITES	52
5.1.1	SEM analyses.....	52
5.1.2	TEM analyses.....	54
5.1.3	The EDS analyses.....	58
5.1.4	UV-Vis spectroscopy	59
5.1.5	The XRD analyses.....	61
5.1.6	BET analyses	63
5.2	PHOTOCATALYTIC ACTIVITY EVALUATION OF NANOCOMPOSITES	67
5.3	KINETICS AND PROPOSED PHOTOCATALYTIC ACTIVITY MECHANISM	71
5.3.1	General overview.....	71
5.3.2	Proposed mechanism.....	77
5.4	SUMMARY	78
CHAPTER 6: CONCLUSIONS AND RECOMMENDATIONS		80
6.1	CONCLUSIONS	80
6.2	RECOMMENDATIONS	80
REFERENCES.....		82

LIST OF FIGURES

Figure 1.1:	Generalised textile production process and the production areas that are the focus of this report (adapted from Johannesson, 2016).....	2
Figure 1.2:	Generic industrial wastewater treatment process.....	4
Figure 2.1:	Distribution of firms employing more than 45 people (from eThekweni Industrial Land GIS database (EDGE, 2014))	11
Figure 2.2:	Flowchart of textile product manufacturing (Le Roes-Hill et al., 2017).....	12
Figure 2.3:	Generalised configuration of a WWTW receiving industrial wastewater, showing the integrated anaerobic pond and activated sludge process (Boyd and Mbelu, 2009)...	15
Figure 2.4:	Structure of Bismarck Brown	17
Figure 2.5:	Structure of CI Acid Red 73	17
Figure 2.6:	Structure of CI Direct Blue 71	17
Figure 2.7:	Summary of primary, secondary and tertiary treatment techniques applied to the treatment of textile wastewater (Le Roes-Hill et al., 2017)	20
Figure 2.8:	Proposed mechanism of action of MWCNTs as electron sink (A) and photosensitiser (B).....	33
Figure 2.9:	Mechanism of action of rare earth metal ions when coupled with TiO ₂ , acting by introducing sub-band gap states beneath the TiO ₂ CB (left) or upconverting lower energy light (NIR and visible photons) into higher energy photons available for use by TiO ₂ (right).....	35
Figure 4.1:	Illustration of laboratory setup of photodegradation experiments.....	51
Figure 5.1:	SEM micrograph of TiO ₂	52
Figure 5.2:	SEM micrograph of Er:TiO ₂	53
Figure 5.3:	SEM micrograph of TiO ₂ @MWCNT	53

Figure 5.4:	SEM micrograph of Er:TiO ₂ @MWCNT	54
Figure 5.5:	TEM image of the MWCNT before acid treatment.....	55
Figure 5.6:	TEM image of the MWCNT after acid treatment.....	55
Figure 5.7:	TEM image of the TiO ₂	56
Figure 5.8:	TEM image of the Er:TiO ₂	56
Figure 5.9:	TEM image of the TiO ₂ @MWCNT	57
Figure 5.10:	TEM image of the Er:TiO ₂ @MWCNT	58
Figure 5.11:	The TiO ₂ EDS spectrum and table of quantities	58
Figure 5.12:	The Er:TiO ₂ EDS spectrum and table of relative quantities.....	58
Figure 5.13:	The Er:TiO ₂ @MWCNT EDS spectrum and table of relative quantities	59
Figure 5.14:	Kubelka-Munk function plots for the TiO ₂ -based Er ³⁺ and MWCNT-modified nano- photocatalysts.....	60
Figure 5.15:	A Kubelka-Munk function plot for the TiO ₂ -based Er ³⁺ and MWCNT-modified nano- photocatalysts	61
Figure 5.16:	The XRD patterns of the TiO ₂ -based Er ³⁺ , CNTs and CA-PCL-modified nano- photocatalysts.....	62
Figure 5.17:	The N ₂ adsorption-desorption isotherms and Barrett, Joyner and Halenda (BJH) pore size distribution for TiO ₂	64
Figure 5.18:	The N ₂ adsorption-desorption isotherms and BJH pore size distribution for Er:TiO ₂ -c	64
Figure 5.19:	The N ₂ adsorption-desorption isotherms and BJH pore size distribution for Er:TiO ₂ -w	65
Figure 5.20:	The N ₂ adsorption-desorption isotherms and BJH pore size distribution for Er:TiO ₂ @MWCNT-c	66
Figure 5.21:	The N ₂ adsorption-desorption isotherms and BJH pore size distribution for Er:TiO ₂ @MWCNT-w	66

Figure 5.22:	The chemical structure of Reactive Red 120.....	67
Figure 5.23:	Percentage dye removal vs. time curves of TiO ₂ and its Er ³⁺ and CNT functionalised composites over a 240-minute period.....	69
Figure 5.24:	Percentage dye removal vs. time bar graph of TiO ₂ and its Er ³⁺ and CNT functionalised composites at 120 minutes' reaction time.....	70
Figure 5.25:	Reactive Red 120 decomposition vs. reaction time curves of TiO ₂ and the Er ³⁺ and CNT-modified composites over a 180-minute reaction time period.....	73
Figure 5.26:	Integrated first-order plot of Reactive Red 120 decomposition vs. reaction time curves of TiO ₂ and the Er ³⁺ and CNT-modified composites presented over a 180-minute reaction time period.....	74
Figure 5.27:	Integrated second-order plot of Reactive Red 120 decomposition vs. reaction time curves of an Er:TiO ₂ @MWCNT composite presented over a 180-minute reaction time period.....	75

LIST OF TABLES

Table 2.1:	Membrane processes and their typical operating parameters.....	25
Table 5.1:	The textural properties of photocatalyst composites.....	66
Table 5.2:	The physicochemical properties of the model dye Reactive Red 120.....	68
Table 5.3:	Amount of Reactive Red 120 dye adsorbed and removed by the photocatalyst at 90 and 240 minutes.....	70
Table 5.4:	Apparent reaction rate constant (k_{App}) for the various composites as estimated from the slope of the linear regression of the straight-line plots of Ln (C ₀ /C _t) vs. time	73

ACRONYMS AND ABBREVIATIONS

$\alpha\text{-Fe}_2\text{O}_3$	Hematite
AC	Activated carbon
AD	Anaerobic digestion
AOP	Advanced oxidation process
AOx	Absorbable organohalogens
ATR-FTIR	Attenuated total reflection-Fourier transform infrared
BET	Brunauer, Emmett and Teller
Bi_2S_3	Bismuth sulphide
BJH	Barrett, Joyner and Halenda
BOD	Biological oxygen demand
C_2H_2	Acetylene
C_0	Initial concentration
CaCO_3	Calcium carbonate
CA	Cellulose acetate
CAPCL	Cellulose acetate-polycaprolactone polymer blend
CB	Conduction band
CBD	Central business district
Cd^{2+}	Cadmium ion
CdS	Cadmium sulfide
Ce	Cerium
CeO_2	Ceric oxide
CI	Colour Index
Co	Cobalt
COD	Chemical oxygen demand

Co(NO ₃) ₂	Cobalt (II) nitrate
CO	Carbon monoxide
CO ₂	Carbon dioxide
CTFL	Clothing, textiles, footwear and leather manufacturing
CTFL-SETA	CTFL Sector Education and Training Authority
CNT	Carbon nanotube
CVD	Chemical vapour deposition
DMF	Dimethylformamide
DRS	diffuse reflectance spectroscopy
DWA	Department of Water Affairs
DWAF	Department of Water Affairs and Forestry
DWS	Department of Water and Sanitation
Dy	Dysprosium
EDS	Energy dispersive X-ray spectroscopy
EDX	Energy dispersive X-ray
Er	Erbium
Er:TiO ₂	Er-modified TiO ₂
Er:TiO ₂ @CNT	Er and MWCNT co-modified TiO ₂ composites
Er ₂ O ₃	Erbium oxide
Er ³⁺	Erbium cations
Er(NO ₃) ₃	Erbium nitrate pentahydrate
Eu	Europium
Fe	Iron
Fe(NO ₃) ₃	Iron (III) nitrate
Fe ₂ O ₃	Ferric oxide
FWHM	Full width at half maximum
GaP	Gallium phosphide

Gd	Gadolinium
Gd ₂ O ₃	Gadolinium oxide
H ₂	Hydrogen
H ₂ O	Water
H ₂ O ₂	Hydrogen peroxide
H ₂ SO ₄	Sulphuric acid
HNO ₃	Concentrated nitric acid
IUPAC	International Union of Pure and Applied Chemistry
KM _n O ₄	Potassium permanganate
La	Lanthanum
L-H	Langmuir-Hinshelwood
MF	Microfiltration
MnO ₄	Permanganate
MoS	Molybdenum disulphide
MWCNT	Multi-walled carbon nanotube
NCMA	Natal Clothing Manufacturers Association
Nd	Neodymium
NF	Nanofiltration
N ₂	Nitrogen
NH ₃ ⁺	Ammonia
NIR	Near infra-red
O ₂	Oxygen
O ₃	Ozone
•OH	Hydroxyl
OH ⁻	Hydroxide
PCA	Principal component analysis
PCL	Polycaprolactone

Poly DADMAC	Polydiallyldimethyl ammonium chloride
PO ₄ ⁻	Phosphates
Pr	Praseodymium
PTFE	Polytetrafluoroethylene
REM	Rare earth metal
RO	Reverse osmosis
Sb ₂ S ₃	Antimony trisulphide
Sc	Scandium
SEI	Secondary electron imaging
SEM	Scanning electron microscopy
Sm	Samarium
SME	Small and medium enterprises
SWI	Specific water intake
TBOT	Titanium (IV) butoxide
TCA	Titanium dioxide cellulose acetate
TEM	Transmission electron microscopy
TiO ₂	Titanium dioxide
TDS	Total dissolved solids
TSS	Total suspended solids
UF	Ultrafiltration
UV	Ultraviolet
UV-Vis	UV-visible
V ₂ O ₅	Vanadium oxide
VB	Valence band
WO ₃	Tungsten trioxide
WRC	Water Research Commission
WWTW	Wastewater treatment works

XRD	X-ray diffraction
Y	Yttrium
Yb ³⁺	Ytterbium ion
ZnO	Zinc oxide
ZrO ₂	Zirconium dioxide
ZnS	Zinc sulphide

CHAPTER 1: INTRODUCTION

1.1 BACKGROUND

South Africa is a water-scarce country due to its location in a water-deficient region that is characterised by variable rainfall, droughts, flooding and increased water losses due to evaporation, with the annual rainfall amounting to 53% of the global average (i.e. 450 mm per annum of the global average of 860 mm per annum). In addition, the water scarcity is compounded by unfavourable rainwater runoff distribution and limited groundwater of variable quality. The collective flow of all the rivers in South Africa amounts to about 49 000 106 m³ per annum, which amounts to less than that of the Zambezi River, comparatively speaking (Muller et al., 2009).

The importance of water to the sustainable development of South Africa cannot be overstated. The reliable availability of water of a quality that is acceptable and suitable for good health, livelihoods and production is critical to economic survival. South Africa has been facing a water resource crisis that continues to be exacerbated by an increasing population, increasing agricultural activity and expanding industries. Typically, the expansion of urban settlements, shifts in agricultural practices and industrial effluent discharged into natural water resources all have serious effects that have proven difficult and expensive to remediate.

Manufacturing industries require large volumes of water for processes such as production, cooling, heating, cleaning, rinsing and sanitation, and consumption by personnel. The industrial sector is responsible for 55% of the total water usage, with mining, power generation, and the food and beverage industry using 23%, 20% and 2%, respectively. The effluent produced by the industrial sector was estimated to be 74%, making it the largest producer of wastewater, followed by the mining sector (10%), food and beverage sector (8%) and power-generation sector (7%) (Cloete et al., 2010). The industrial, mining and power-generation sectors make water withdrawals of only 10.3% of South Africa's freshwater sources, with municipalities withdrawing 62.6%. However, it should be noted that smaller industries draw water directly from municipalities (Donnenfeld et al., 2018). Consuming such large volumes of water is an issue in that the over-exploitation of a renewable resource at unsustainable levels, combined with post-production wastewater discharged from these industries, left unregulated,

poses an imminent threat to natural water resources because the effluent load and quality, volume and destination of the effluent are important factors that further aggravate the water stress loss. Therefore, water conservation and water demand management are national priorities as demand for water of an acceptable quality grows.

The textile industry is potentially one of the biggest threats to the environment because of its large water usage, high energy consumption, and the release of chemicals and undesirable emissions to fresh water sources. In South Africa, the textile industry has been identified as one of the top 80% of industrial water users (Cloete et al., 2010). The entire supply and production chain of textiles is related to numerous negative environmental issues. For example, vast quantities of gas, liquid and solid waste are generated from the cultivation of natural raw fibres like cotton, jute and flax, which require irrigation and pesticides that have an impact on ecosystems and natural water sources, followed by the weaving of the fibres into cloth and ultimately the manufacture of the finished, dyed fabric. In the wet processing phase of the textile production process, water is used primarily for the dissolution and application of chemicals onto the textiles and rinsing. The textile finishing and dyeing process involves steps such as scouring, bleaching, dyeing, dye-fixing and fabric softening. These processes are all very water-intensive and require large volumes of water (Şen and Demirer, 2003). This study focused on the wet processing of the textile manufacturing process, with the dyeing unit operations (Figure 1.1 highlighted in red) and the wastewater effluent generated from it being the main focus. The yarn and fabric production operations are also within the scope of this process (Figure 1.1 highlighted in blue).



Figure 1.1: Generalised textile production process and the production areas that are the focus of this report (adapted from Johannesson, 2016)

Like many industrial processes, textile dyeing has inherent inefficiencies. The water that remains after the dyeing process has been completed is heavily laden with unspent dye. Depending on the type of dye and the fabric, it is estimated that nearly 50% of the dye remains unfixed in fabrics (Ghaly et al., 2014). The multitude of chemicals used in textile manufacturing results in the dye being discharged

together with the wastewater into natural water sources, making it aesthetically displeasing. Furthermore, textile wastewater has highly variable content and characteristics, depending on the textiles and dyes applied to it. Notable fluctuations in physicochemical parameters such as colour, pH, temperature, salinity, COD and BOD stem from the fact that numerous other substances are used before and after dyeing: lubricants, stabilisers, caustic soda, peroxide, acetic acid and detergents to name just a few (Ntuli et al., 2009; Chequer et al., 2013). In addition to the depreciation in the aesthetic quality of the water, the release of dye-containing wastewater into the environment poses major risks to aquatic, terrestrial and human life because of the resultant eutrophication of water bodies, the reduction in sunlight penetrating contaminated waters and the harmful byproducts that are formed when the wastewater is subject to the biotic and abiotic processes that occur in the environment (Akpan and Hameed, 2009).

In both industrial and municipal WWTW, wastewater is generally treated in three steps: primary, secondary and tertiary. Within these steps, physical, biological and chemical techniques are used (Figure 1.2). A major challenge posed by dye from household water is that, in addition to the dye, many other chemicals, such as detergents, softeners and other additives, are also used to improve the dyeing process. Furthermore, the effluent characteristics may vary daily and seasonally. This increases the difficulty of treatment (Ntuli et al., 2009). Many currently used industrial wastewater treatment systems were built for primary and secondary treatment because most WWTW are designed to handle domestic effluent (Eckenfelder, 2000). This means that primary and secondary treatment is rather inadequate in treating dye from household wastewater with a higher organic load, and there is a greater incidence of water pollution by industrial effluent discharge into WWTW and ultimately surface water, thus treatment facilities must be fitted with additional systems to handle recalcitrant organic pollutants and toxic residuals. Following secondary treatment, techniques can be applied to the refractory organic pollutants that are present in textile wastewater. These are broadly divided into biological, chemical and physical techniques. Among the tertiary treatment techniques that have been used for textile effluent are membrane technologies, adsorption, oxidation, electrolytic precipitation, electrochemical processes, ion exchange, thermal evaporation and photocatalytic degradation (Le Roes-Hill et al., 2017).

Photocatalytic degradation falls within a class commonly referred to as advanced oxidation processes (AOPs). These involve the photochemical activation of already oxidising substances like ozone (Shu

and Chang, 2005), hydrogen peroxide (Aleboye et al., 2003), Fenton's reagent (Lucas and Peres, 2006), etc. to yield highly reactive and oxidising free radicals. Reports frequently state that the use of photoactivated oxidising agents for the treatment of dye effluent is largely superior to using only UV radiation or the oxidants on their own (Ghaly et al., 2014), primarily because photochemical processes completely destroy organic pollutants as opposed to transferring them to another phase, as is the case with physical treatment processes.

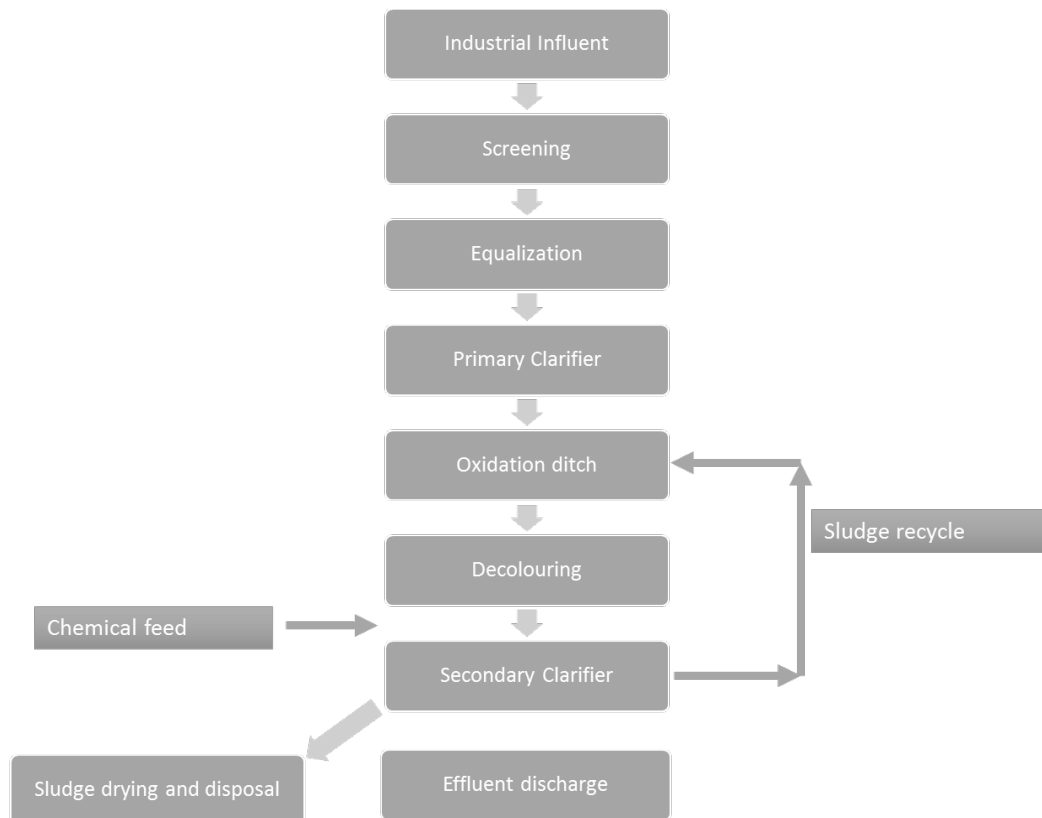


Figure 1.2: Generic industrial wastewater treatment process

One of the most viable AOPs for the elimination of organic pollutants in wastewater is semiconductor-mediated heterogeneous photocatalysis. Its viability, relative to other treatment processes, is based on the premise that there is no mass transfer. It can be carried out under ambient conditions (extreme pressure and temperature are not required). Atmospheric oxygen can be used as the oxidant, and the complete mineralisation of target pollutants can be achieved (Konstantinou and Albanis, 2004). Titanium dioxide remains the most studied semiconductor photocatalyst as it demonstrates high activity under UV irradiation, photostability, biological inertness, relative chemical stability, low operational temperature and low energy consumption, water insolubility under typical environmental conditions,

disinclination to photo corrosion and it is naturally abundant, therefore cheaper than other semiconductor photocatalysts (Zangeneh et al., 2015).

A fundamental problem that prevails with the use of TiO₂ in as far as environmental pollutants, decontamination and many other applications are concerned, is that it has a relatively wide band gap energy ($E_g \sim 3.10$ and 3.23 eV for rutile and anatase, respectively) (Zangeneh et al., 2015), so it only displays photoactivity under UV irradiation at wavelengths of ~ 387 nm. This means that only about 4% of the solar energy incident on earth can be used, and the use of TiO₂ in wastewater treatment is rendered impractical (Teh and Mohamed, 2011). In addition to this, the high rate of electron-hole recombination and low interfacial charge-transfer rates of the photogenerated carriers in TiO₂ particles result in a lowered quantum yield and inefficient photocatalysis (Xu et al., 2010). Studies on TiO₂-mediated heterogeneous photocatalysis have focused on improving the efficiency of the photocatalytic process in TiO₂. Multiple strategies have been employed, not only to improve the photocatalytic performance of TiO₂, but to enhance its visible light photoactivity. This is because visible light accounts for nearly 50% of the solar energy spectrum incident on earth, and much of the cost associated with photocatalysis for environmental clean-up derives from the energy-cost implications of powering UV-light sources.

Enhancement strategies can be divided into chemical and physical methods. Typically, chemical methods involve the doping and co-addition of metal and non-metals or coupling with secondary semiconductors. Physical methods involve the introduction of microwave or ultrasonic radiation into titania photoreaction systems (Xu et al., 2010). In an ideal situation, a catalyst to be employed in photocatalytic oxidation should be photostable, chemically and biologically inert in natural systems, abundant and cheap. The works studied proposed the development of nanoparticulate TiO₂-based catalysts, which would retain all the favourable properties of TiO₂ as a photocatalyst, but would impart visible light activity. The use of Er³⁺ and MWCNTs would improve the visible light activity of TiO₂ nanoparticles by decreasing the band gap of the parent TiO₂, decreasing the electron-hole recombination rate and enhancing interfacial charge-transfer efficiency, while improving photocatalyst pollutant pre-adsorption and retention (Reszczyńska et al., 2015; Etacheri et al., 2015). Additionally, the photoactive nanocomposite was immobilised on a biodegradable polymer matrix to improve the photocatalyst retention after the depollution of dye-containing wastewater.

1.2 AIM AND OBJECTIVES

The main aim of the project was to develop nano-sized TiO₂ particles modified with erbium ions, combined with MWCNTs and embedded onto a naturally derived, biodegradable polymer film. The nanocomposite was intended for and applied to the remediation of organic azo dyes found in textile wastewater. The aim of the project was realised through the following specific objectives:

- To prepare MWCNTs using the chemical vapour deposition method.
- To prepare TiO₂ nanoparticles via the sol-gel method.
- To prepare erbium ion-modified TiO₂ nanoparticles via the sol-gel method and the wet-impregnation of the titania by the Er³⁺ ions.
- To prepare a MWCNT-modified titania nanocomposite.
- To prepare an erbium and MWCNT-co-modified titania-based nanocomposite.
- To immobilise the erbium and MWCNT-co-modified titania-based nanocomposite onto a cellulose acetate and polycaprolactone biopolymer blend.
- To evaluate the powder nanocomposites and biopolymer-immobilised photocatalysts for the degradation of synthetic solutions of model diazo dye Reactive Red 120 under visible light irradiation.

1.3 SCOPE AND LIMITATIONS

The Er and MWCNT-modified TiO₂ nano-photocatalysts applied to the decolourisation through the photodegradation of Reactive Red 120 proved that the inclusion of Er and TiO₂ improves MWCNT visible light activity. However, photocatalyst efficiency was limited by immobilisation onto the biopolymer matrix and requires refinement of the polymer synthesis to avoid light penetration limitation and decomposition when subject to radicals present in solution during the photocatalysis process. Because the study was limited to the application in modelized solutions prepared with a singular dye, the laboratory-scale experiments yielded valuable fundamental data in so far as the research objectives were concerned. The project met all the stated research objectives. The results of this investigation were not proven with real wastewater. Therefore, more extensive research is required with more complex real-time wastewater. During the course of the project, the research team visited textile dyeing mills in the eThekweni Hammarisdale Textile Hub where a working relationship was established with

factories and the Department of Water Affairs and Sanitation (DWS) regarding the continuous collection of wastewater and establishing a partnership for the application of the nanocomposites in the mills. Beyond the scope of the proposal was an endeavour to raise awareness in the textile milling operations and plant managers of the importance of removing azo dye and pigments prior to discharging wastewater.

CHAPTER 2: LITERATURE REVIEW

2.1 THE CLOTHING, TEXTILE, FOOTWEAR AND LEATHER INDUSTRY IN SOUTH AFRICA

2.1.1 Introduction and definition of the clothing, textile, footwear and leather industry in South Africa

The South African clothing, textiles, footwear and leather manufacturing (CTFL) industry is a diverse and mature industry. “Textile industry” is a broad term referring to the CTFL industry as a collective because the inter-relation of these industries’ starting materials and production processes means that they form an organic grouping in the manufacturing industry. However, for the purposes of this report, “textile industry” refers specifically to “the industry that consists of companies that are involved in the manufacture and processing of textiles through various processes: the production of yarn from natural raw materials (e.g. cotton, wool, mohair) and/or man-made fibres (e.g. viscose, rayon); the production of woven or knotted fabrics from spun yarn; the dyeing and printing of fabrics; and the application of finishing processes (e.g. the production of technical textiles or textiles with industrial applications)” as defined in “National Survey 13: Water and Wastewater Management in the Textile Industry” (Le Roes-Hill et al., 2017).

During the early 1920s the CTFL industry in South Africa was nearly non-existent, as clothing and fabrics were tailored and imported. The catalyst for growth in the production of local clothing was the supply restrictions experienced during World War I. During the 1930s until the 1950s, a steady growth occurred in the industry until the clothing sector was producing about 87% of local demand. Growth slowed down and peaked again during the 1980s, partly due to a depreciating rand and the subsequent reduction in imports to such an extent that local production made up about 93% of total domestic demand. During the early 1990s, there was a crisis, and production and employment declined due to

an increase in imports. Between 1993 and 1994, the sector seemed to recover, albeit slowly (October, 1996). Historically, the South African textile industry has been concentrated primarily in two large regional agglomerations: Western Cape and KwaZulu-Natal, where the bulk of clothing production has been in Western Cape. Partly driven by the large retail chains in the region, Cape Town became the heart of the South African clothing industry (Chaddha et al., 2009).

When South Africa implemented trade liberalisation in the 1990s, however, levies on imported machinery limited upgrading, while the liberalisation and restructuring of the sector simultaneously created major reductions in employment. The increases in productivity were as a result of downsizing and cost-cutting. The industry incurred about 30 000 job losses between 1996 and 1999 as companies competed by saving costs through downsizing (Morris et al., 2005). The economic openness and trade liberalisation policies were intended to increase export potential and thus the growth of the industry. However, these policies had a detrimental impact on the CTFL sector in South Africa, where the challenges of global competition exposed previously protected domestic industries to international competition. The South African CTFL industry was burdened when the rapid increase in clothing imports hastened the decline of the industry. Its consequences were marked in the 2000s when rapid increases in job losses were incurred and smaller firms went completely out of business (Van der Westhuizen, 2007). The CTFL industrial complexes in Gauteng and KwaZulu-Natal were hardest hit; more so than the Western Cape cluster.

As part of the process of gathering information on textile production processes and wastewater sampling and collection, the researchers visited textile mills in the Hammarsdale Industrial Complex in KwaZulu-Natal during the course of this project.

2.1.2 Profile of the KwaZulu-Natal Textile Cluster

The KwaZulu-Natal CTFL industry goes as far back as 1935 with the formation of the Natal Clothing Manufacturers Association (NCMA) and grew in the 1960s with the relocation of firms in the former province of Transvaal to KwaZulu-Natal (then known as Natal). These firms were concentrated primarily in the Isithebe, Pinetown and Hammarsdale industrial agglomerations, with their headquarters in Durban. Despite fluctuations over the years, the CTFL industry in KwaZulu-Natal grew rather steadily until 2000 when it showed a decline. It has been estimated that, between 2000 and 2011, there were

about 17 000 formal job losses (EDGE, 2014). Historically, the CTFL firms in KwaZulu-Natal had family-oriented ownership, displaying a markedly entrepreneurial base, which allowed the KwaZulu-Natal-based firms to participate in the informal and wholesale hawker markets (Prinsloo, 1996).

This diversification was once an advantage in the region. However, over time and with trade liberalisation, cheaper production costs, a favourable currency and productivity enabled the Asian manufacturing sector, in particular the CTFL sector, to expand rapidly and seize markets abroad. In response to the industry losing a large share of the domestic retail market, the Ministry of Trade and Industry and the eThekweni Municipality launched various support measures, such as the Competitiveness Improvement Programme, the formation of the Clothing and Textiles Cluster and Fashion Council, and the Fashion Fair held during 2013, to bolster growth in the sector (EDGE, 2014). Despite these interventions, sections of the industry have and are continuing to experience a degree of informalisation as they have found it increasingly harder to compete and have resorted to downsizing and informalisation operations to survive.

It is difficult to accurately determine the number and size of the companies in the CTFL industry, primarily because of the informal nature of the sector and by virtue of the fact that it is an unobtrusive industry. Operations can almost always be set up anywhere. The CTFL Sector Education and Training Authority (CTFL-SETA) has approximately 2 000 active registered companies. Most of these companies are small and medium enterprises (SMEs) employing between 20 and 200 people (Jauch et al., 2006; Prinsloo, 1996). Figure 2.1 shows CTFL firms in eThekweni with more than 45 employees.

Of the textile mills visited during this project to determine their water usage and wastewater generation, it was found that trade liberalisation in previous years forced small and medium textile factories employing less than 200 people to downsize and informalise their operations to survive in a market that had opened to foreign trade. One of the negative outcomes of economising was the compromise of water management practices by these companies, where the only best practices implemented to minimise wastage related to water intake were to turn off running taps and hoses, turn off the water when machines were not in use and to repair defective valves and leaks. Wastewater and effluent were subjected to preliminary and primary treatment such as screening, settling and neutralisation on-site prior to being discharged into the WWTW. Some companies stated that they did not have the resources

and infrastructure to treat their wastewater and only diluted it with river and/or borehole water prior to discharging it into the WWTW.

The CTFL industry in KwaZulu-Natal has registered factories mainly in industrial and commercially zoned areas, while the unregistered “garage” factories are predominantly in the central business district (CBD) (along Grey Street) and in the Phoenix, Chatsworth and Inanda residential areas. Nodes of manufacturers are found in the industrial hubs in Mobeni, Jacobs, Clairwood, in the Durban CBD near Grey Street, in the Umbilo and Rosburgh area, in Stamford Hill and in the Mayville/Overport area, as well as in the centres further north, such as Phoenix, Verulaam and Tongaat (Prinsloo, 1996). The textile industry has a strong presence, especially in Pinetown and Hammarsdale in the west, where the fibre weaving and dyeing mills are concentrated, forming a textile dyeing, processing and manufacturing industrial complex as shown in Figure 2.1 (see the green circle).

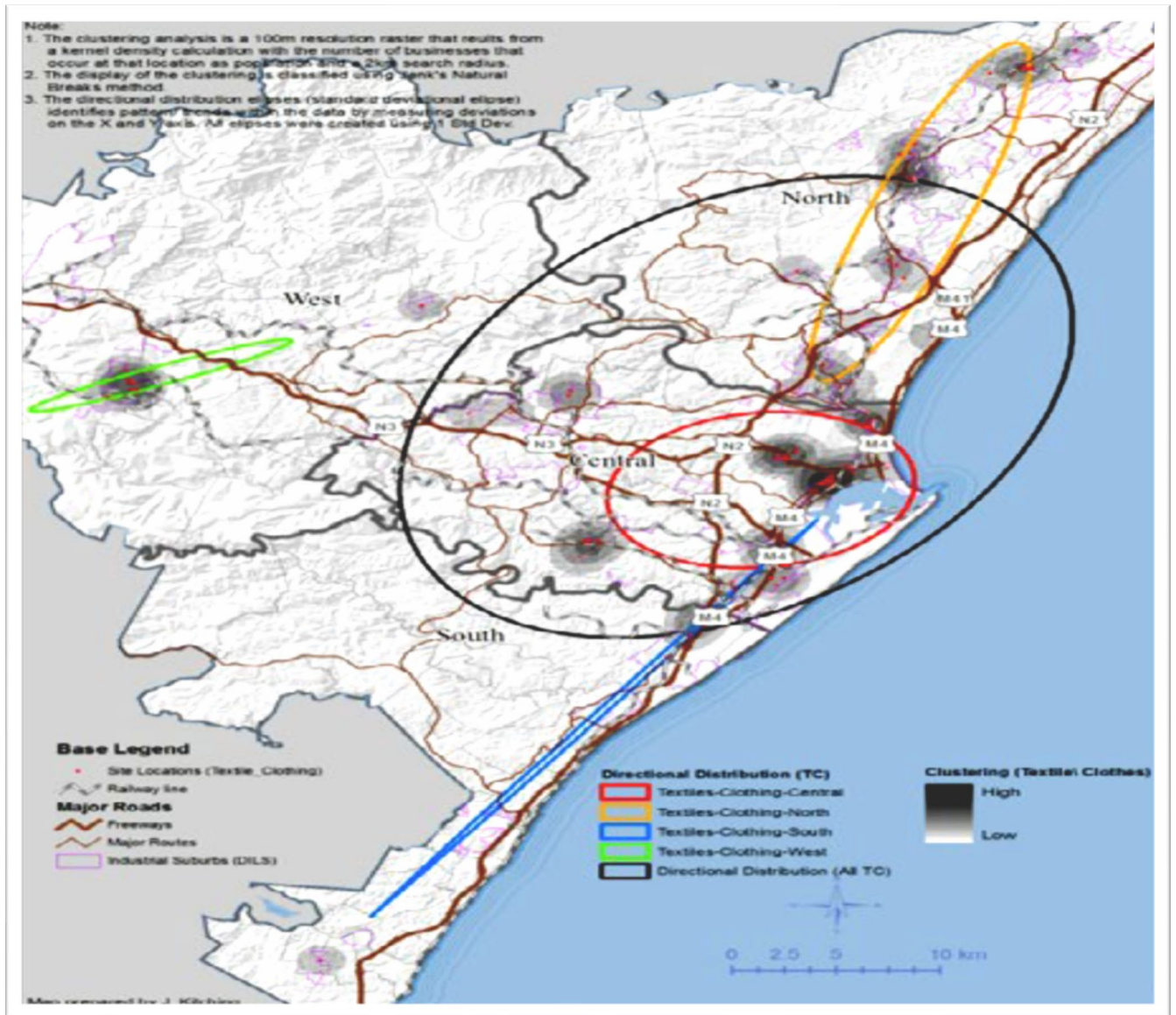


Figure 2.1: Distribution of firms employing more than 45 people (from eThekweni Industrial Land GIS database (EDGE, 2014))

2.2 WATER USE AND WASTEWATER MANAGEMENT IN THE TEXTILE INDUSTRY

2.2.1 Water use in the textile industry

The diversity of the textile industry and its operations make it virtually impossible to outline simple categories, as the processing of textiles from start (raw materials to produce yarn) to finish (the final textile goods) can be carried out by various related industries or it can take place in one factory. Typically, natural and/or synthetic fibres are spun to produce yarn, which is woven into fabrics that are subjected to various chemical treatments, such as bleaching, dyeing, printing and finishing (Le Roes-

Hill et al., 2017). Broadly speaking, the textile industry can be categorised into dry processing (yarn manufacturing, weaving and knitting) and wet processing (preparation, dyeing and finishing). For the purposes of this report, the focus is on wet processes in general, and particularly dyeing and finishing, together with the wastewater generated from these processes (Figure 2.2).

The textile industry poses a threat to the environment because it is so water intensive during all stages. Cloete and co-workers (Cloete et al., 2010) conducted a study in which they found that the textile industry was ranked among the top 80% of industrial water users in the eThekweni Metropolitan Municipality (being the largest consumer of water, accounting for about 36% of total water use). The City of Cape Town Metropolitan Municipality and Amathole District Municipality are the second- and third-highest users respectively, consuming about 29% and about 2% of the total available water (Cloete et al., 2010).

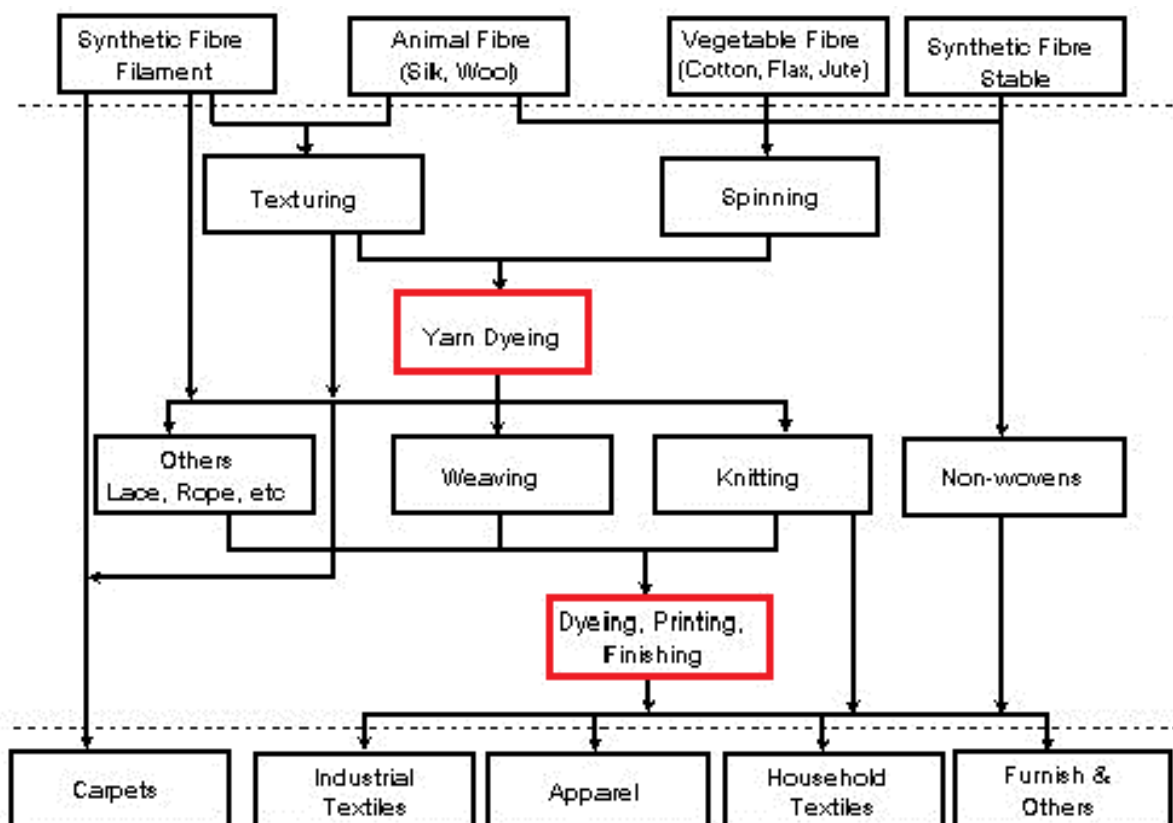


Figure 2.2: Flowchart of textile product manufacturing (Le Roes-Hill et al., 2017)

More recently, the WRC commissioned a national survey that focused on the water use and wastewater management practices in the South African textile industry. As part of the survey, various textile

companies were asked to provide information pertaining to the source of the water used in their production processes, the water quality requirements and pre-treatments they carried out, and their water use per unit of production. It was found that some of the textile companies used varying sources of water to supplement municipal water, such as rivers, boreholes and reclaimed waste streams. Based on the information provided by the companies surveyed and the specific water intake (SWI) estimations, it was found that the water usage varies from 0.36 kℓ to 600 000 kℓ per annum (Le Roes-Hill et al., 2017). The variations in the source of water, water quality and water usage were due to the fact that water is used for various activities, such as the dissolution and application of chemicals onto the textiles and rinsing, washing the plant equipment, steam generation, cooling systems, air conditioning, staff consumption and sanitation. Functions such as steam generation, air conditioning, human consumption and textile processing require a higher quality of potable water, while water of a lower quality can be used for other purposes (Groves et al., 1990). With regard to textile wet-processing operations, this wide variation in water usage depends on factors such as the type of fibres being processed, treatment and pre-treatment processes, and the type of dye and dyeing process used.

The fabric dyeing process involves steps such as scouring, bleaching, dyeing, dye-fixing and fabric softening, which are all very water intensive and require large volumes of water (Şen and Demirer, 2003). It has been estimated that between 0.00015 ℓ and 113 ℓ of water is used a day during the wet process to manufacture 1 kg of fabric (Le Roes-Hill et al., 2017).

2.2.2 Wastewater generation and management in the textile industry

Total effluent production in the textile industry followed a similar trend to water usage, where specific effluent volumes were about 80-90% of the specific water intake value (Cloete et al., 2010; Le Roes-Hill et al., 2017). However, what is more important is the pollutant load of the effluent caused by the wide variety of chemicals, such as detergents, lubricants, wetting agents, caustic soda, salts, bleach, mineral oils, metal ions (from pigments and dyes) and finishes, which also go into the waste stream (Ntuli et al., 2009). These substances, which are used in textile manufacture, in combination with the dye already present in the water, cause the wastewater to show notable fluctuations in physicochemical parameters, such as colour, pH, temperature, salinity, COD and BOD (Chequer et al., 2013).

Due to the fact that textile effluents are generally not biodegradable, discharging this water into the WWTW causes colour and COD problems, while those that are discharged into the environment pose

major risks to aquatic and terrestrial wildlife because of the resultant eutrophication of water bodies, high BOD, limitation of light penetrating contaminated waters and harmful byproducts formed when the wastewater is subject to biotic and abiotic processes that occur in the environment (Akpan and Hameed, 2009). The non-biodegradability and variant nature of textile wastewater creates a challenge for WWTW operators to produce non-toxic, remediated effluent prior to discharging it into rivers and natural water sources. Figure 2.3 illustrates the generic configuration of a WWTW receiving industrial wastewater with an integrated anaerobic pond and activated sludge process. Textile effluents may interfere with these municipal WWTW operations because the preliminary, primary and secondary treatment operations are not suitable for textile wastewater.

The South African textile companies surveyed indicated that they do not recycle effluent because they require good-quality water for production processes. The majority does not pre-treat effluent due to insufficient resources and infrastructure, while others discharge their effluent to a central off-site facility run by a private service provider that treats it at a cost. Those that treat their own wastewater, carry out rudimentary treatments such as screening, settling and pH neutralisation prior to discharging it to the WWTW. Of the 21 companies surveyed, only three had on-site treatments that applied primary, secondary and tertiary techniques such as three-pit settling dams, flocculating with lime and ferric chloride and implementing a newly piloted filtration and reverse osmosis (RO) system (Le Roes-Hill et al., 2017).

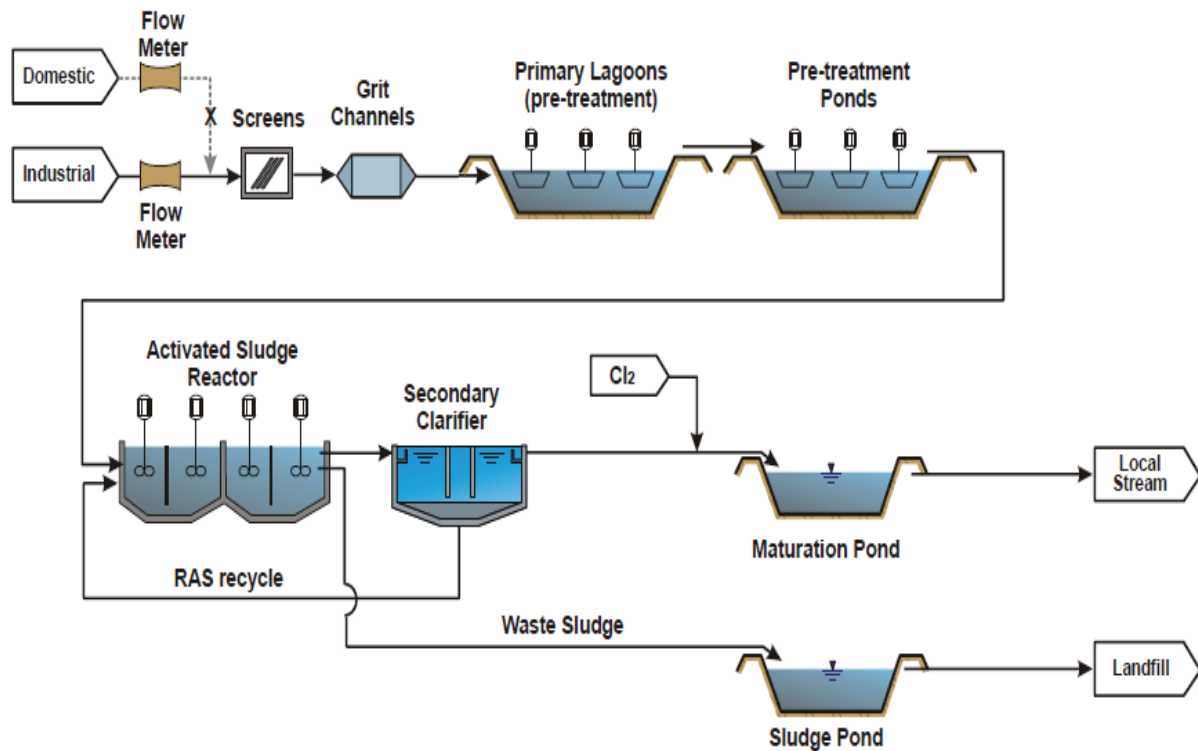


Figure 2.3: Generalised configuration of a WWTW receiving industrial wastewater, showing the integrated anaerobic pond and activated sludge process (Boyd and Mbelu, 2009)

Cloete et al. (2010) conducted a study in which the environmental threat posed by the resultant effluent from various industries was assessed. Furthermore, risks associated with certain chemical constituents in the effluent that pose the greatest harm to natural water sources and the environment were evaluated (Cloete et al., 2010). Wastewater components of special interest, such as micro-organisms, biodegradable organic materials and their associated BOD, synthetic organic materials, nutrients, metals, inorganic substances, such as mineral acids and bases, thermal effects, odour and taste, were the primary considerations. Based on information provided by the City of Cape Town, eThekweni, Buffalo City and Tshwane metropolitan municipalities, it was found that that textile mill effluents indicated COD values ranging from 537 mg/l to 9 553 mg/l. Phosphate concentrations ranged from 1 mg/l to 39 mg/l and pH values were alkaline, ranging from 5 to 12. The high COD and phosphate levels would lead to oxygen depletion and eutrophication if discharged to natural water bodies. A related industry in the same study is the dyeing and colouring sector, which is involved in the manufacture of dyes, pigments and textile dyehouses. Based on information from the City of Cape Town Metropolitan Municipality, it

was found that wastewater from the dye manufacturing process exhibited a high COD (217 mg/l to 1 992 mg/l), where COD concentrations, by the Department of Water Affairs and Forestry (DWAF)'s standards, should be less than 50 mg/l. The pH values ranged from alkaline (7-10) to highly alkaline (11-12). What was interesting to note was that, in textile effluent risk assessment, nonylphenols and nonylphenol ethoxylates were the primary environmental risk considerations for textile mills. Briefly, nonylphenols and their ethoxylates are chemicals present in surfactants and detergents used in the manufacture of textiles. Upon release in textile and laundry effluents via WWTW or into natural water sources, they decompose into toxic nonylphenols, which are persistent organic pollutants that tend to bioaccumulate (Brigden et al., 2013).

In the literature surveyed, synthetic organic dyes such as azo dyes and their partial decomposition intermediates, which are present in veritable amounts in textile effluents, were not highlighted as pollutants that posed significant environmental risk in South African textile mills (Cloete et al., 2010; Le Roes-Hill et al., 2017). Instead, parameters for quantifying pollutant load such as COD, ammonia (NH_3^+), phosphates (PO_4^-), pH, temperature, conductivity, total suspended solids, total solids, nitrate/nitrite, chlorides and sulphates are the primary parameters considered to be of importance. However, considering that the dyeing process results in wastewater that contains high colour from dyes and pigments, as well as pollutants such as halogens, metals, amines, salts, reducing and/or oxidising agents and antifoaming agents, it would be negligent not to prioritise the polluting effects of synthetic organic dyes prevalent in dyehouse waste.

2.2.2.1 Azo dyes

Azo dyes are strictly of anthropogenic origin. However, some substances that contain *N*-oxide azo (azoxy) are known to occur in nature (Hunger, 2003). They are the outcome of the work of Peter Griess, who discovered diazo compounds and went on to prepare dyes from them (Griess, 1858). Azo dyes contain at least a single azo group ($-\text{N} = \text{N}$). However, they may contain two, three and, in rare cases, four azo groups. Figures 2.4 to 2.6. show the structures of typical azo dyes.

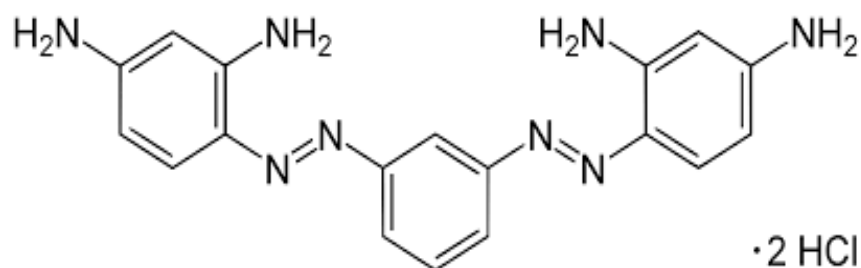


Figure 2.4: Structure of Bismarck Brown

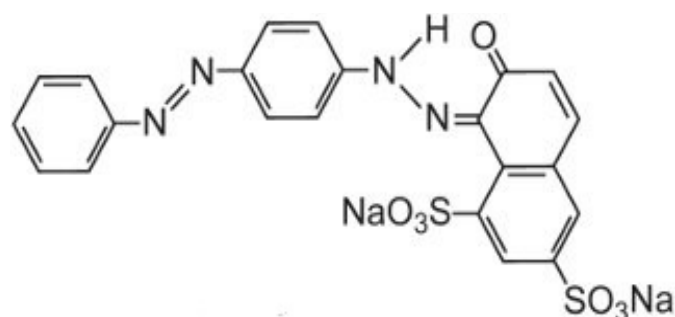


Figure 2.5: Structure of CI Acid Red 73

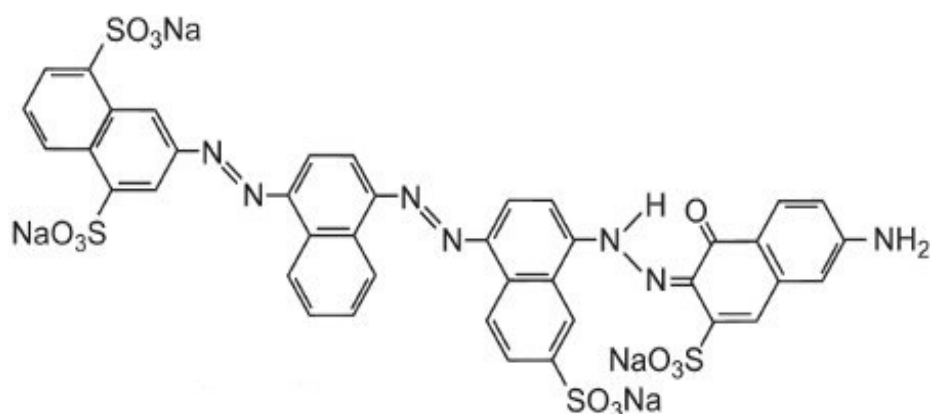


Figure 2.6: Structure of CI Direct Blue 71

In 1991, the world was consuming about 668 000 tonnes of dyestuffs, of which, with the exclusion of the non-azo dyes, such as indigo, sulphur and vat dyes, 527 000 tonnes of dyes remain. There is a lack of statistics on the actual share of azo dyes consumed relative to the total amount of dyes. However, there is agreement that azo dyes represent the majority of all dyes consumed all over the world: about 60-70%, and thus represent the “majority” (Øllgaard et al., 1998).

Commercially, azo dyes constitute the most important class of dyestuffs, as they account for over 60% of the total dyes manufactured. Moreover, the textile industry is the largest consumer of organic azo dyes (Gordon and Gregory, 1983; Allen, 1971). The estimations of global dye consumption show that synthetic colourants represent a fairly large proportion of the organic chemicals encountered in daily life. The removal of organic dye from wastewater is often considered to be more urgent than the removal of other organic contaminants as the colourants present in water, even at minute concentrations, are clearly visible and affect water quality. In addition to depreciating the aesthetic quality of water bodies, azo dyes and their aromatic amine intermediates have long been established as carcinogens (Dietrich and Golka, 2012). Other risks of chronic interaction with azo colourants and their intermediates are acute toxicity, causing methemoglobinemia, acute haemolysis, dermatitis and allergies, with the major hazard to humans being the induction of cancer, particularly in the urothelial tract and urinary bladder as a result of occupational exposure (Fishbein, 1984).

The biodegradation of azo dyes has been said to occur in both aerobic and anaerobic bacteria. However, synthetic dyes are generally xenobiotic. The micro-organisms that occur in humans, in terrestrial and aquatic life, as well as in rivers and lakes, seldom possess enzymes designed by nature to fully mineralise synthetic dyes (Zollinger, 1987). Because dyes, by their very nature, are manufactured to be thermally, chemically and photolytically stable, the photodecomposition of azo colourants in nature is generally slow and depends on factors such as oxygen levels, pH, light intensity and the chemical structure of the azo dye, where mono-azo dyes have shown to readily decompose, as opposed to trisazo dyes. The inability of biotic and abiotic processes to fully degrade azo dyes (and other organic compounds) that are discharged into the environment causes compounds to be transformed into aromatic amines, which are generally recalcitrant and will ultimately, through processes such as sorption into sediment, bioaccumulate in nature and have a lasting effect on the environment, humans, and aquatic and terrestrial life.

2.2.2.2 *Aromatic amines*

Aromatic amines are a class of chemical compounds with one or more aromatic rings bearing one or more amino substituents in their molecular structure. The simplest aromatic amine is aniline, although the structures become increasingly complex, where the conjugated aromatic or heterocyclic structures

can contain multiple substituents (Pineiro et al., 2004). Aromatic amines are also used in the synthesis of dyes and pigments, as has previously been elaborated. Other sources of aromatic amines into the environment include, but are not limited to the combustion of organic matter, such as the burning of tobacco and protein-rich plant matter and forest fires, and exhaust fumes generated by the combustion of fossil fuels (Lewtas, 2007). The carcinogenicity of *N*-substituted aryl compounds used in the azo dye manufacturing industry has been known since the late 19th century, when, in 1895, a German clinician, Ludwig Rehn, found that several individuals working in factories producing dye intermediates had bladder cancer that was likely caused by exposure to polycyclic aromatic amines such as 2-naphthol thylamine (Dietrich and Golka, 2012).

2.3 TEXTILE WASTEWATER TREATMENT TECHNOLOGIES

2.3.1 Overview

In 2010, the Department of Water Affairs (DWA) conducted a water quality review in South Africa at the resource-directed management of water quality planning level. It was found that the majority of South Africa's WWTW were overloaded. This made pollution from WWTW a point of concern (Moodley et al., 2011). Part of the pollution load to WWTW stems from the large volumes of textile wastewater that requires disposal. Pollution, such as high salinity, high COD load and colour, necessitates adequate care to be exercised, otherwise it will pose serious and long-lasting threats to the environment and water resources. Due to the complex and variable nature of industrial textile wastewater, there is not one single wastewater treatment technology that is a panacea, therefore a multi-barrier approach to the control and removal of pollutants remains one of the best practices to be applied. For example, the treatment of textile wastewater has traditionally included methods such as neutralisation, flocculation, coagulation, activated carbon absorption, biological treatment and advanced oxidation using UV irradiation, combined with hydrogen peroxide (H_2O_2) solutions and ozone (O_3). Figure 2.7 presents the conventionally used treatment methods at the primary, secondary and tertiary treatment levels for textile effluent (Le Roes-Hill et al., 2017). However, it must be stressed that, separately, all treatment processes have associated advantages and disadvantages.

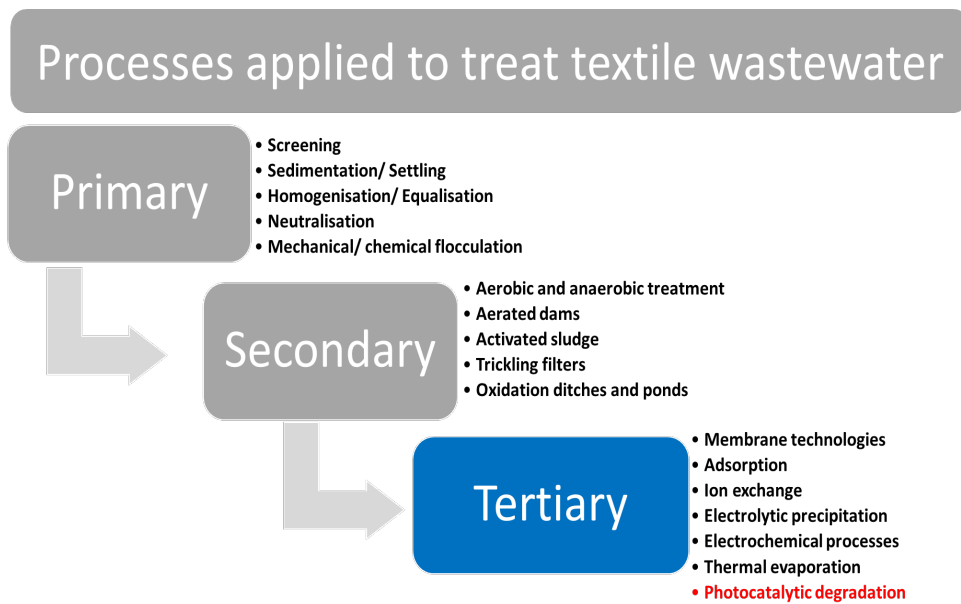


Figure 2.7: Summary of primary, secondary and tertiary treatment techniques applied to the treatment of textile wastewater (Le Roes-Hill et al., 2017)

The conventional wastewater treatment processes listed in Figure 2.7 under primary and secondary treatment techniques are usually adequate in combination for the removal of classical pollutant parameters, such as BOD, COD, total suspended solids (TSS), total dissolved solids (TDS), nitrogen content, phosphorous and metals arising from process chemicals (Vandevivere et al., 1998). The tertiary techniques are used for the treatment of refractory pollutants (viz. synthetic organic dyes and pigments, persistent organic pollutants, toxicants, absorbable organohalogens (AOx) and surfactants) that present problems in conventional WWTW. The following discussion focuses on a few technologies used in the treatment of textile wet-processing wastewater, with an emphasis on the removal of azo dyes and the resultant colouring present in the effluents.

2.3.2 Biological methods

Biological wastewater treatment refers to processes that use naturally occurring micro-organisms to feed on complex organic matter, thereby converting them into simpler substances. Biological methods of wastewater treatment are divided into two broad classes based on the oxygen required as aerobic or anaerobic and anoxic or facultative methods, or a combination of these. Aerobic methods apply micro-organisms for the treatment of wastewater in the presence of oxygen, while anaerobic methods use micro-organisms in the absence of oxygen. The aerobic biological treatment method can

decontaminate wastewater via aerobic and facultative bacteria in an aerobic environment. Both aerobic and anaerobic methods can be applied in combination on real textile wastewater to treat wastewater with a high COD (anaerobic process), followed by the treatment of the resulting low COD wastewater (aerobic process) (Wang et al., 2011). The configurations of both anaerobic and aerobic biological treatment are virtually innumerable and are beyond the scope of this report. The following discussion highlights a few biological treatment methods that have been applied to the treatment of textile wastewater with an emphasis on dye and colour removal.

During anaerobic treatment, also known as anaerobic digestion (AD), microbes transform the organic matter present in wastewater into biogas in the absence of oxygen. In WWTW, an oxygen-free environment is achieved by using gas-tight covers over the anaerobic tanks. Anaerobic digestion is often used to treat warm industrial wastewater. Aerobic treatment, on the other hand, is a process in which organic matter is converted into carbon dioxide (CO_2) and new biomass in an oxygenated atmosphere. In WWTW, air can be forced into the wastewater by compressors or blowers, where the aerobic microbes feed on the wastewater. Aerobic treatment is often used for the removal of nitrogen and phosphorous. This is also known as biological nutrient removal (EvoquaWater Technologies, n.d.).

For textile wastewater treatment, the anaerobic and aerobic methods are typically implemented in combination, where the anaerobic process is used to treat textile wastewater with a higher COD, followed by the aerobic polishing treatment to treat the resulting wastewater with a low COD. The reason for the combination of the anaerobic and aerobic processes in textile wastewater treatment is that textile wastewater comprises various types of highly concentrated organic water from processing, such as desizing, that contains both biodegradable organic compounds, such as polyvinyl alcohol or starch, and non-biodegradable constituents, such as azo dyes. The anaerobic treatment uses anoxic hydrolysis or acidification to improve the biodegradability of the wastewater from dyeing and finishing. The following aerobic process is used to polish anaerobically pre-treated wastewater by further lowering the BOD and suspended solids, degrade ammonia, convert nitrite into nitrate and remove phosphates. The hydrolysis or acidification of wastewater occurs during anaerobic treatment. It uses anaerobic bacteria and facultative bacteria in an oxygen-free environment.

The organic acid that is produced during hydrolysis can neutralise the alkalinity of the textile wastewater, thereby creating a neutral environment for the subsequent aerobic treatment. There have been differing views on the ability of biological treatment to completely degrade textile wastewater with special reference to dyes. Reviewers have argued that biological methods for the complete degradation of textile wastewater are eco-friendly, cost-competitive, produce less sludge, yield non-hazardous metabolites, and consume less water due to their capacity to process highly concentrated effluents compared to physical or oxidation methods (Holkar et al., 2016). Mierzwa et al. (2018) pose that azo dyes are hard to degrade via conventional biological wastewater treatment processes because dyes are designed to resist degradation. Furthermore, WWTW that rely on sorption and aerobic biodegradation show low removal efficiency for reactive and other anionic soluble dyes. The stability of azo dyes under aerobic conditions is related to their structural complexity and makes them harder to decompose.

In the same light, azo dyes are easily cleaved to aromatic amines under anoxic conditions because the azo bond only functions as an electron acceptor in the transport chain when a carbon source is available and nitrates are absent. The resultant aromatic amines are not further metabolised under anaerobic conditions, but are easily biodegraded in aerobic conditions (Vandevivere et al., 1998).

Biological treatment methods are arguably one of the greener approaches to textile wastewater remediation in that they are economically feasible, environmentally friendly and the sludge generated, despite requiring disposal, can be used as a soil enhancer. Studies have been conducted to determine the ability of bacteria to survive anaerobic and aerobic conditions for the full decomposition of azo dyes. The research into the micro-organisms used in biological wastewater treatment methods is based on the premise that the microbes would adapt themselves to textile dyes and evolve into new resilient strains that grow naturally in these highly coloured and concentrated wastewaters. In order to survive, they would use enzymes, such as laccase, hexane oxidase, aminopyrine *N*-demethylase and lignin peroxidase, to convert dyes into less hazardous organic substances (Solis et al., 2012).

Numerous laboratory-scale trials have shown the potential of biological treatment for colour removal. However, the large-scale installations that use biological treatment in the pre-treatment step seldom achieve full decolourisation (Vandevivere et al., 1998). The Hammarsdale WWTW in KwaZulu-Natal

primarily receives textile wastewater. It has a five-stage bar-d-enpho nutrient-removal process that is used to treat intensely coloured textile effluents. The entire anaerobic-aerobic system has achieved 95% decolourisation, 60% of which occurs in the first anaerobic state. However, the final effluent remains excessively (Carliell et al., 1995). In a study conducted by Carliell and co-workers (Carliell et al., 1995), dyebath effluents were fed directly to anaerobic digesters used to treat primary sludge from sewage works. The reactive dyebath effluent was completely decolourised. However, it was found that methanogens were being inhibited after a few days of operation at higher loading as a result of the build-up of sulphide originating from the sulphate concentrations in the dyebath wastewater (Carliell et al., 1996).

Numerous reviews detail studies that have been conducted using different microbes, such as bacteria, fungi and algae (Holkar et al., 2016). The biological treatment of textile wastewater does not always yield consistent, reasonable results because some of the dyes and processing chemicals used in wet processing are either toxic to the microbes or completely unaffected (Oller et al., 2011). Furthermore, oxygen, pH, temperature, dye concentration, the chemical structure of the dye, carbon and nitrogen sources and concentrations, as well as electron donor and redox mediators are a few of the pertinent physical and chemical operating parameters that are critical to the performance of biological treatment methods. The thrust is that the efficacy of the biological treatment applied depends on the micro-organisms' ability to adapt to the wastewater environment and the substances in it, and therefore the enzymes produced (Holkar et al., 2016; Bhatia et al., 2017).

2.3.3 Physical methods

Textile wastewater treatment involves a series of unit processes: physical, chemical, biological and other hybrid combinations. Traditionally, the first stage in treatment involves physical processes (Figure 2.7). Subsequent to that, physicochemical processes, such as chlorination, coagulation-flocculation, electrochemical techniques, chemical oxidation techniques, adsorption and membrane separation, are applied. The complexity of textile wastewater requires these techniques to be used in varying combinations, since each has its own advantages and disadvantages.

2.3.3.1 Adsorption

Adsorption is a commonly employed technique that is used to remove a wide variety of compounds from ground water, drinking water and process water. It is also a tertiary polishing technique that is conventionally used to remove low concentrations of non-biodegradable refractory organic and inorganic compounds, including metal ions. Adsorption is a surface phenomenon where a solution that contains an absorbable solute encounters a solid that displays a highly porous surface structure in which liquid-solid intermolecular forces of attraction cause solute molecules from solution to concentrate and are deposited on the solid surface. The adsorbent is the solid surface onto which the adsorbate (the solute retained on a solid surface) adheres. The surface buildup of the adsorbate onto the adsorbent is called adsorption (Rashed, 2013).

Activated carbon is the most commonly applied adsorbent for the removal of a wide variety of environmental pollutants at very low concentrations. It is a popular adsorbent as decolourisation is affected by the affinity of the dye to the adsorbent. This affinity is influenced by physicochemical parameters such as surface area, particle size, pH, temperature and contact time (Patel and Vashi, 2010). Activated carbon exhibits the desirable properties that are required to remove colour, such as a high specific area, and stability in both acidic and basic media. It is structurally stable at elevated temperatures and is easily and widely available. However, AC is expensive and difficult to regenerate. It is also difficult to separate from depolluted solutions and may be discarded with process sludge, resulting in secondary pollution. This presents a limitation in the use of AC for the decolourisation of textile waste water (GilPavas et al., 2019).

Research has been conducted on low-cost alternatives to AC for the removal of dyes from textile wastewater. The search for alternatives to AC is aimed at developing an adsorbent that displays superior adsorption capacity, has a higher surface area and is mechanically stable in terms of performance. There have been reports on the use of waste materials for the development and synthesis of low-cost adsorbents in the removal of dyes from textile wastewater, such as shredded corn cobs and barley husks (Robinson et al., 2002). Biopolymers such as chitosan have also been applied, grafted and cross-linked to form polymeric matrices for the removal of dyes from aqueous solutions (Crini and Badot, 2008). Nanocomposites have also proven capable of removing dye from aqueous solutions and

real wastewater. Composites can combine various desirable properties of numerous adsorbents such as natural clays like zeolites, bentonite, montmorillonite, fly ash, activated carbon, polymeric isomers, activated clay and biopolymers, to form a high-performance adsorbent in which the uptake of the various pollutants in textile wastewater has been enhanced. Kamaruddin et al. (2013) and Rashed (2013) present comprehensive reviews detailing developments in adsorption technology as it pertains to the removal of dyes and pollutants present in textile wastewater (Rashed, 2013; Patel and Vashi, 2010; GilPavas et al., 2019; Robinson et al., 2002; Crini and Badot, 2008; Kamaruddin et al., 2013). Adsorption technology has proven to be a capable and efficient technology for the removal of dye in wastewater. However, upscaling adsorption technology is a challenge, especially with regard to the regeneration and retention of the adsorbents after the depollution of wastewater.

2.3.3.2 Filtration

Filtration by membrane processes is the transport of substances between two fractions with the help of membranes, which are permeable or non-permeable for specific substances to be removed from the matrix or to be concentrated (Marcucci et al., 2002). Different membrane processes are applied for different separation purposes and are classed by particle size and separation mechanism (see Table 2.1) (Arslan et al., 2016). Membrane filtration techniques like microfiltration (MF), ultrafiltration (UF), nanofiltration (NF) and reverse osmosis have been used in the recovery and reuse of textile wastewater, as well as the removal of dyes (Marcucci et al., 2002).

The membrane separation process relies on the membrane's pore size and selective permeability to separate various compounds from wastewater. Membrane filtration can be applied to textile wastewater as a separation process or in combination with other treatment processes as a tertiary polishing treatment step because membranes clarify, concentrate and, more importantly, are able to separate dyes from effluent (Robinson et al., 2001).

Table 2.1: Membrane processes and their typical operating parameters

Membrane process	Pore width [nm]	Pressure interval ΔP [bar]	Permeability [L/m ² .h.bar]	Membrane type	Application
------------------	-----------------	------------------------------------	--	---------------	-------------

Microfiltration	50-5 000	0.1-2	>50	Porous membrane	Separation of suspended solids
Ultrafiltration	2-200	1-5	10-50	Porous membrane	Concentration, fractioning and treatment of macromolecules in fluid systems
Nanofiltration	1-2	5-20	1.4-12	Non-porous membrane	Fractioning of dissolved materials in fluid systems
Reverse osmosis		10-100	0.05-1.4	Solution-diffusion membrane	Concentration of dissolved materials in fluid systems

(Arslan et al., 2016)

The choice of filter, permeability and therefore the type of membrane process is dictated by the pollution load and temperature of the textile wastewater. Membranes have key performance features, such as the ability to resist microbial attack, and to withstand a harsh chemical environment and elevated temperatures typical of dyebath wastewater. The use of membrane filtration has been shown to be able to separate and concentrate the hydrolysed reactive dyes and auxiliary process chemicals used during the dyeing process for possible recycling. Moreover, this reduces the BOD, COD and colour from the textile wastewater (Chollom et al., 2015). The main advantage of membrane filtration processes is that the chemicals required for wastewater treatment are not used. This technology has promise in textile wastewater remediation. However, it has significant limitations for industrial-scale application as it suffers from clogging and fouling by insoluble dyes (e.g. indigo dye) and starch that need further treatment. It also requires specialised equipment that has a high initial investment cost and the membranes need replacement (Hoek et al., 2013).

2.3.4 Chemical methods

2.3.4.1 Coagulation-flocculation

Chemical coagulation and flocculation have been cited as being essential in the decontamination of industrial wastewater. This process can be applied either before or after the treatment of textile mill wastewater, or as the main treatment method. Inorganic coagulants, which are primarily salts of

multivalent metals (alum, ferric chloride, magnesium chloride, polyaluminium chloride, lime and ferrous sulphate) (Lee et al., 2014) and synthetic (aminomethyl polyacrylamide, polyalkylene, polyamine, polyethylenimine, polydiallyldimethyl ammonium chloride (poly DADMAC)) or naturally derived polymers (Zahrim et al., 2010; Mishra and Bajpai, 2005; Bolto et al., 1996), are added to wastewater, thus destabilising colloidal material and causing the aggregation of small particles into larger flocs that are easier to remove by sedimentation (Stephenson and Duff, 1996). Dye-containing wastewater has been treated by coagulation for many years as a prior or main treatment due to the low capital costs incurred. However, there are drawbacks related to coagulation. These include the fact that adding chemicals only slightly alters the physical state of dissolved and suspended solids, and removal is affected when particles are entrapped in a voluminous coagulate that consists mostly of the coagulant. Chemical addition can also cause a net increase in dissolved content in the wastewater. Finally, sludge generation is a major limitation of this process (Verma et al., 2012). The ability of coagulation and flocculation to remove colour is determined by the dye concentration and solubility of the dye. This is further aggravated by the process chemicals, such as the hydrolysing and fixing agents that are present in the dyebath water, and which interfere with the coagulants (Zahrim et al., 2010). Another problem with the use of chemical coagulants is that the overdosing of alum leads to high residual aluminium concentrations in the wastewater that is discharged. This has been linked to serious health issues, such as Alzheimer's disease and senility (Freitas et al., 2015). As an alternative to sludge production resulting from alum, researchers have reported the use of biopolymers, such as chitosan, as a bioflocculant, citing its biodegradability as a boon because micro-organisms can effectively degrade this sludge (Guibal and Roussy, 2007).

2.3.4.2 Chemical oxidation

Among the chemical methods used for textile wastewater treatment, oxidation is one of the more commonly used methods for the decolourisation of effluents, primarily because of its simple application. Oxidising agents such as H_2O_2 , O_3 and permanganate (MnO_4) achieve chemical decolourisation by oxidation. This removes the dye from effluents when oxidation cleaves the aromatic rings (chromophoric moieties) of the dye molecule. Ozone and H_2O_2 are widely used as they are highly reactive with dyes and have shown good removal efficiencies (Alaton et al., 2002). The main problem with chemical oxidants has been low colour removal rates for non-soluble disperse dyes and vat dyes because they

react slowly. In addition, decolourisation by chemical oxidants is subject to pH. While pH decreases, the ozonation of hydrolysed dye decreases (Marmagne and Coste, 1996). Chemical oxidation methods, such as H_2O_2 and O_3 , often need to be activated by external means such as UV irradiation. Moreover, ozonation has the added disadvantage of cost. Constant and continued ozonation is necessary as O_3 has a very short half-life (about 10 to 20 minutes in an aqueous medium with a pH of 7). This half-life can be further reduced by chemicals that are present in the dyebath water, as well as by being destabilised by salts, pH and temperature (Gosavi and Sharma, 2014).

Fenton's reagent is another method of textile wastewater decontamination, which uses a solution of H_2O_2 with ferrous iron (H_2O_2 -Fe (III) salts). It is used especially for wastewaters that are resistant to biological treatment or are toxic to live biomass. This method applies chemical separation, in which sorption or bonding removes dissolved dyes from the wastewater. It is thus effective in decolourising both soluble and insoluble dyes. However, cationic dyes do not coagulate at all, while acid, direct, vat, mordant and reactive dyes coagulate. However, the floc is of a poor quality and does not settle. This technology is problematic in that the sludge generated during the flocculation of Fenton's reagent and recovered dye contains concentrated impurities and requires disposal (Robinson et al., 2001).

2.4 DECOLOURISATION OF DYE AND TEXTILE EFFLUENT USING ADVANCED OXIDATION PROCESSES

2.4.1 Overview

Advanced oxidation processes refer to processes in which hydroxyl ($\bullet\text{OH}$) radicals are produced as the primary oxidant. Hydroxyl radicals are extremely unstable and therefore highly reactive and very powerful oxidants (oxidation potential NHE 2.33 V) and exhibit rapid rates of oxidation relative to their conventional counterparts, such as H_2O_2 or potassium permanganate (KMnO_4) (Holkar et al., 2016). Advanced oxidation processes are similar by virtue of the way the hydroxyl radicals participate in most mechanisms that occur during the reactions in each process. The hydroxyl radicals are generated by means of chemical oxidising agents such as H_2O_2 , O_3 , and Fenton's reagent with H_2O_2 in combination with UV irradiation, ultrasound, and homogeneous and heterogeneous photocatalysts.

Advanced oxidation processes can react with complex organic and inorganic compounds. They can be applied to contaminated groundwater, surface water and wastewater that contains refractory, toxic compounds that are resistant to biodegradation.

Hydroxyl radicals attack organic molecules either by the abstraction or the addition of a hydrogen atom from or to the double bonds present in organic compounds. These radicals can break down complex synthetic organic dyes into smaller oxidised intermediates and ultimately CO₂ and water (H₂O) upon complete mineralisation. Furthermore, the hydroxyl radicals that are generated are non-selective in nature and can act without other chemical additives. The reader is referred to numerous reviews that detail studies conducted on AOPs for wastewater treatment (Mohajerani et al., 2009; Kalra et al., 2011; Asghar et al., 2015).

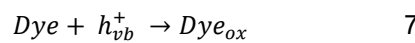
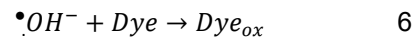
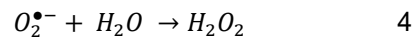
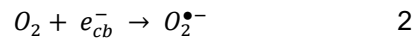
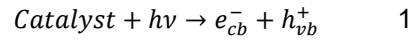
2.4.2 Semiconductor-mediated photocatalysts

Fujishima and Honda (1972) discovered the photolysis of water on TiO₂ electrodes in 1972. This discovery signaled the advent of an era in heterogeneous catalysis, with the story of TiO₂ photocatalysis beginning in the late 1960s. Some of the burgeoning research interests are photoelectrochemical solar energy conversion and environmental photocatalysis, self-cleaning surfaces and, later, photoinduced hydrophilicity. Research into photoelectrochemical solar cells started with the investigation of TiO₂, where the possibility of solar photo-electrolysis was demonstrated; and thus the decomposition of water using UV-visible light into oxygen and hydrogen (Fujishima et al., 2000). Since then, extensive research has been conducted to understand the fundamental processes and to optimise the photocatalytic activity of TiO₂. Studies carried out to that end were mostly related to renewable energy sources and energy storage (Bard, 1982; Gratzel, 2012).

Briefly, in a heterogeneous photocatalytic system, photo-induced molecular transformations and reactions take place at the surface of a catalyst. Depending on where the initial excitation occurs, the process could be a catalysed or a sensitised photoreaction. In the former, the initial photoexcitation occurs in the adsorbed molecule, which subsequently interacts with the catalyst substrate. In the latter, the initial photoexcitation takes place in the catalyst substrate, and the electronically excited catalyst transfers electrons (or energy) to the adsorbed molecule, thereby inducing a reaction (Linsebigler et al., 1995). Titania-mediated photocatalytic oxidation mechanisms have been detailed previously in

literature (Akpan and Hameed, 2009; Zangeneh et al., 2015; Linsebigler et al., 1995; Rauf and Ashraf, 2009) and will only be summarised here.

Briefly, the process is initiated by the generation of electron-hole pairs in the semiconductor when electrons are excited from the VB to the CB by the absorption of photons with energy equal to or greater than the band gap (E_{bg}) of the semiconductor. Upon excitation, there are several de-excitation pathways the electron-hole pair may follow. The photo-generated electrons (e^-_{cb}) could react with electron acceptors such as oxygen (O_2) absorbed onto the catalyst surface or dissolved in water, reducing them to superoxide radical ions ($O_2^{\bullet-}$). The photo-generated holes (h^+_{vb}) can react with surface-bound H_2O , oxidising it to $\bullet OH^-$ radicals and H^+ ions. These, in combination with other highly oxidising species such as peroxide radicals, are reported to be responsible for the TiO_2 -based photocatalytic decomposition of organic substances such as dyes and other organic contaminants. The generalised possible reactions that occur at the semiconductor surface are outlined below:



Various other metal chalcogenide semiconductors, such as zinc oxide (ZnO), zirconium dioxide (ZrO₂), ceric oxide (CeO₂), ferric oxide (Fe₂O₃), tungsten trioxide (WO₃), vanadium oxide (V₂O₅), cadmium sulphide (CdS), gallium phosphide (GaP) and zinc sulphide (ZnS), have been used as photocatalysts that have demonstrated high efficiency in the degradation of a range of organic pollutants to reduce toxic substances and, in some instances, to complete mineralisation. As an example, transition metal sulphides, such as CdS, ZnS, antimony sulphide (Sb₂S₃), bismuth sulphide (Bi₂S₃) and molybdenum disulphide (MoS₂), are some of the more frequently studied semiconducting materials with narrow band gaps (~1.3-2.40 eV) that are appropriate for visible light photocatalysis. However, they are generally unstable and readily deactivated as a result of photocorrosion or self-oxidation by holes (positive charge) generated in the materials themselves (Yamashita and Li, 2016). Cadmium sulphide, a representative chalcogenide photocatalyst used for hydrogen (H₂) evolution under visible light irradiation, is one such example. It has severe limitations, such as its toxicity in aqueous media as a result of its tendency to undergo photoanodic corrosion, thereby releasing dangerous metal ions (such as cadmium ions (Cd²⁺)) into solution (Hernández-Ramírez and Medina-Ramírez, 2014). Despite this, it has shown potential in the degradation of dyes and organic pollutants in aqueous media.

Transition metal oxides of the *d*-transition metals, such as TiO₂, ZnO and Fe₂O₃, are the most extensively researched metal oxides that demonstrate photocatalytic ability. However, some drawbacks exist. Zinc oxide is the second to be employed to TiO₂ because of its good optoelectronic, catalytic and photochemical properties, but ZnO is susceptible to photo-corrosion and facile dissolution at lower pH values limits its application in photocatalysis. Hematite (α -Fe₂O₃) also has a narrow band gap (~2.2 eV) and is active within the visible region of the solar spectrum. Its photocatalytic performance is a result of the generation of electron-hole pairs through the narrow band gap illumination, and it has received attention in photocatalytic applications because of its aqueous stability at pH values greater than ~3 (Zhu et al., 2012). However, despite its wide application as a photocatalyst, the process's low quantum yield hinders its process kinetics and therefore its efficiency (Bandara et al., 2007). The activity decline of iron oxide presents a problem because of the rapid (within nanoseconds) electron-hole charge recombination on the oxide surface, requiring the deposition of noble metal supports (Bai et al., 2012). The work of Kraeutler and Bard (1978) was the earliest description of the heterogeneous photocatalytic decomposition of acetic acid on *n*-type TiO₂ to yield methane and CO₂, and since then, applications to

environmental cleanup using titania became one of the most active research areas in heterogenous photocatalysis (Pelaez et al., 2012; Paz, 2010; Spasiano et al., 2015).

2.4.3 Improving the photocatalytic activity of TiO₂ using carbonaceous nanomaterials

The use of carbonaceous nanomaterials is one of the many ways of improving the photocatalytic activity of TiO₂ nanoparticles. Increasingly, research has been aimed at exploiting the intrinsic properties of nanocarbon materials and TiO₂ in order to enhance the photocatalytic performance via synergy between the materials as shown in Figure 2.8. Since the mid-1990s, it has been understood that carbon acts as one of the more exceptional catalyst supports as it is thought to offer unmatched flexibility in the tailoring of catalyst properties for niche applications. Carbon has more recently received attention as a catalyst. However, its primary use as far as heterogenous catalysis is concerned remains as a catalyst support. Titanium dioxide-carbon nanotube (CNT) composite studies have proven that the combination of MWCNTs with titania can improve the decolourisation of azo-dyes under UV-light irradiation. The explanation proffered was that the MWCNTs served as a catalyst support and increased the available reactive surface area of TiO₂. The report suggests that the intimate interphase contact between the MWCNT and TiO₂ had a synergy that resulted in improved photochemistry (Wang et al., 2005). Another group varied TiO₂ MWCNT arrangements to find the optimal arrangement that yielded a higher reactive surface area by dispersing the TiO₂ on the MWCNT surface, thereby hindering charge recombination and ultimately enhancing photocatalytic oxidation. The study's outcomes showed that a hydration/dehydration synthesis process creates a situation where the MWCNTs were attached to the surface of TiO₂. The relative position of the edge of the MWCNT band allowed the transfer of electrons from the titania surface, permitting charge separation, stabilisation and impeding electron-hole recombination. The MWCNTs allowed the electrons to be shuttled freely within their conducting network (Yao et al., 2008).

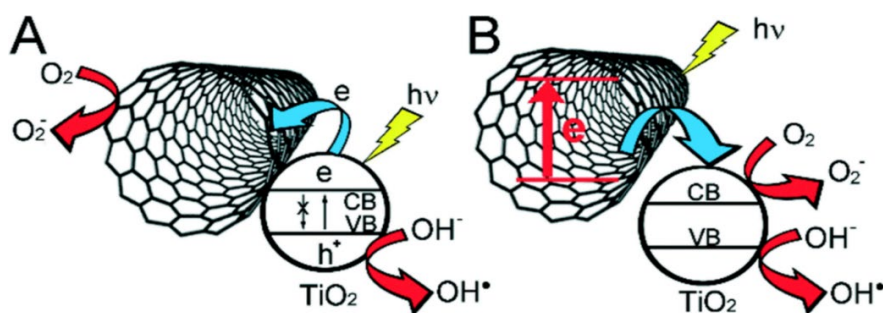


Figure 2.8: Proposed mechanism of action of MWCNTs as electron sink (A) and photosensitiser (B)

To curb costs, the synthesis of MWCNT TiO₂ nanocomposites using facile and green methods is key to large-scale water treatment applications (Xu et al., 2010). Yu et al. (2005) describe the synthesis by the simple mechanical mixing of TiO₂ (P25) with MWCNTs to improve the photocatalytic activity of TiO₂ for the decolourisation of azo-dyes. The premise of the study was that one proposed mechanism for the photooxidation of organic compounds is initiated when the organic compound is adsorbed onto the photocatalyst surface and subsequently reacts with the excited electron-hole pairs and/or hydroxyl radicals to form the decolourised oxidation products.

The photocatalytic activities of TiO₂ and MWCNTs have been reported to decolourise a variety of dyes and organic compounds, such as methylene blue, methyl orange, phenols and volatile organic compounds (Saleh, 2013).

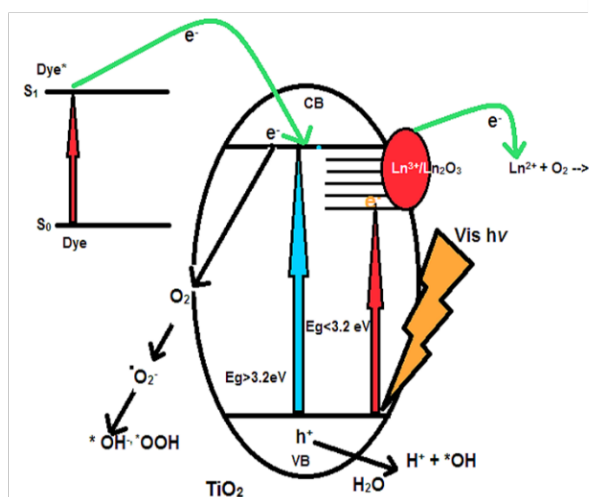
Adsorption of the organic molecules and other species onto the photocatalyst is considered an important parameter in the determination of degradation rates. This is achieved through the insertion of MWCNTs that provide a large surface area and high-quality reactive sites. The MWCNTs behave as an effective electron transfer unit because of their high electrical conductivity and large electron storage capacity. Their ability to capture photo-excited electrons prompts the transfer of electrons from the CB of the metal oxide semiconductor towards the MWCNTs surface due to their lower Fermi level. The Schottky barrier that is formed at the interface between the MWCNTs and the metal oxide semiconductor means that the photogenerated electrons may move unhindered towards the surface of the MWCNT, thereby leaving the holes to move towards the VB. Studies that have been conducted provide compelling evidence that mixing MWCNTs with titania would provide a superior route for the improvement of the photocatalytic activity of TiO₂ for the degradation of organic contaminants and other environmental cleanup applications.

2.4.4 The use of rare earth metals to improve the photocatalytic activity of TiO₂

Rare earth metals (REMs) refer to elements that comprise the lanthanide series and include the chemically similar metals scandium (Sc) and yttrium (Y). The electronic configurations of lanthanoids in the ground state are $[\text{Xe}]4f^n 6s^2$ and $[\text{Xe}]4f^{n-1} 5d^1 6s^2$. Lanthanum, cerium and gadolinium belong to the $[\text{Xe}]4f^n 6s^2$ configuration, while praseodymium, neodymium, promethium, samarium, europium, terbium, dysprosium, holmium, erbium, thulium, ytterbium and lutetium belong to the $[\text{Xe}]4f^{n-1} 5d^1 6s^2$ configuration. The inclusion of scandium and yttrium in this subgroup, despite the fact that they do not have 4f electrons, stems from the fact that they have similar chemical properties to lanthanide elements because their outermost electrons have the $(n-1)d^1 ns^2$ configuration (Huang, 2011). The lanthanide ions display fascinating optical properties, and it is this ability to interact with light that has seen them applied as catalysts, in ceramics, permanent magnets and optoelectronics, where phosphors that contain europium, cerium and terbium have been found in many common fluorescent lighting and colour displays (Van Eldik and Stochel, 2011).

The unique spectroscopic properties are a result of the shielding of the 4f orbitals by the filled $5p^6 6s^2$ subshells. Furthermore, this shielding by the $5p^6 6s^2$ causes the REM ions to be less affected by the micro surroundings. It is these 4f energy levels that impart excellent photostability, a large anti-Stokes shift, a long luminescence lifetime and sharp-band emission to the REM ions (Sun et al., 2015). With regard to titania-based heterogeneous photocatalytic applications, the goal is not only to increase photocatalytic efficiency, but to extend the spectral response of titania so that it can be visible and near-infrared (NIR) light-active. One avenue is the insertion or doping of the TiO₂ lattice using rare earth elements. The doping should produce a narrowing of the band gap of titania, or introduce mid-states in the titania band gap, resulting in a broadened absorption towards the visible and NIR region of the solar spectrum as illustrated in Figure 2.9 (Tobaldi et al., 2013). (Stengl et al., 2009) reported a one-step synthesis for the preparation of rare earth(s)-doped titania. They used various REMs (lanthanum (La), cerium (Ce), praseodymium (Pr), neodymium (Nd), samarium (Sm), europium (Eu), dysprosium (Dy), gadolinium (Gd)) as dopants in the titania. It was found that, for the photocatalytic decomposition of Orange II dye in an aqueous slurry irradiated by UV and visible light, the Neodymium cation (Nd³⁺) doped titania had the best results.

Sub-bandgap states below TiO₂ CB



Spectral upconversion of Vis/NIR photons

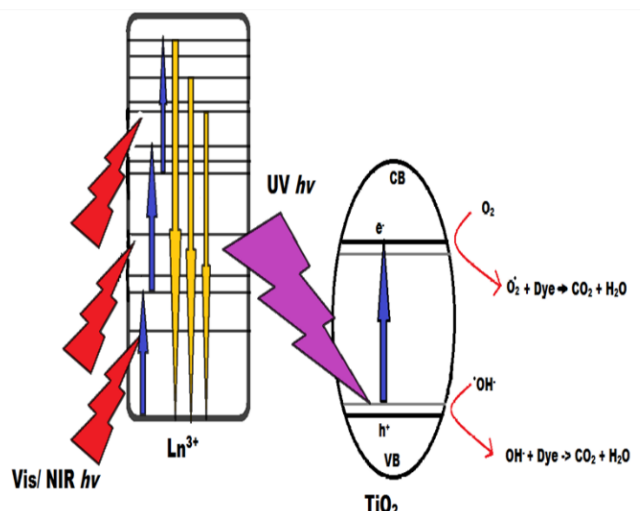


Figure 2.9: Mechanism of action of rare earth metal ions when coupled with TiO₂, acting by introducing sub-band gap states beneath the TiO₂ CB (left) or upconverting lower energy light (NIR and visible photons) into higher energy photons available for use by TiO₂ (right).

The increased photocatalytic activity was attributed to the transitions of the 4f electrons in the REMs that led to the enhancement of the optical absorption of the catalyst, as well as supporting the photo-generated electron-hole pair separation. Enhancement of the visible light photoactivity of TiO₂ was due to the redshift of the optical adsorption band edge of titania by doping of the rare earth ions. Other researchers also report the use of lanthanide ions as dopants in titania for use as photocatalysts in the degradation of Direct Blue and Phenol (Reszczyńska et al., 2015; El-Bahy et al., 2009). El-Bahy et al. (2009) found that catalyst photoactivity depends on band gap, particle size, surface area and pore volume. Their research showed that (Gadolinium) Gadolinium cation (Gd³⁺)/TiO₂ had the lowest band gap and particle size, highest surface area and largest pore volume, and was thus the most effective photocatalyst in the degradation of Direct Blue 53. Reszczyńska et al. (2015) report on the visible light activity of erbium (Er³⁺), ytterbium (Yb³⁺) and Er³⁺/Yb³⁺-doped titania in the decomposition of phenol.

The TiO₂ doped with Er³⁺ or Er³⁺/Yb³⁺ showed up low-intensity conversion emission, with Yb³⁺-doped TiO₂ showing the highest photocatalytic activity under visible light irradiation. Reszczyńska et al. (2015) proposed that the primary mechanism for the visible light sensitisation was due to the availability of higher adsorption sites, BET surface area, a decrease in crystallite size and prevention of electron-hole

recombination. It was found that, overall, the improved photocatalytic activity could be attributed to the synergetic effects of large surface areas, small crystallite size, lattice distortion and a greater charge imbalance of holmium-doped TiO₂.

The results of investigations conducted on the effects of rare earth ion-doping into photocatalytic semiconductors clearly present a promising approach to preparing a visible light-driven catalyst for the decomposition of dyes and organic pollutants in wastewater. The use of REMs shows great promise in the enhancement of the optical response of photocatalysts to a broader solar spectrum. Understanding the enhancement mechanism would make the remediation of organic dyes in wastewater via titania-mediated heterogeneous photocatalysis a commercially viable application as it would circumvent the need for powering UV-light sources.

2.4.5 Biopolymers as photocatalyst supports

2.4.5.1 Definition of terms

Humans have used natural polymers and their derivatives for millennia for survival. These include wood, cotton, silk, animal skin and natural rubber (Cheremisinoff, 1997). Humans had a long-standing relationship with naturally derived polymers until the advent of the synthetic polymers that dominated the 20th century, along with the petrochemical industries. The rapid development of synthetic polymers and the migration from natural polymers has been ascribed to the scarcity of natural polymers during the World War I and II (Maya and Sabu, 2012). In addition to this, the high cost of extracting natural monomers from plants, animals and micro-organisms relative to their petroleum-based counterparts has also been cited as motivation for the great development and popularity of synthetic polymers (Teramoto, 2011).

An imminent problem faced by mankind is the depletion of fossil fuel resources and resilient polymer wastes that persist in the environment. Therefore, it stands to reason that the development and use of polymers produced from resources that can be replenished at rates comparable to their consumption, as well as those that would biodegrade to harmless and environmentally benign products is inevitable. Literature surveys show that there are no strict definitions of the terms used to describe biopolymers. These terms include “bio-based”, “biodegradable”, “biopolymer” and “bioplastic polymer”. Instead, it

appears that these terms have several and intersecting meanings. The synonymous and interchangeable use of the terms “bio-based plastic”, “biopolymer” and “biodegradable plastic” is erroneous.

The International Union of Pure and Applied Chemistry (IUPAC) has proposed terminology that can be used across scientific disciplines (Vert et al., 2012). “Biomass” refers to living systems and a collection of organic substances produced by living systems that are exploitable as *materials*, including recent post-mortem residues. “Bio-based” refers to materials composed or derived in whole or in part of biological products issued from the biomass (including plant, animal, and marine or forestry materials).

“Biodegradable” qualifies *macromolecules* or polymeric substances as being susceptible to *degradation* by *biological activity* by lowering the molar masses of *macromolecules* that form the substances. “Biomacromolecule” refers to macromolecules (e.g. proteins, nucleic acids and polysaccharides) that are formed by living organisms. “Biopolymer” refers to macromolecules (including proteins, nucleic acids and polysaccharides) that are formed by living organisms. The need for the definition of terms becomes apparent when different scholars attempt to delineate biopolymers and bioplastics in accordance with the source of the feedstock material and/or biodegradability.

Currently, there are no standards for what can be called a “biopolymer”. However, there are intuitive ways one could qualify the “bio” element of biopolymers: “naturally occurring” or “derived from biomass” and “biodegradable” seem to be useful delimitations under the context of environmental decontamination and sustainability. Thus, biopolymers that are produced from fossil fuels and are biodegradable, as well as “green polymers”, have been described. It is important, however, to note that bio-based polymers are not always or necessarily environmentally friendly, biocompatible or biodegradable, but there are fossil fuel-based polymers that are biodegradable.

2.4.5.2 Immobilisation of photocatalysts on supports

The necessity of the immobilisation of titania-mediated heterogeneous photocatalysis demonstrates high potential as an alternative method for the decontamination of wastewaters. However, there are significant challenges as far as its realisation as an industrial technology is concerned.

It is fundamentally inadequate for harnessing energy or for the treatment of large volumes of water because its light energy density is primarily low and TiO₂ can only utilise the minute amounts of UV light contained in solar radiation (Kazuhito et al., 2005). Another obstacle that has to be overcome is the retention, recycling and recovery of the photocatalyst powders because commercial grade TiO₂ has agglomerate particles in the micron size (>0.5 μ) range and nanomaterial elementary particles in the nanometre (10-100 nm) range (CEFIC, 2012). Research endeavours focus mainly on improving both the photocatalytic activity and visible-light activation of TiO₂ in order to circumvent the expenses incurred from powering UV light sources used for the treatment of massive volumes of wastewater. These strategies involve the use of both physical and chemical methods. Examples of physical techniques include microwave or ultrasound irradiation. Chemical methods refer to the use of metal and non-metal dopants; and coupling TiO₂ with different semiconductors (Xu et al., 2010).

Traditionally, photocatalyst particles were applied as a powder and were found to demonstrate a large surface area and efficiency (Singh et al., 2013). However, in order to achieve full-scale industrialisation of this technology, certain shortcomings that are inherent to powdered photocatalysts must be overcome. Firstly, immobilisation of the photocatalyst is critical, simply because “decontaminated” water cannot be allowed to contain particles of catalyst. Secondly, the very essence of photocatalysis is light. Therefore, critical to the efficacy of a heterogeneous photosystem is the optimal use of radiation. The most important factors that affect process performance is the photoactivity of the catalyst. Therefore, from a practical viewpoint, immobilised photoreactor systems are preferred as post-depollution catalyst recovery and retention have been circumvented. However, it can be countered that slurry photoreactor systems could be more efficient due to greater reactant accessibility by the suspended catalyst.

2.4.5.3 Features of an immobilising support

The choice and development of a catalyst support is generally informed by its role. Since the photocatalyst requires maximum access to light and target contaminants, a good support must demonstrate the following features (Singh et al., 2013; Shan et al., 2010):

- There must be strong adherence of the photocatalyst to the support in order to provide anchorage.
- The catalytic activity must remain unaffected by the method of fixation.

- It must provide a large specific surface area.
- It must have a strong capacity for the adsorption of pollutants in order to improve their removal.
- The contact mass must be stable for extended periods of time.
- The immobilising support must be resistant to oxidative degradation when it is subjected to radiation and radicals.
- The photocatalyst must not leach from the support under various reaction conditions.
- Light transparency and low light-scattering by the support are a boon, but not always possible.

2.4.5.4 *Approaches used for the immobilisation of the photocatalyst*

The anchorage of the photocatalyst onto a support can be achieved via physical surface forces or chemical bonds, where the physical usually involves at least one thermal step and includes all procedures that utilise previously manufactured titania; and chemical refers to the “in-situ” generation of catalysts deposited straight onto a suitable support, often from a precursor (Fabiyyi and Skelton, 2000). Most important is that, regardless of the deposition means used, the photocatalytic activity (PCA) of the catalyst must remain unhindered or at least retain the catalytic activity of the powder form as much as possible. In addition to this, the support-catalyst junction must be resilient to strain caused by particle-particle and particle-fluid mechanical interactions inside the reactor environment in order to avoid the shedding of the catalyst particles from the support (Robert et al., 2013). A wide variety of substrates have been tested as supports for the immobilisation of titania.

Some of these that have been reported in literature include, but are not limited to glass, SiO₂ beads, activated carbon, aluminium, Teflon, fibreglass and polymeric materials (Tryba, 2008), fly ash, vycor glass, hollow glass spheres, polyethylene sheets, reactor walls, fibre glass, silica gel, fabric or wool, micro-porous cellulose membranes, quartz, optical fibres, alumina clays, ceramic membranes and monoliths, stainless steel, zeolites and anodised iron (Fabiyyi and Skelton, 2000).

The techniques that have been used for the deposition of titania onto solid supports can be roughly categorised as those using either TiO₂ powders or titania precursors, and those either employing binders or not. Any of these approaches could be used alone or in combination, but the choice depends on the nature of the support employed. A credible solution to challenges, such as catalyst decantability after depollution and recovery, mass transfer limitations inherent to heterogeneous catalysis systems,

the substrates' ability to concentrate the intended pollutants onto the contact surface, a stable contact mass over extended periods of time, a high specific surface area and strong adhesion between catalyst and support, may present itself via the use of a suitable stabilising matrix that can be found in biopolymers.

2.4.5.5 Cellulose acetate and polycaprolactone as immobilisation support

Cellulose and its derivatives have also received attention in a wide variety of applications outside the traditional paper and textiles industry, such as water filtration membranes, biomedical applications and, in later years, as magneto-responsive composites, bio-imaging materials and supports for catalysts (Wittmar et al., 2015). Several groups have tested the ability of cellulosic polymers to act as immobilisation supports and co-adsorbents for various semiconductor-mediated heterogeneous photocatalyst adsorbents (Zhou et al., 2016; Gadiyar et al., 2013; Prado et al., 2005). During the design of immobilising supports, attention must be given to attaching the photocatalyst particles on a support without compromising its reactivity. However, an immobilising powdered photocatalyst reduces the photocatalyst activity due to the decrease in reactive sites. Traditional supports are vulnerable to photo-oxidative degradation. Thus, the current challenge is a convenient synthesis of a photocatalyst that retains the same level of activity as its powder counterpart on a stable support.

Jin et al. (2014) fabricated a flexible hybrid film using CA and TiO₂. The composite film was designed for use first as a recyclable photocatalyst and ultimately to be optimised for use as a self-cleaning material or in other applications. Mesoporous anatase TiO₂ microspheres were synthesised using a facile solvothermal technique. The prepared TiO₂ powder was subsequently coated onto the CA gelatum to form the hybrid TiO₂ CA (TCA) film. The photocatalytic activity was evaluated using Methylene Blue as a model dye. It is reported that the TCA film, with a 0.01 g TiO₂ catalyst load, degraded almost all the Methylene Blue after three hours, which demonstrated excellent performance when compared to a similar study where 0.1 g of ZnO was used while keeping all the experimental conditions the same (Xu et al., 2011).

The aforementioned studies demonstrate the importance of an immobilising support in as far as concentrating the pollutants onto the substrate for greater accessibility to the photocatalyst. The

photocatalysis process consists of two parts: adsorption and degradation, where the dye is initially adsorbed onto the surface of the photocatalyst and the photogenerated oxidising radicals react with the organic compound to mineralise it to CO₂ and H₂O. In addition to this, the TCA film exhibits good recyclability, where the CA film was stable in water and more so after being transferred to a new dye system for three cycles. The degradation rates of the Methylene Blue barely showed a decrease and thus the TCA film remains photocatalytically active and the photocatalyst has been retained on the CA support. The study further reports that the CA film shows some photodegradation effect on the model dye and long-term stability in water during exposure to UV irradiation.

The work carried out by Jin et al. (2014) was thorough and yielded a proof of concept in the endeavours for sustainable, economically viable, green techniques for the fabrication of an efficient photocatalytic system, where the obstacle of photocatalyst retention, recycling and recovery has been circumvented. Another group's work that deserves attention is that carried out by Sökmen et al. (2011). Titanium dioxide was directly immobilised onto and into a biodegradable polymer. This work has attracted the researchers' attention from a material processing point of view in that the method is simple and easily scalable, and because biodegradable polymers present a good alternative to synthetic non-biodegradable polymeric matrices for environmental reasons previously stated at length. Polycaprolactone is a readily available, reasonably cheap aliphatic polyester. Despite the fact that it is a petroleum-based polymer, it is biodegradable and biocompatible, which has made it suitable for biomedical applications, such as drug delivery and tissue engineering (Elizubair et al., 2010).

The authors recognised the characteristics of PCL, such as its resistance to water, oil, solvent and chlorine, its relatively easy processability, its good mechanical properties and the fact that it takes up to two years to completely break down, making it suitable for longer-term applications. However, shortcomings such as low melting temperature present a problem in as far as the fabrication of photocatalytically active films is concerned. Physical and chemical methods used to fix photoactive titania powders, such as sputtering, electrophoretic deposition, spray pyrolysis, chemical vapour deposition (CVD) and thermal oxidation are inappropriate for use on polymeric substrates as these methods require high temperature treatments to obtain the desired photoactive titania layer with strong adhesion to the substrate (Yaghoubi et al., 2010).

Sökmen et al. (2011) found that wet-coating fixation methods such as spray or the dip-coating of nanocrystalline sols present a viable avenue for the immobilisation of TiO₂ onto a polymeric substrate. They were able to immobilise anatase TiO₂ nanoparticles into and onto PCL using solvent-casting to fabricate a biodegradable and photocatalytically active material that was able to remove a typical model dye (Methylene Blue). It also possessed antimicrobial properties as demonstrated by its ability to kill *Candida albicans*, also a model fungus of medical importance. The fabricated materials were successful in the removal of Methylene Blue. Where the TiO₂ immobilised into the PCL, PCL-1 showed an 83.2% effective removal of Methylene Blue, and where the TiO₂ immobilised onto the PCL, PCL-2 had a 94.2% effective removal of Methylene Blue. This result is credible, since it has already been established that the direct mixing of the catalyst with the polymer solution significantly reduces the available reactive surface sites, therefore the photocatalytic activity (Wittmar et al., 2015). The PCL-2 also had a killing efficiency of 54% for *C. albicans* under near-visible light irradiation after only 60 minutes of exposure.

The authors considered the elements that were important to a good support: the capacity of the support to adsorb organic contaminants and the support's chemical inertness and resistance to photo-oxidative degradation. The PCL exhibited minimal degradative changes after long-term UV and visible light exposure, corresponding to a slight shift in the melting point as revealed by the thermo-gravimetric analyses. Attenuated total reflection-Fourier transform infrared (ATR-FTIR) spectra of the polymer after the treatment of the Methylene Blue solutions revealed that the PCL and TiO₂ complemented each other in their functions, where the Methylene Blue was adsorbed by the PCL and significantly decomposed by the TiO₂.

A problem with the use of PCL is its low melting point. As seen by morphological changes after UV exposure, which causes some localised heating that, in turn, deforms or melts the composite film surface. The SEM analyses of the PCL-2 revealed that the addition of TiO₂ to the PCL creates an uneven surface with TiO₂ nanoparticle aggregates, visible cracks and pinholes on the hybrid film, combined with the low compatibility of TiO₂ with PCL. These results highlight the other problem with the use of organo-inorganic metal oxide composite materials. The degree of homogeneity significantly influences and possibly commands the ultimate properties of the composites.

Therefore, in terms of material development and processing, issues such as scale of mixing and dispersion of the nanoparticles into polymeric matrices could be resolved through the use of alternative techniques such as autoclaving or ultrasonication of the polymer-titania mixture prior to casting.

2.5 SUMMARY

The environmental and health problems resulting from textile wastewater have been highlighted in the review. The South African textiles dyeing and finishing industries consume significant volumes of water with nearly equal amounts of effluent produced. Furthermore, they do not pre-treat effluent due to insufficient resources and infrastructure and do not recycle effluent because they require good-quality water for production processes. Textile wastewater is complex and non-biodegradable and it is a challenge for WWTW operators to produce non-toxic remediated effluents. Therefore, a multi-barrier approach to the control and removal of pollutants is required. Biological treatment methods are economically feasible, environmentally friendly, and the sludge generated, despite requiring disposal, can be used as a soil enhancer. However, their efficacy depends on the microbe's ability to adapt to the textile wastewater environment, while poisoning the micro-organisms is a possibility. Adsorption technology can remove dye from textile wastewater. However, upscaling adsorption technology is challenging because adsorbents are difficult to regenerate and retain after the wastewater has been depolluted. Membrane filtration techniques have been used in the removal of dye from wastewater. The main advantage of membrane filtration processes is that the chemicals required for wastewater treatment are not used. However, upscaling proves to be difficult because of fouling with the membranes needing replacement and the need for specialised equipment that has a high investment cost. Chemical coagulation and flocculation can be applied either before or after treatment, or as the main treatment method for textile mill wastewater. However, sludge generation and disposal are major limitations of this process. The use of oxidising agents, such as H_2O_2 , O_3 and MnO_4 can achieve chemical decolourisation by oxidation. The main problem with chemical oxidants has been the low colour removal rates for non-soluble disperse dyes and vat dyes because they react relatively slowly.

Advanced oxidation processes refer to processes in which hydroxyl ($\bullet\text{OH}$ -) radicals are produced as the primary oxidant and exhibit rapid rates of oxidation relative to their conventional counterparts, such as H_2O_2 or KMnO_4 . Titania-mediated heterogeneous photocatalysis is an AOP in which photo-induced

molecular transformations and reactions take place at the surface of TiO₂. Depending on where the initial excitation occurs, the process could be a catalysed or a sensitised photoreaction.

In titania-mediated photocatalytic oxidation, ultra-violet light ($\lambda < 400$ nm) is used as an energy source. Photons that possess energies greater than the band gap (E_g) of TiO₂ excite the VB electrons to the CB. This electron migration creates positively charged holes (h^+) in the VB and excited electrons (e^-) in the CB. The positive holes oxidise H₂O and the organic pollutants to form numerous highly reactive radical species such as hydroxyl ($\bullet OH$), superoxide ($\bullet O_2^-$) and hydroperoxyl ($\bullet HO_2$). The result of this chain reaction is the decomposition of organic pollutants into lower molecular weight molecules, and when complete mineralisation has been attained, CO₂ and H₂O are produced. Titanium dioxide can only be excited by UV light, which makes it expensive to use in large industrial-scale applications because powering UV-light sources increases the capital cost, and its electron-hole pair cause rapid recombination rates, which reduce the quantum yield of TiO₂ and lead to decreased photocatalytic activity and incomplete mineralisation of refractory organic compounds. Thus, other metal oxide semiconductors with narrower band gap values than TiO₂ have been studied for the degradation of organic pollutants. However, their instability and propensity to photo-corrosion and self-oxidation deactivate the semiconductors and make them ineffective.

The non-selectivity of TiO₂ in oxidation reactions makes it a superior semiconductor. However, in order for its large-scale application to be feasible, spectral response must be extended so that it can be visible and NIR-light active, while increasing its photocatalytic efficiency by accelerating charge carrier generation. The use of nanocarbon materials such as MWCNTs can improve the photocatalytic activity of TiO₂ by acting as supports and dispersing agents to reduce TiO₂ nanoparticles' agglomeration, thus increasing the surface area and available surface-active sites. The MWCNTs also act to enhance pollutant adsorption onto the photocatalyst surface.

Rare earth elements display unique spectroscopic properties because of the partially filled $4f$ orbitals and empty $5d$ orbitals. Lanthanides can make TiO₂ visible-light active through doping by forming sub-bandgap states beneath the CB of TiO₂. Valence band electrons in TiO₂ can be excited by visible light into the new lowest unoccupied molecular orbitals beneath the TiO₂ CB, thereby narrowing the

bandgap. Rare earth ions doped into TiO₂ and combined with MWCNTs present a promising approach to preparing a visible-light-driven catalyst for the decomposition of dyes and organic pollutants in wastewater.

Photocatalyst particles have been applied in powder form because they have a large surface area and efficiency. However, immobilisation of the photocatalyst is necessary because depolluted water cannot be allowed to contain particles of photocatalyst. Naturally derived biopolymers such as CA can be used as immobilisation supports because they can provide a large specific surface area, have a good capacity for the adsorption of dyes and may improve their removal. The use of rare earth metals shows great promise in the enhancement of the optical response of photocatalysts to a broader solar spectrum. Understanding the enhancement mechanism would make the remediation of organic dyes in wastewater via titania-mediated heterogeneous photocatalysis a commercially viable application as it would circumvent the need for powering UV-light sources.

This study has synthesised nanocomposites that offer advantages over the conventional wastewater treatment methods detailed above as follows:

- It harnesses freely and abundantly available solar radiation to photolyse the dyestuff, thus destroying the dyes, as opposed to transferring them to another phase, which requires secondary depollution as is the case with coagulants, flocculants and adsorbents.
- The nanocomposite can be applied under ambient conditions (room temperature and atmospheric pressure).
- The synergy created between the titania, the carbonaceous nanomaterial and the Er₂O₃ will overcome the slow rates of degradation experienced with pure titania and increase photo-efficiency.
- Embedment in a natural polymeric matrix was anticipated to improve catalyst retention.

CHAPTER 4: EXPERIMENTAL WORK

4.1 REAGENTS

All chemical reagents that were used were obtained from commercial sources, primarily Sigma Aldrich, South Africa (unless otherwise specified) and used without further purification. The following reagents and materials were used:

Iron (III) nitrate nonahydrate ($\text{Fe}(\text{NO}_3)_3 \cdot 9\text{H}_2\text{O}$), cobalt (II) nitrate hexahydrate, ($\text{Co}(\text{NO}_3)_2 \cdot 6\text{H}_2\text{O}$), calcium carbonate (CaCO_3), acetylene (C_2H_2), titanium (IV)butoxide (97% $\text{Ti}\{\text{O}(\text{CH}_2)_3\text{CH}_3\}_4$, TBOT), Erbium (III) nitrate pentahydrate ($\text{Er}(\text{NO}_3)_3 \cdot 5\text{H}_2\text{O}$), Poly- ϵ -caprolactone ($M_w \sim 80\,000$, PCL), Cellulose acetate (39.8 wt% acetyl content, CA), polyethylene glycol ($M_w \sim 600$ PEG₆₀₀), anhydrous ethanol, 2-propanol, 2-butanol, formic acid (~99.9%), concentrated hydrochloric acid (HCl), nitric acid (HNO_3) and sulphuric acid (H_2SO_4), hydrogen peroxide (30% H_2O_2), dimethyl formamide (DMF), dimethyl sulphoxide (DMSO), acetone, Reactive Red 120. Milli-Q Deionized/ distilled water will be used for all the reactions and treatment processes

4.2 SYNTHESIS METHODS

4.2.1 Synthesis of Fe-Co catalyst

To prepare the different catalysts, $\text{Fe}(\text{NO}_3)_3 \cdot 9\text{H}_2\text{O}$ and $\text{Co}(\text{NO}_3)_2 \cdot 6\text{H}_2\text{O}$ were used (Sigma-Aldrich, St Louis, Missouri, USA). Calculated amounts of the iron (Fe) and cobalt (Co) nitrates were mixed, ground to a fine powder and dissolved in distilled water to make a 0.3 mol l^{-1} Fe-Co (50:50 m/m) precursor solution. This solution (28 ml) was added to the CaCO_3 support (10 g) and the mixture was left to stir for 30 minutes. The metal support mixture was then filtered and the insoluble product was dried in an air oven at $120 \text{ }^\circ\text{C}$ for 12 hours, cooled to room temperature, ground and finally screened through a $150 \text{ }\mu\text{m}$ sieve. The catalyst powder was then calcined at $400 \text{ }^\circ\text{C}$ for 16 hours in a static air oven.

4.2.2 Carbon nanotube synthesis

Carbon nanotubes were synthesised by the decomposition of C_2H_2 (Afrox) in a tubular quartz reactor (51 cm × 1.9 cm inner diameter (i.d.)) that was placed horizontally in a furnace. The furnace was electronically controlled so that the heating rate, reaction temperature and gas flow rates could be accurately maintained as desired. The catalyst (0.2 g) was spread to form a thin layer in a quartz boat (120 mm × 15 mm). The boat was then placed in the centre of the quartz tube, and the furnace was heated at $10\text{ }^\circ\text{C min}^{-1}$ under flowing N_2 (40 ml min^{-1}). Once the temperature had reached $700\text{ }^\circ\text{C}$, the N_2 flow rate was set to 240 ml min^{-1} and C_2H_2 was introduced at a constant flow rate of 90 ml min^{-1} . After 60 minutes of reaction time, the C_2H_2 flow was stopped and the furnace was left to cool to room temperature under a continuous flow of N_2 (40 ml min^{-1}). The boat was then removed from the reactor and the carbon deposit that formed along with the catalyst was weighed.

4.2.3 Synthesis of TiO_2

Titanium dioxide was prepared via the homogeneous hydrolysis of TBOT using the sol-gel method. Briefly, TBOT was dissolved in 2-butanol and sonicated. Formic acid and deionised water were added drop-wise to the solution and left to stir at room temperature. The sol was aged to allow gelation. The gel was dried and ground into a fine powder and calcined in an electrically controlled tubular furnace. The dried mass was weighed and kept in an airtight container.

4.2.4 Synthesis of Er-modified TiO_2

The same procedure for the synthesis of TiO_2 was followed for the synthesis of Er-modified TiO_2 . After the calcination of TiO_2 , a weighed amount of $Er(NO_3)_3 \cdot 5H_2O$ was dissolved in distilled water and added to the calcined, powdered TiO_2 while stirring at a slow speed at room temperature. The slurry was dried in an oven and ground to a fine powder. The powder was calcined and labeled Er: TiO_2 . In an alternative synthesis, erbium ions were added to the hydrolyser solution of the sol and allowed to co-precipitate with the titania sol.

4.2.5 Synthesis of Er-modified TiO_2 grafted onto MWCNT

The MWCNTs were synthesised via the decomposition of C_2H_2 over a bimetallic Fe-Co@ $CaCO_3$ support using the procedure reported by Mhlanga et al. (2009). The MWCNTs were purified by stirring

the products in concentrated HNO₃ at room temperature. The acid-treated MWCNTs were subsequently washed with distilled water until the washings were neutral. The MWCNTs were dried in an oven overnight and stored in an airtight container.

Titanium dioxide was synthesised as detailed previously, save for the addition of MWCNTs to the sol. An amount of 10 ml of TBOT was dissolved in 2-butanol and sonicated. A weighed amount of MWCNTs were dispersed via ultrasound in 2-butanol and added to the TBOT solution. Formic acid and deionised water were added drop-wise to the suspension and left to stir at room temperature. The sol was aged to allow gelation. The gel was dried in an oven and the dried sample was ground into a fine powder and calcined in air in an electrically controlled tubular. The Er(NO₃)₃·5H₂O was dissolved in distilled water and added to the calcined, powdered TiO₂@MWCNT while stirring at a low room temperature. The slurry was dried in an oven and ground to a fine powder. The powder was calcined. The dried mass was weighed and kept in an airtight container and labeled Er:TiO₂@MWCNT.

4.2.6 Synthesis of Er-modified TiO₂ grafted onto MWCNTs and embedded onto PCL and CA blended

A weighed amount of PCL was dissolved in a dimethylformamide (DMF) and trichloromethane solution and stirred. In a separate vessel, CA was weighed and dissolved in a solution of acetone and DMF and stirred. Some Polyethylene glycol, molecular weight 600 (PEG 600), was weighed and dissolved in acetone and left to stir. The solutions were mixed together and stirred. Various blend ratios of PCL/CA were prepared along with neat PCL and CA. A weighed amount of the photocatalyst was dispersed in trichloromethane under sonic vibration and added to the polymer blend solution while stirring vigorously. The emulsion was then cast onto a glass plate, covered and left to stand for the solvent to evaporate slowly. The dry film was dried in a vacuum oven for 48 hours at room temperature. The same procedure was repeated without the addition of the photocatalyst. The polymer was cast onto a glass plate and allowed to slowly evaporate until semi dry. Before it was completely dried, the photocatalyst, suspended in trichloromethane, was sprayed onto the partially solidified polymer blend film. The film was covered and left to evaporate at room temperature and then dried in a vacuum oven for 48 hours.

4.3 CHARACTERISATION

4.3.1 Microscopy analyses

The surface morphology of the prepared photocatalysts was investigated using microscopy techniques. Transmission electron microscopy analysis was done on a Jeol JEM 2100 TEM (Japan) under a bright field at 120 kV. A small amount of the sample was sonicated for a few minutes in methanol and a small drop of the suspension was put on a copper grid. The grid was left to dry in air before being mounted on the sample holder for analyses. Scanning electron microscopy images were obtained from a Jeol JSM- 7500F field emission SEM (Japan) (the working distance was 3.9-6.5 mm, the acceleration voltage 2.00 kV). The secondary electron imaging (SEI) mode was coupled with an INCA energy dispersive x-ray (EDX) analyser (at an acceleration voltage of 15 kV) for qualitative elemental analysis. Sample powders were mounted on glass slides using double-sided carbon tape and coated with carbon before being loaded in the field emission SEM for analysis.

4.3.2 UV-Vis spectroscopy

The optical properties of the samples were studied using UV-Vis spectroscopy. UV-Vis absorption spectra of the photocatalysts were collected on a Shimadzu UV-2450 UV-Vis spectrophotometer (Japan) fitted with an IRS 240A integrating sphere, and barium sulphate was used as a reference. Small amounts of powdered samples were mixed with barium sulphate and ground using a pestle and mortar to ensure adequate mixing of the sample and the reference. The mixture was then mounted in the UV-Vis solid sample holder and introduced into the instrument for analysis.

4.3.3 X-ray diffraction measurements

X-ray diffraction gave insight into the mineral phases of titania, degree of crystallinity and the average crystallite size of the titania particles. A Rigaku Ultima IV X-ray diffractometer (Japan) was used to obtain the diffraction patterns of the prepared nanocomposites from a 2θ range of 20-80° at a scanning rate of 5° min⁻¹. The diffractometer was operated at 40 kV and 40 mA. A Cu α radiation beam with an excitation wavelength of 0.15406 nm was used as an X-ray source. The average crystallite size of anatase TiO₂ (D) was computed from Scherrer's equation (Equation 3.1) for a specific angle (θ), full width at half maximum (FWHM) for the (101) anatase peak (β) and a shape factor (k) of 0.9.

$$D = \frac{k\lambda}{\beta \cos\theta} \quad 9.$$

4.3.4 Surface area analysis

The BET surface area analysis was employed to determine the surface areas of the prepared nanocomposites. A larger surface area is desirable in a photocatalyst as it presents a larger number of active sites for the degradation of the organic pollutants. The BET analyses were done on a Micromeritics ASAP 2020 surface using a porosity analyser (USA). Prior to analysis, the photocatalyst samples were degassed at 200 °C under vacuum to remove moisture and other solvents.

4.4 EVALUATION OF PHOTOCATALYTIC ACTIVITY

The prepared photocatalytic materials were evaluated for the adsorption and degradation of an aqueous solution of Reactive Red 120 under simulated solar light. The photocatalyst was mixed with 150 ml of 70 mg/l Reactive Red 120 dye, and the mixture was stirred in the dark for a time to establish adsorption equilibria. Samples were drawn from the solution and taken as the initial concentration (C_0). Thereafter, samples were drawn at equal intervals for 240 minutes. The samples were filtered using a Polytetrafluoroethylene (PTFE)-fitted syringe and analysed using a UV-Vis spectrophotometer at the wavelength of maximum absorption (512 nm for Reactive Red 120). The solar simulator was equipped with a xenon lamp and set at an input power of 400 W. The solar simulator was fitted with a dichroic UV filter ($\lambda > 420$ nm). A calibration curve was plotted from which the percentage colour removal was calculated using the equation:

$$\% \text{ Colour Removal} = \frac{C_0 - C_t}{C_0} \times 100 \quad 10$$

Where C_0 is the initial dye concentration and C_t is dye concentration after time, t .

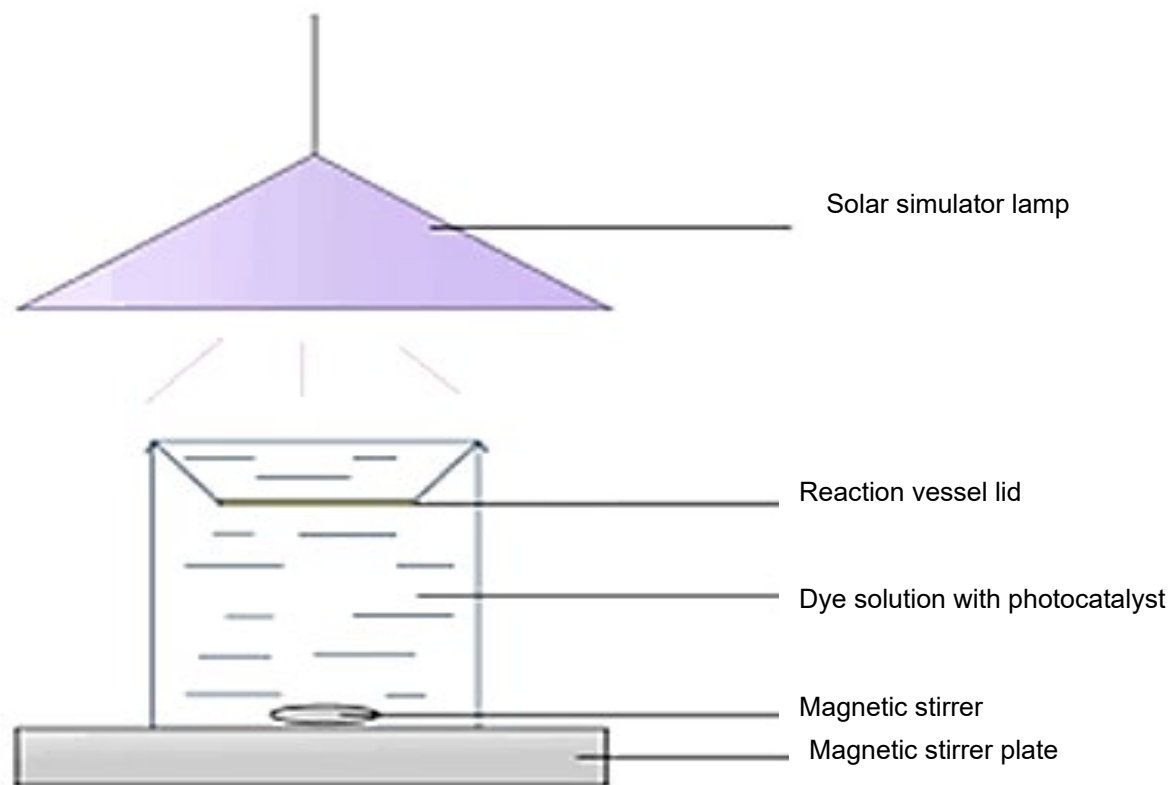


Figure 4.1: Illustration of laboratory setup of photodegradation experiments

CHAPTER 5: RESULTS AND DISCUSSION

5.1 CHARACTERISATION OF NANOCOMPOSITES

5.1.1 SEM analyses

Figures 5.1 to 5.4 show SEM images of the synthesised composites. The SEM analysis showed that the neat TiO_2 was brittle and crystalline in nature with large lumpy structures and smooth surfaces. After modification with erbium, the surface of the $\text{Er}:\text{TiO}_2$ remained crystalline and brittle. However, the surface exhibited a porous microstructure with diameters of around 1-2 μm . When TiO_2 was modified with MWCNTs, there was a marked change in the structure and morphology. The wet impregnation method of grafting TiO_2 onto MWCNTs was effective and, in fact, formed a continuous layer on the surfaces of the MWCNTs. After calcination, the TiO_2 coating surrounding the MWCNTs was transformed into clusters. The modification of TiO_2 with Er and MWCNTs has a remarkable effect, where the particle sizes became significantly smaller and adhered to the MWCNT.

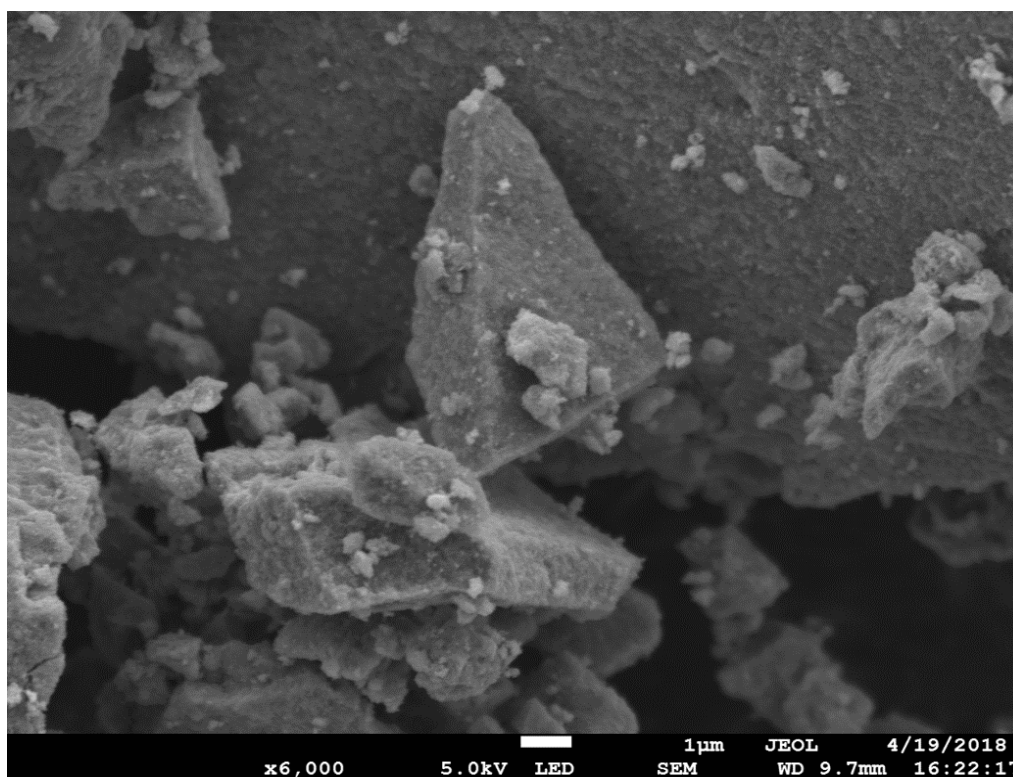


Figure 5.1: SEM micrograph of TiO_2

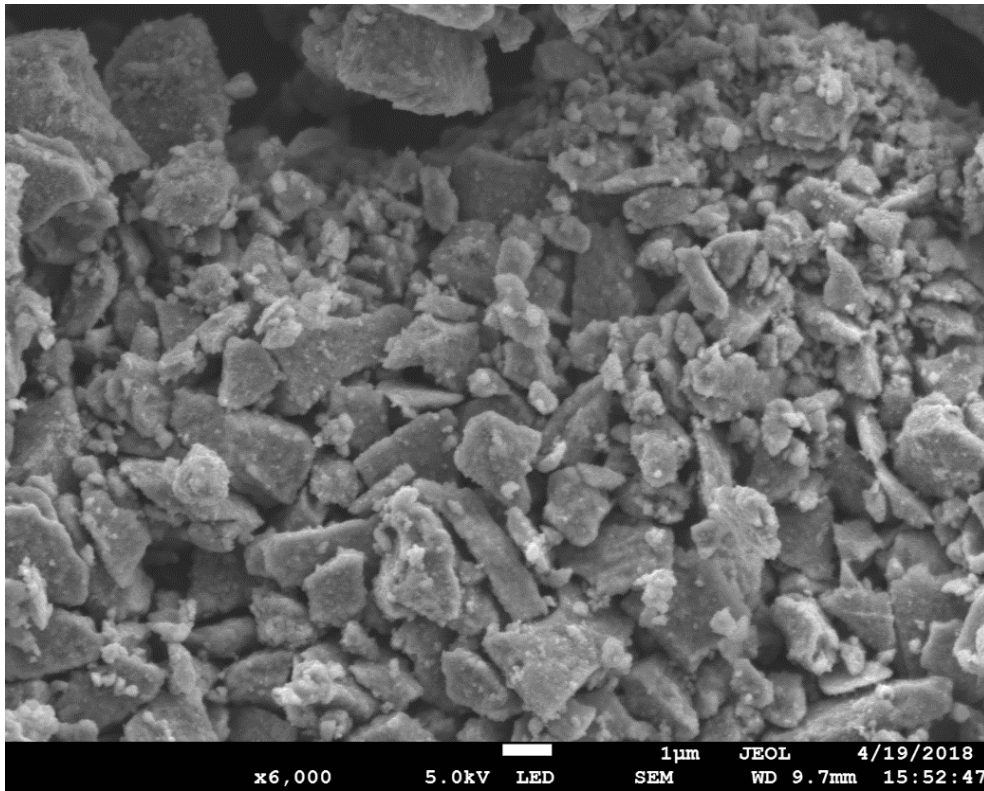


Figure 5.2: SEM micrograph of Er:TiO₂

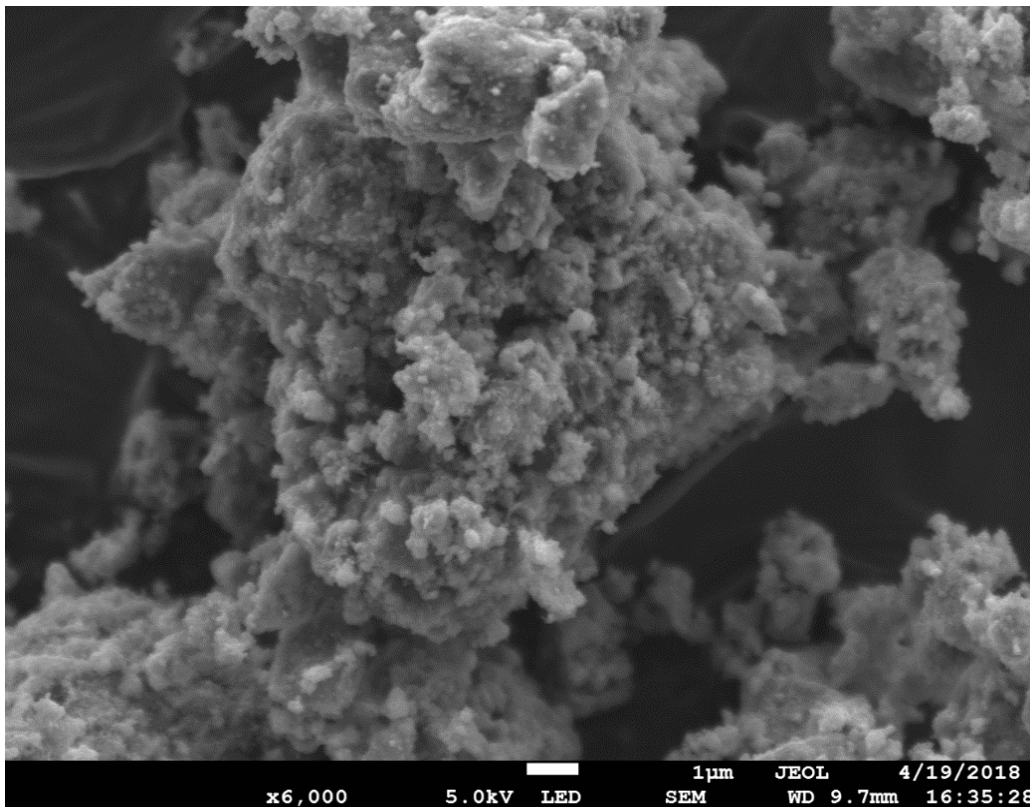


Figure 5.3: SEM micrograph of TiO₂@MWCNT

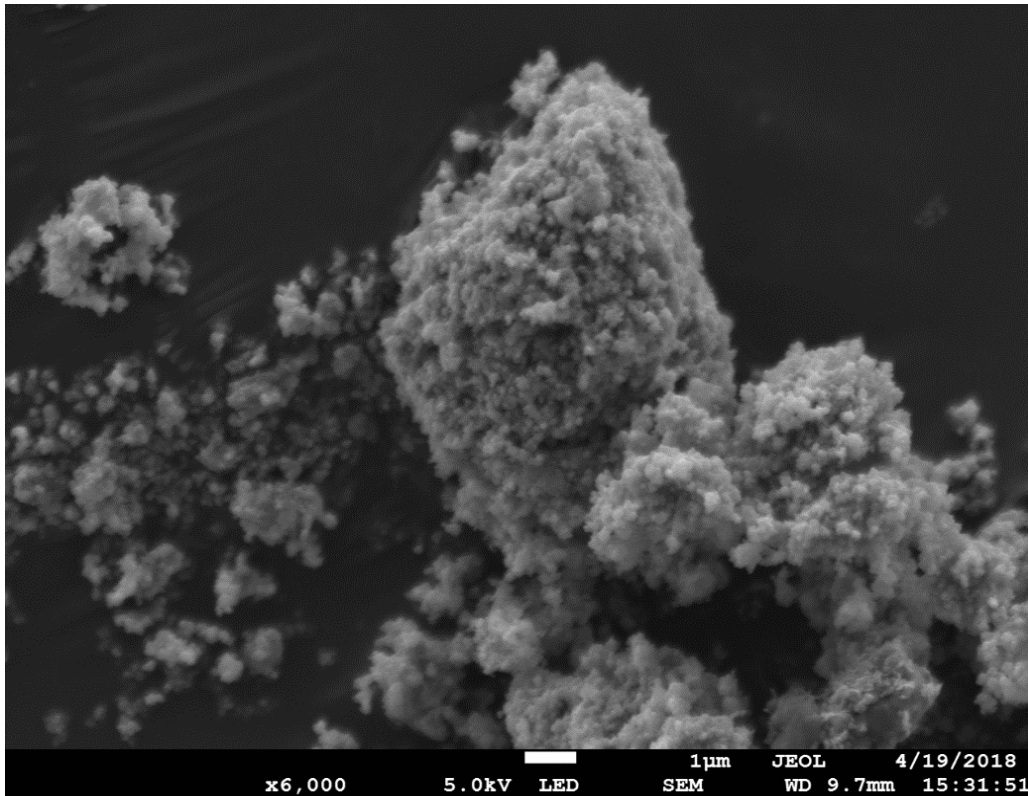


Figure 5.4: SEM micrograph of Er:TiO₂@MWCNT

5.1.2 TEM analyses

A TEM analysis of the MWCNTs, Er:TiO₂ and Er:TiO₂@MWCNT was used to observe morphological changes from the parent materials to the nanocomposite. The TEM images shown in Figures 5.5 to 5.10 reveal that the MWCNTs were multi-walled and randomly oriented. Prior to acid treatment, the MWCNTs showed the presence of a catalyst. However, the MWCNTs showed catalyst particles in the MWCNT with minimal metal residue inside the tube cavities, which implies that the MWCNTs form via a basal-growth mechanism. The MWCNTs were surrounded by amorphous carbon on the outer thicker walls and varied in diameter with tight kinks. After acid treatment and ultrasonic vibration, the MWCNTs remained intact and retained their length, while straightening, which was indicative of the non-destructive nature of the acid treatment (Boussouari and Baitoul, 2014; Osswald et al., 2007). The Er-modified TiO₂ particles were ellipsoid in shape with sizes ranging from ~7 to ~15 nm. The Er-modified TiO₂ that was grafted onto the MWCNTs had uniform inorganic particles that adhered well to the MWCNTs in clusters.

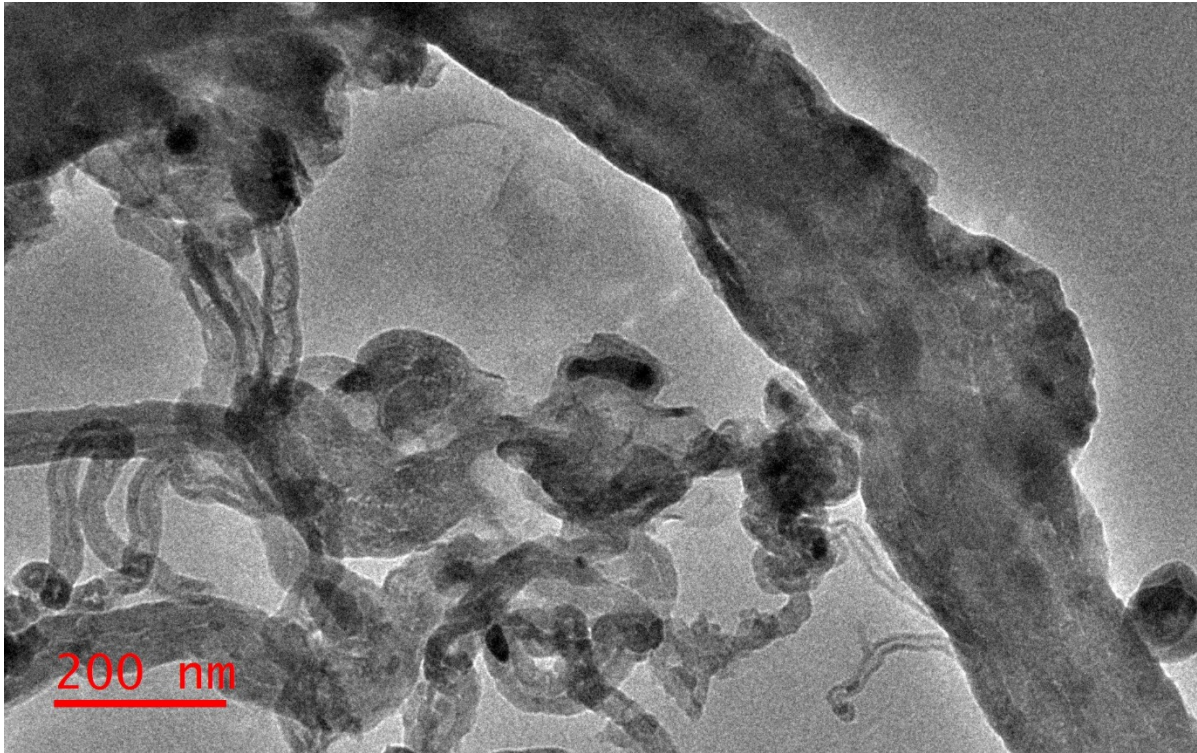


Figure 5.5: TEM image of the MWCNT before acid treatment

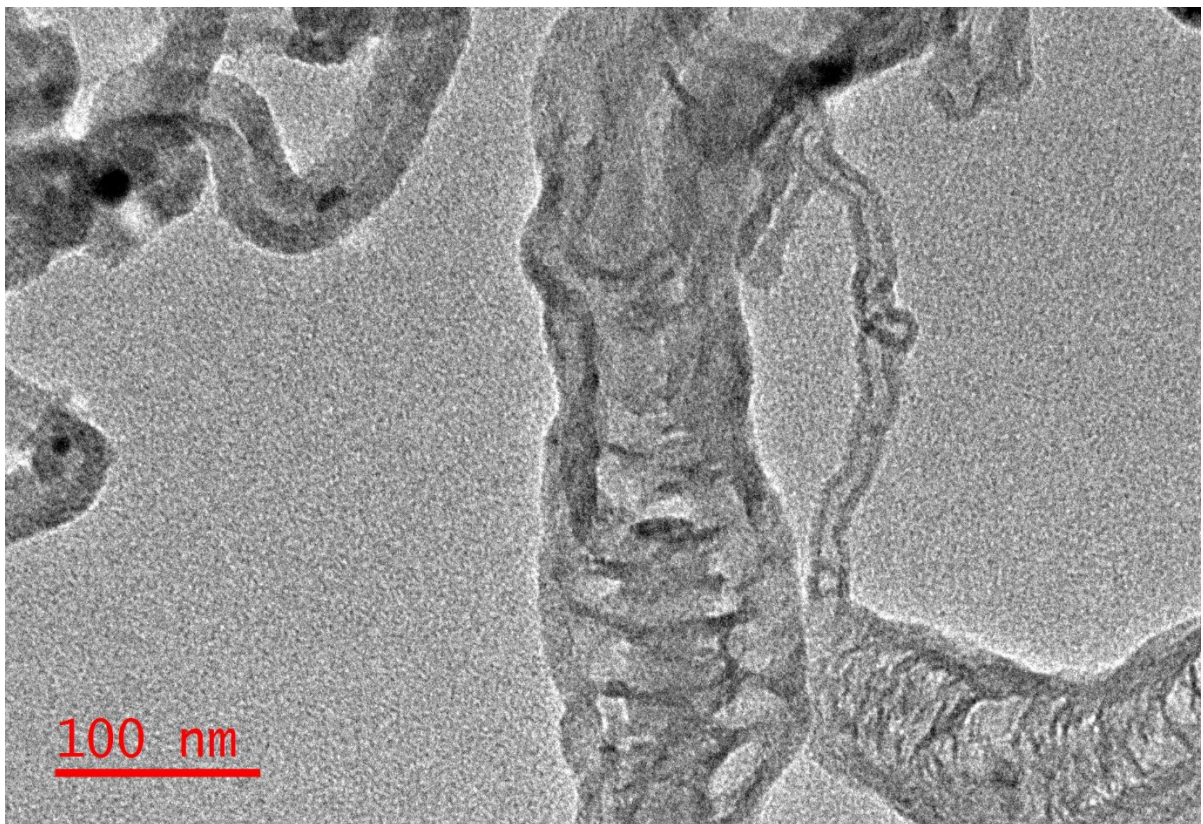


Figure 5.6: TEM image of the MWCNT after acid treatment

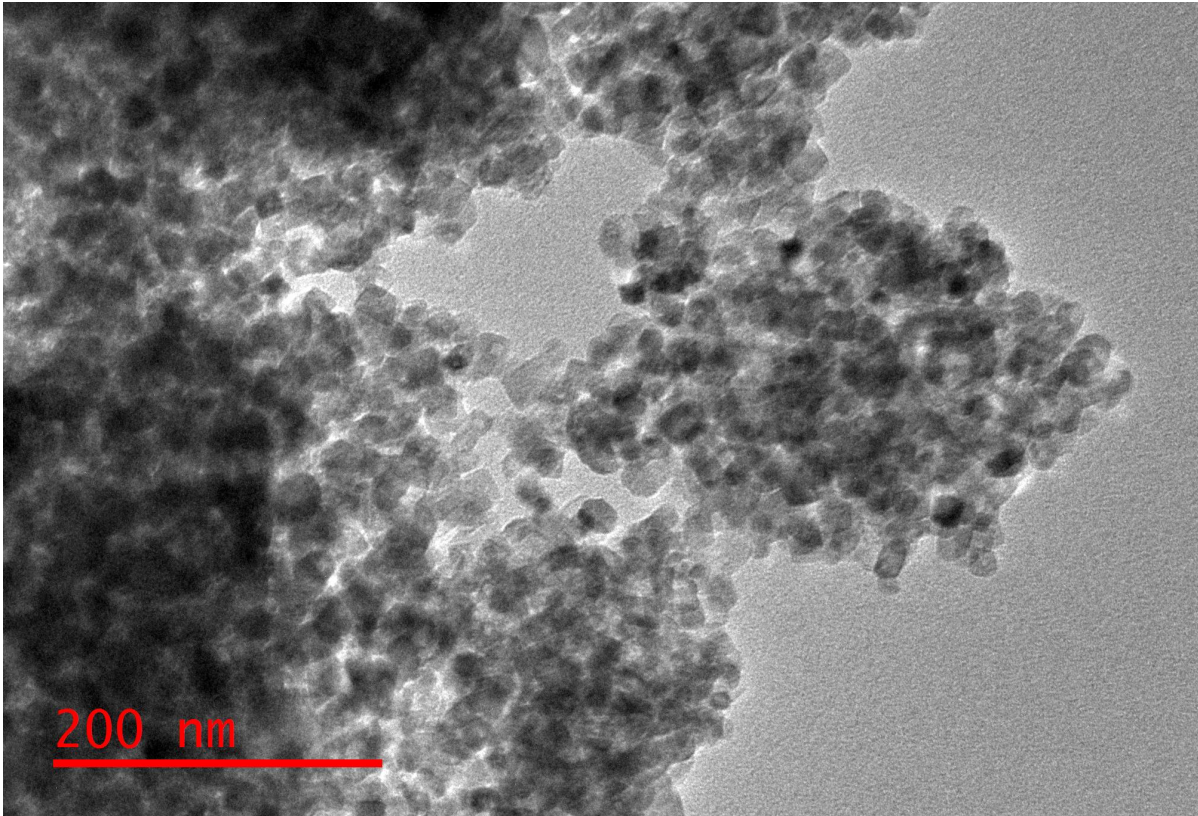


Figure 5.7: TEM image of the TiO_2

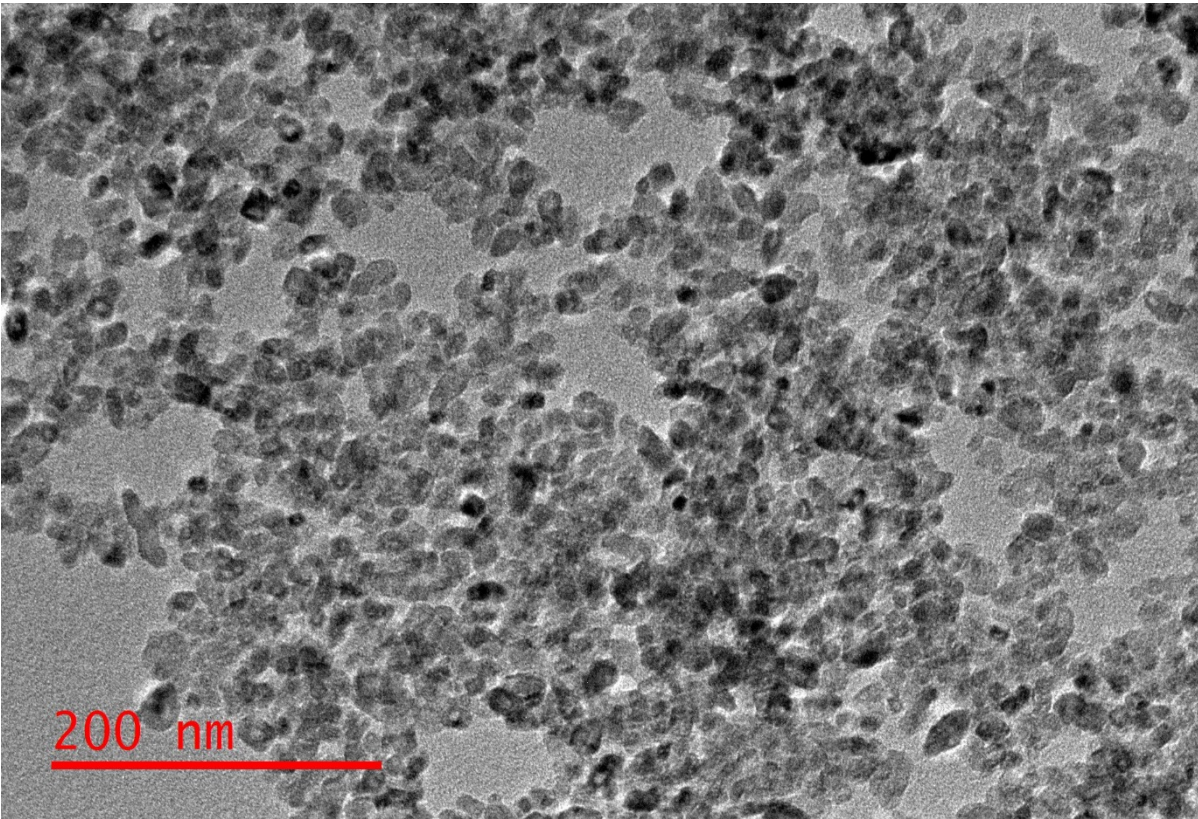


Figure 5.8: TEM image of the Er:TiO_2

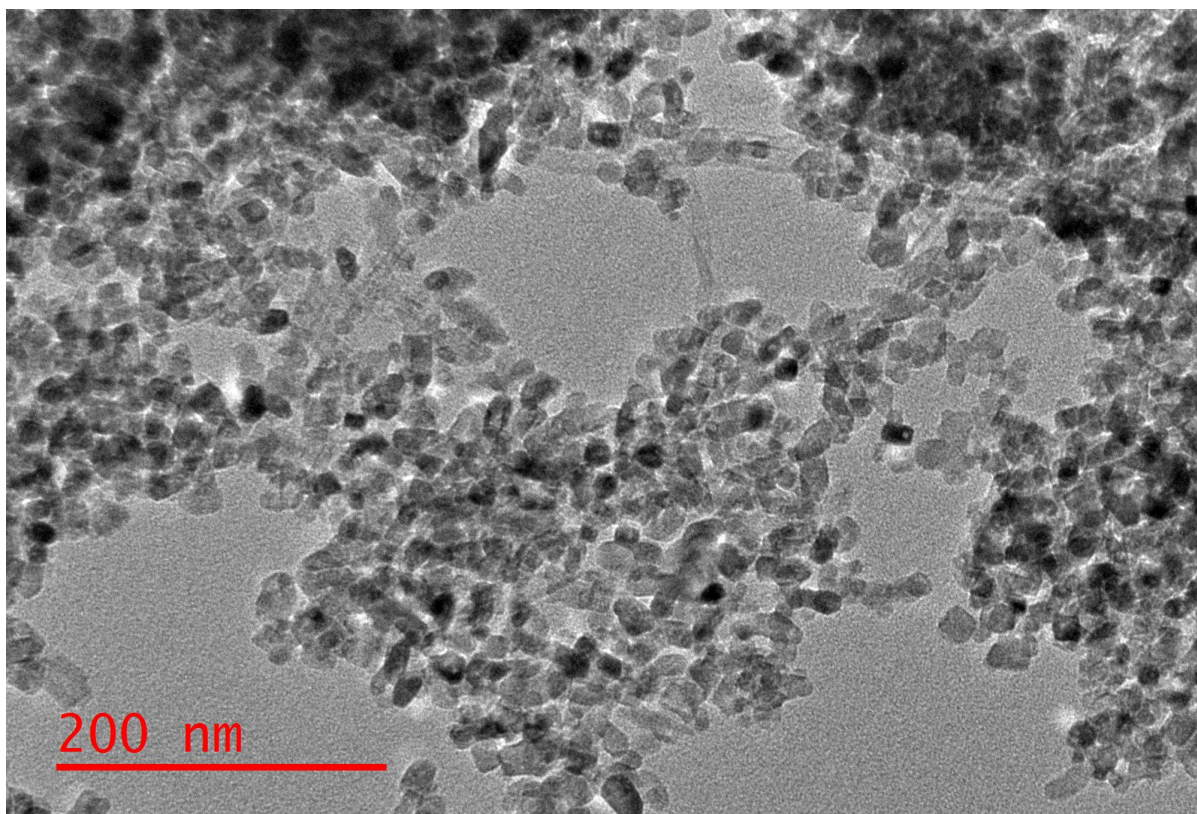


Figure 5.9: TEM image of the TiO₂@MWCNT

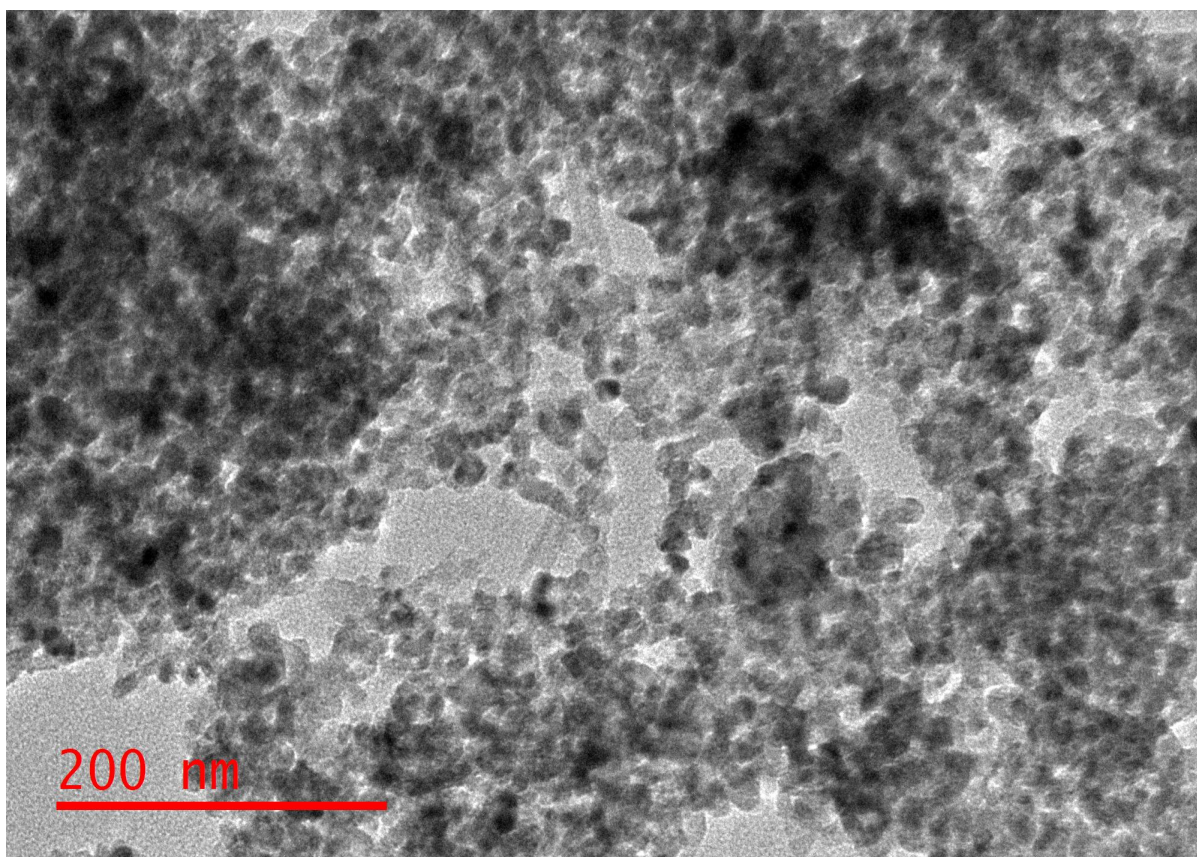


Figure 5.10: TEM image of the Er:TiO₂@MWCNT

5.1.3 The EDS analyses

The EDS mapping results displayed in figures 5.11 to 5.13, with their accompanying tables, confirmed the successful synthesis of all TiO₂, MWCNTs and nanocomposites. The TiO₂, erbium and MWCNTs were successfully combined: the EDS map confirms the 1% (wt %) presence of Er as calculated during synthesis.

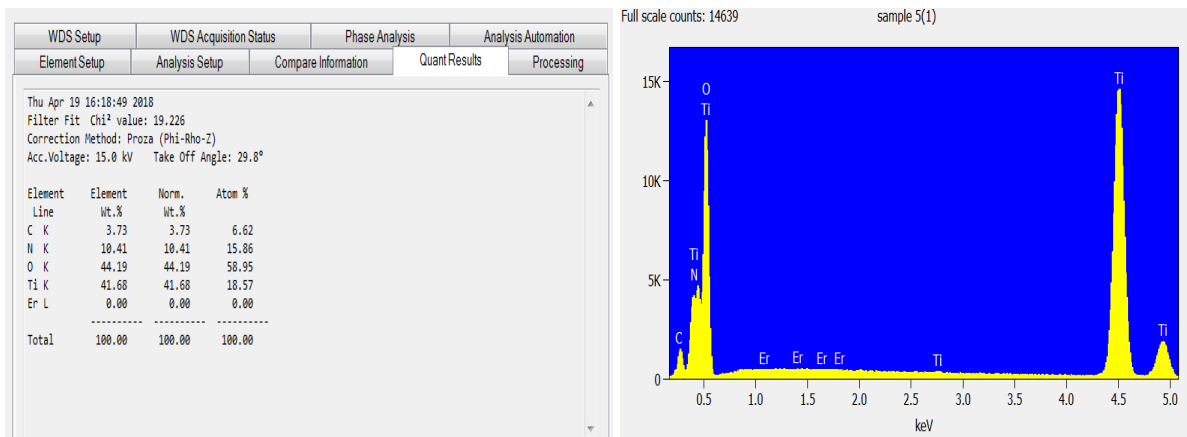


Figure 5.11: The TiO₂ EDS spectrum and table of quantities

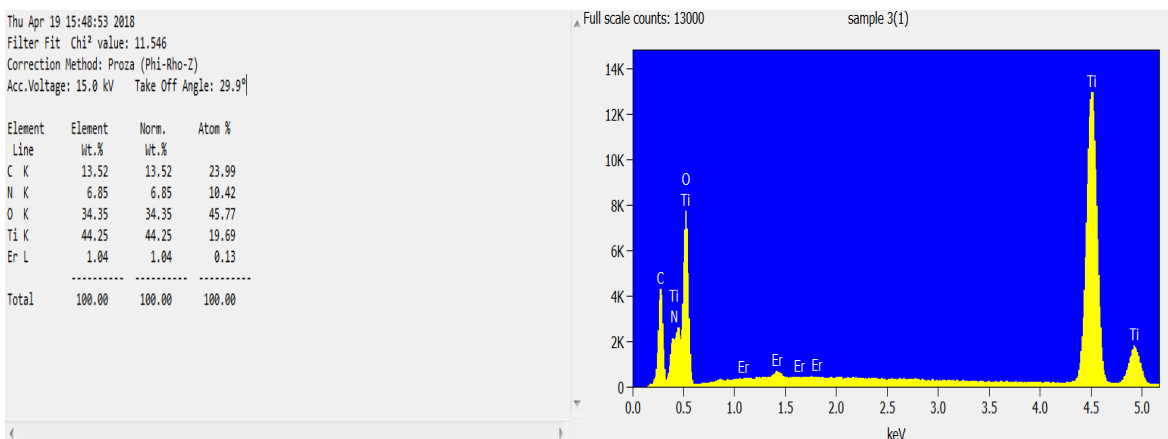


Figure 5.12: The Er:TiO₂ EDS spectrum and table of relative quantities

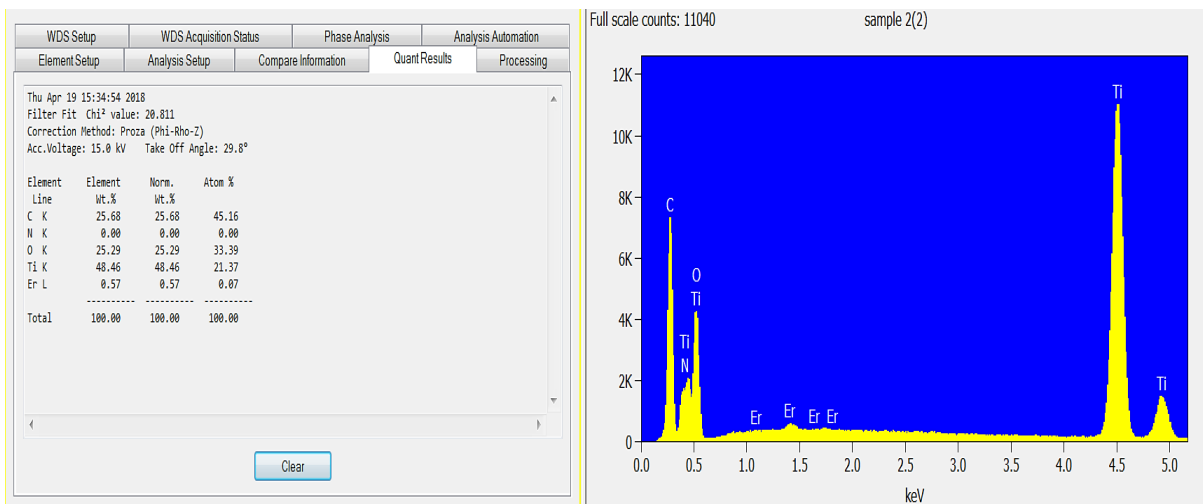


Figure 5.13: The Er:TiO₂@MWCNT EDS spectrum and table of relative quantities

5.1.4 UV-Vis spectroscopy

Optical absorption measurements were conducted at room temperature for all samples. The spectra are shown in figures 5.14 and 5.15. The acid-treated MWCNTs show two significant peaks at ~320 and ~360 nm. These major absorption peaks are due to π - π^* transition of the aromatic C-C and the n - π^* transition of the C=O in the sp^3 regions. The composite photocatalyst materials absorb at higher wavelengths than the unmodified TiO₂. As expected, all samples showed broad intense absorption below ~390 nm. It is the characteristic absorption that results from the excitation of electrons from the VB to the CB in anatase TiO₂.

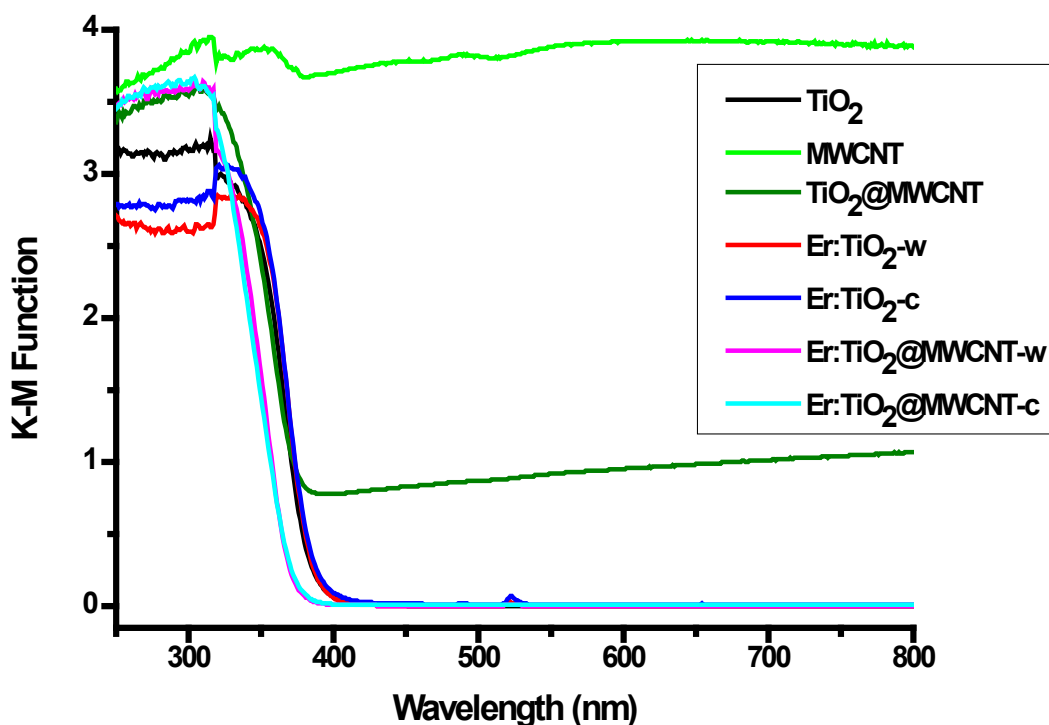


Figure 5.14: Kubelka-Munk function plots for the TiO₂-based Er³⁺ and MWCNT-modified nano-photocatalysts

The neat TiO₂ shows the characteristic spectrum with its absorption peak at ~365 nm. The TiO₂@MWCNT shows absorption over the entire UV-Vis spectrum. When comparing neat TiO₂ and MWCNT, it becomes obvious that there is a correlation between the MWCNT content and the change in the spectra, i.e. the visible range absorption is markedly improved in the TiO₂@MWCNT composite. Furthermore, the TiO₂@MWCNT shows a reduced absorption intensity than the purified MWCNTs. This reduction in absorption intensity in the visible range of the TiO₂@MWCNT is due to the TiO₂ nanoparticles adhering to and wrapping themselves around the surface of the MWCNTs and effectively limiting the light intensity reaching the MWCNTs. The Er-modified TiO₂ absorption edge shifts slightly into the visible light region. This slight red shift exists due to the charge transfer between the TiO₂ and Er³⁺ intra 4*f* electrons. In all the Er-modified composites, absorption peaks are located at ~455, ~480, ~525 and ~660 nm (Figure 5.15). These are ascribed to the transition from the ⁴I_{15/2} ground state to the Er ions' excited states.

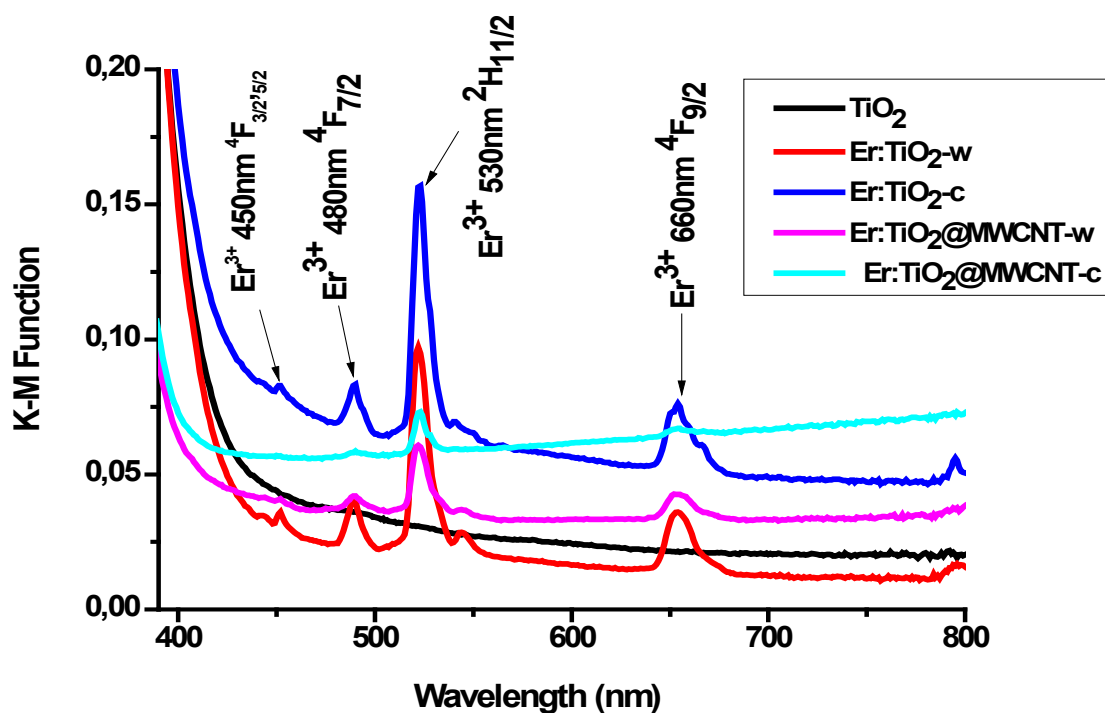


Figure 5.15: A Kubelka-Munk function plot for the TiO₂-based Er³⁺ and MWCNT-modified nano-photocatalysts

5.1.5 The XRD analyses

Figure 5.16 presents the XRD patterns of the synthesised nanocomposites. Titanium dioxide has three crystallographic polymorphs: anatase, rutile and brookite. All three contain the six coordinated titanium ions. Anatase is the more stable, low-temperature form (<600 °C). X-ray diffraction patterns were obtained of the Er-doped TiO₂ grafted onto the MWCNT nanocomposite. The most prominent diffraction peaks were indexed according to JCPDS Card No 70-6826, which corresponds to the pure anatase phase without a rutile phase due to the low-temperature calcination (400-500 °C). Detailed inspection of the diffractograms showed no rutile phase and Er was not detected. This is ascribed to the low Er³⁺ dopant content. The Er:TiO₂@MWCNT was highly crystalline. It showed no peaks at 2θ positions ~26° and 43° corresponding to the MWCNTs. The absence of the MWCNT peaks could be due to overlapping by the main peak of anatase at ~25.3° because they are so close to Er³⁺ and MWCNTs lead to a reduction in crystallite sizes with regard to TiO₂. Wet impregnation does not reduce the crystallite size because the Er³⁺ ions were added after the formation of TiO₂. With the composites formed via co-precipitation, a marked decrease was found in the crystallite size as the Er³⁺ ions are present during

the crystallisation of TiO₂. This means that the Er³⁺/Er₂O₃ forms at the TiO₂ crystal boundary and effectively deters TiO₂ crystal growth, thus the small crystallite size.

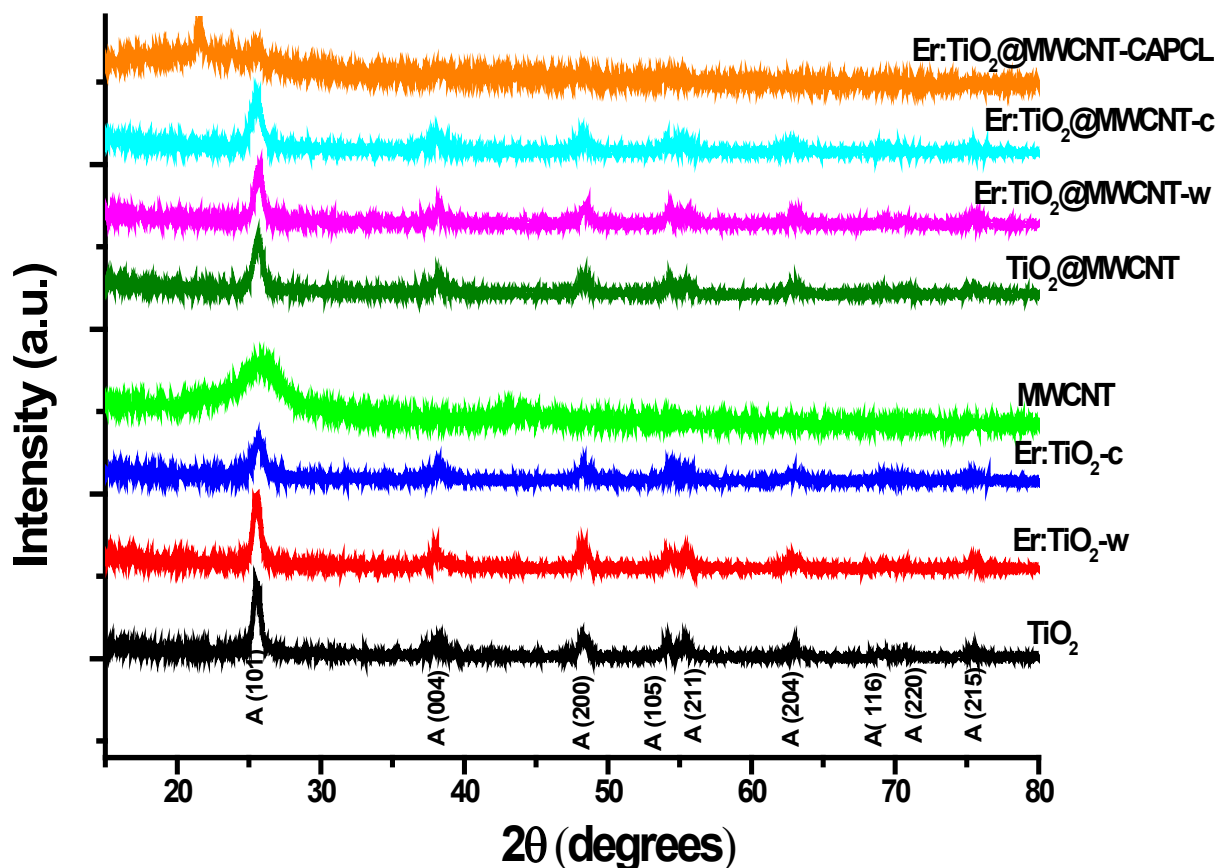


Figure 5.16: The XRD patterns of the TiO₂-based Er³⁺, CNTs and CA-PCL-modified nano-photocatalysts

The Er:TiO₂@MWCNT sample formed via wet impregnation has the smallest crystallite size. This can be ascribed to the MWCNTs acting as a core shell-type template for Er₂O₃ to grow on TiO₂, where the TEM analysis shows that particles changed from hollow cubes to elliptical structures formed around the MWCNT as they partially collapse during calcination. The best-performing photocatalyst during the photodegradation experiments (Er:TiO₂@MWCNT-w) was embedded in a CA-PCL polymer blend film (Er:TiO₂@MWCNT-CAPCL).

The XRD pattern shows the successful blending of CA and PCL. There are two peaks at $2\theta = \sim 21.3^\circ$ and $\sim 23.5^\circ$, which were attributed to the diffraction of the (110) lattice plane and the (200) lattice plane

of semi-crystalline PCL, respectively. However, CA has an amorphous character, manifesting as a broadened, weak diffused background pattern with a singular diffraction halo around $2\theta = \sim 20^\circ$. The weak, broadened diffuse halo of the CA-PCL blend evinces decreased crystallinity and successful blending of the semicrystalline PCL with CA. Moreover, the intensity of the strong reflections of anatase TiO_2 present in the other samples have been noticeably decreased, suggesting that the $\text{Er}:\text{TiO}_2@\text{MWCNT}$ composite has been successfully blended into the CA-PCL polymer matrix (Klébert et al., 2009).

5.1.6 BET analyses

To investigate the effect of Er^{3+} and MWCNT on the surface area of TiO_2 -based nano-photocatalysts, BET N_2 adsorption-desorption measurements were carried out and pore size distribution was estimated by the BET method. The results displayed in figures 5.17 to 5.21 showed that the composites had type IV and type V adsorption isotherms with H1 and H3 hysteresis loops. This implies that the photocatalysts have narrow and open-ended mesopores that are filled or condensed with N_2 , demonstrating the presence of two types of pores. An N_2 sorption and pore size distribution analysis was performed and the results indicate that all composites exhibit mesoporosity through a type IV adsorption isotherm (Matthias Thommes et al., 2015).

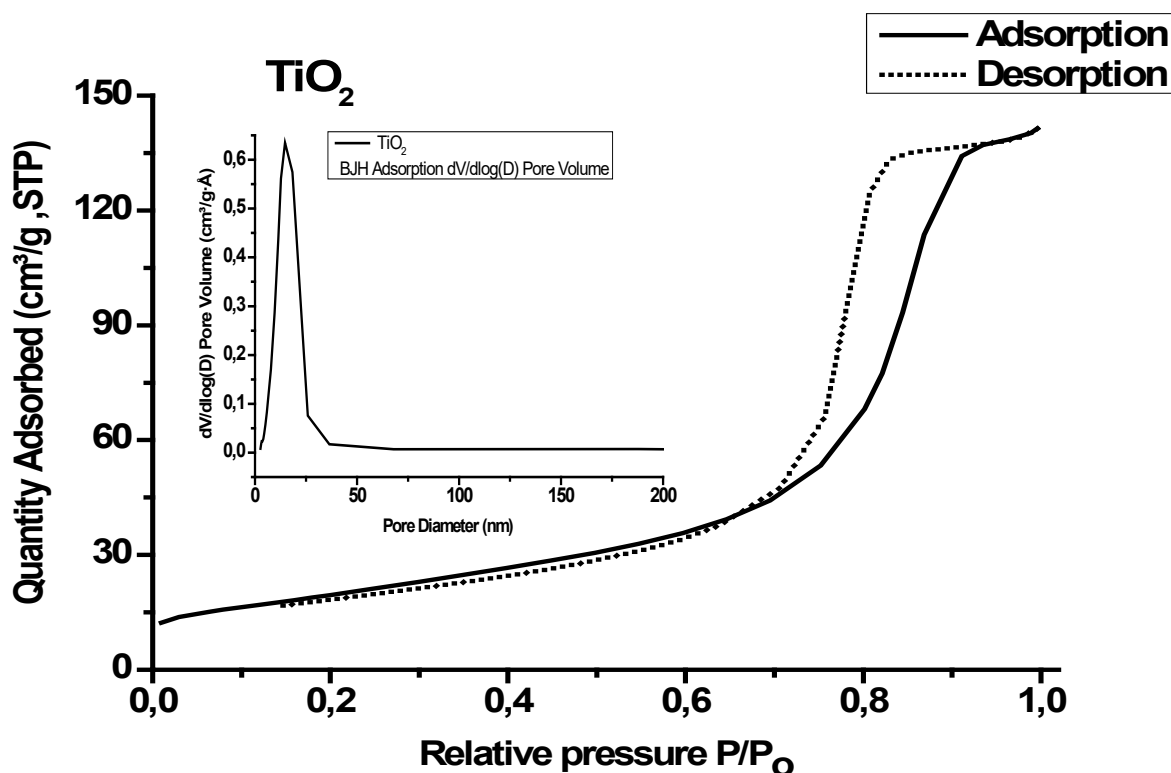


Figure 5.17: The N₂ adsorption-desorption isotherms and Barrett, Joyner and Halenda (BJH) pore size distribution for TiO₂

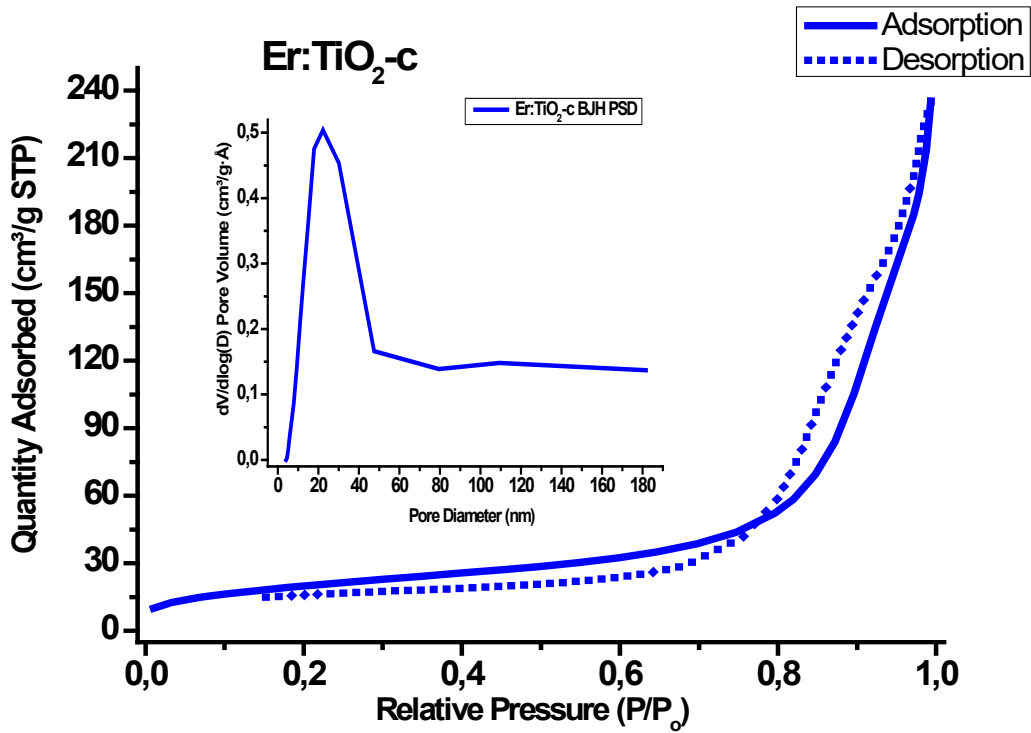


Figure 5.18: The N₂ adsorption-desorption isotherms and BJH pore size distribution for Er:TiO₂-c

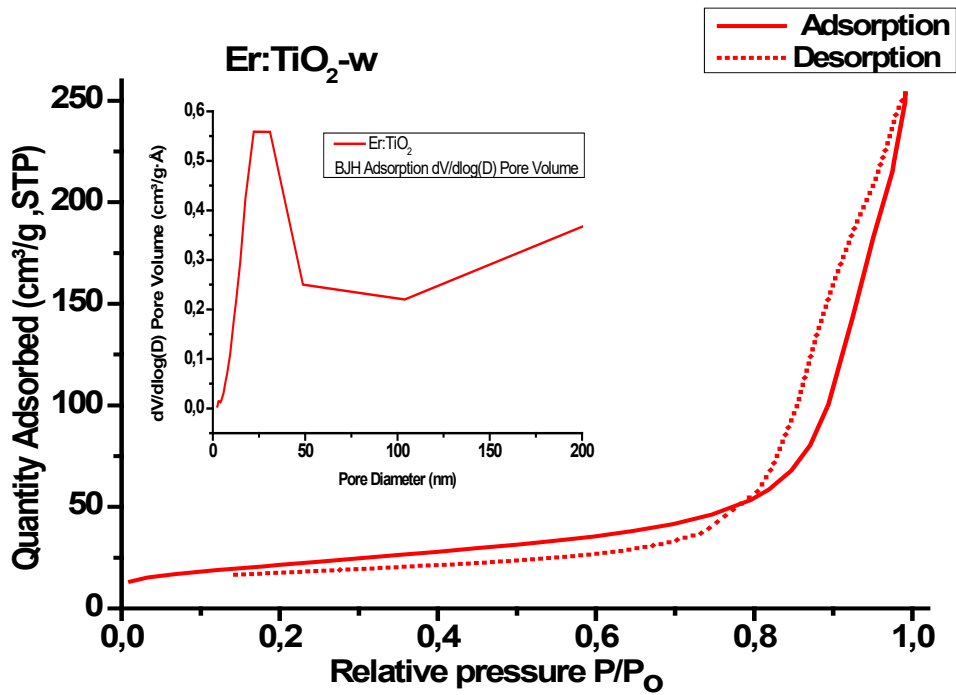


Figure 5.19: The N₂ adsorption-desorption isotherms and BJH pore size distribution for Er:TiO₂-w

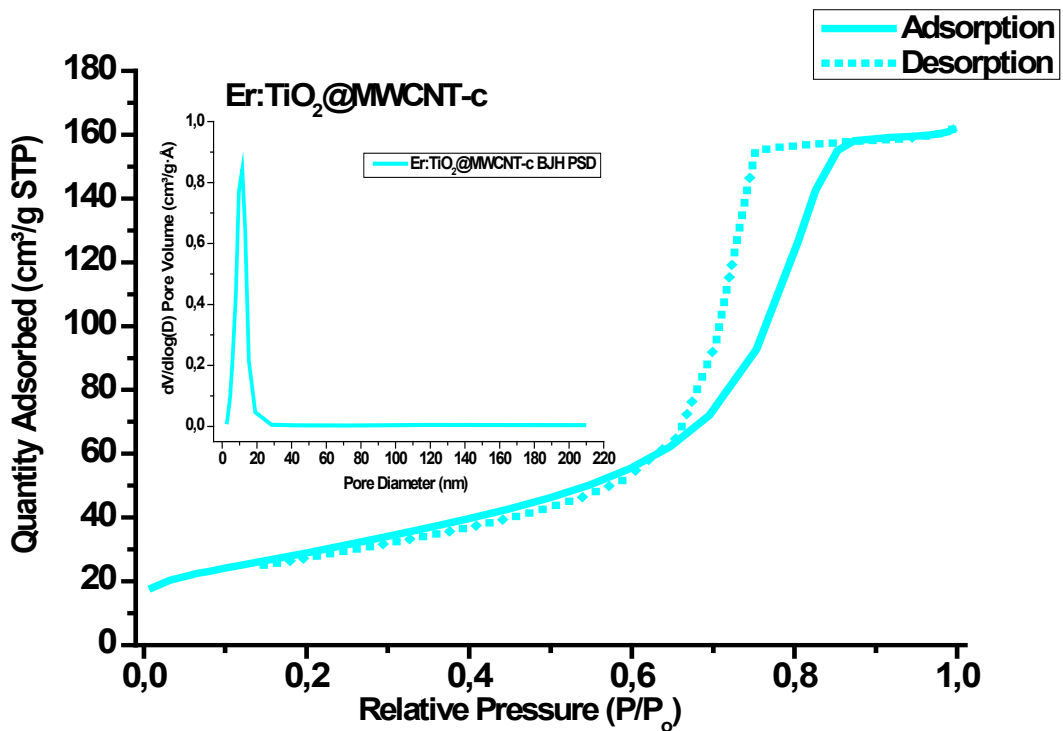


Figure 5.20: The N₂ adsorption-desorption isotherms and BJH pore size distribution for Er:TiO₂@MWCNT-c

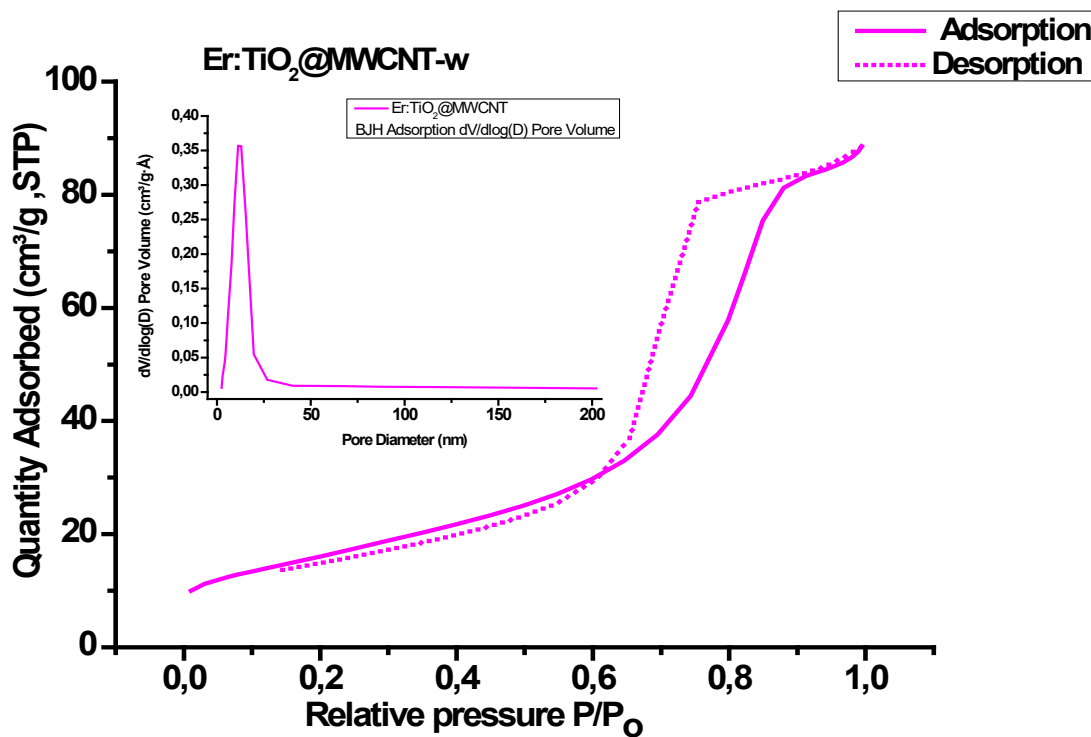


Figure 5.21: The N₂ adsorption-desorption isotherms and BJH pore size distribution for Er:TiO₂@MWCNT-w

The surface areas were different for all samples and ranged from 67.91 to 100.62 m²/g (Table 5.1). The highest BET surface area was observed for the Er:TiO₂@MWCNT-w sample. The presence of Er₂O₃ and MWCNTs increased the TiO₂-based composite BET surface area compared to pure TiO₂ nanoparticles. Higher specific surface areas are anticipated to improve the adsorption ability of photocatalysts because the photocatalytic activity strongly depends on the better adsorption of the organic substrate. The interfacial charge transfer can also be improved. This was the case, where it was observed that the best-performing photocatalyst showed the highest dye adsorption (q_t), in keeping with its large surface area.

Table 5.1: The textural properties of photocatalyst composites

Sample	S _{BET} (m ² /g)	V _{total} (cm ³ /g)	Pore diameter (nm)
1. TiO ₂	67.91	0.2173	12.33

2. Er:TiO ₂ -w	74.48	0.3856	19.98
3. Er:TiO ₂ -c	69.35	0.3305	17.81
4. Er:TiO ₂ @MWCNT -w	103.14	0.4464	16.75
5. Er:TiO ₂ @MWCNT-c	100.62	0.2490	9.49

5.2 PHOTOCATALYTIC ACTIVITY EVALUATION OF NANOCOMPOSITES

The photocatalytic activity of the nanocomposites was evaluated by measuring their ability to decolourise solutions of the model dye Reactive Red 120 over 240 minutes under simulated solar irradiation. Figure 5.22 presents the structure of the diazo dye Reactive Red 120 with absorption maxima at 512 and 535 nm (λ_{max}). Table 5.2 presents the physical and chemical properties of the model dye Reactive Red 120.

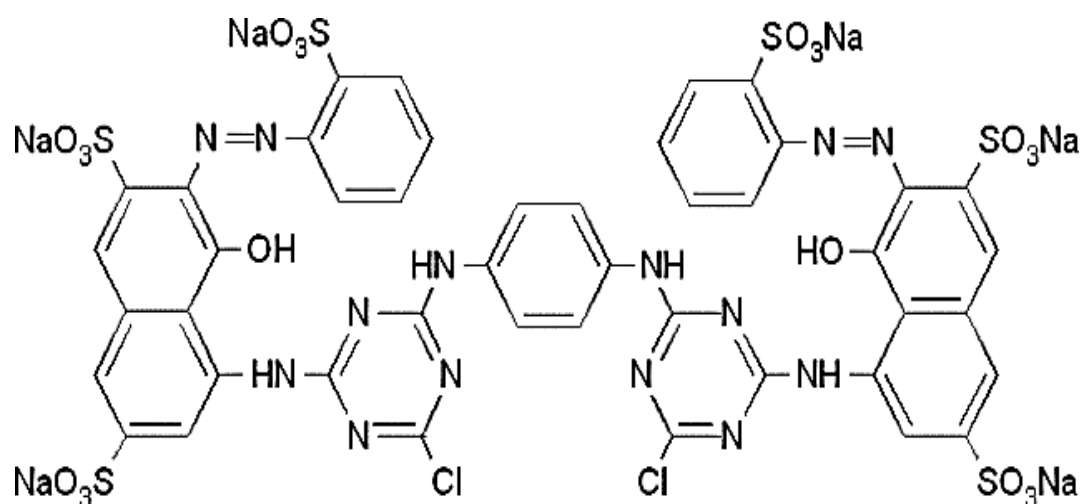


Figure 5.22: The chemical structure of Reactive Red 120

Table 5.2: The physicochemical properties of the model dye Reactive Red 120

Characteristics of Reactive Red 120	
Molecular formula	$C_{44}H_{24}C_{12}N_{14}Na_6O_{20}S_6$
Colour Index (CI) name	Reactive Red 120
Molecular weight (M_w)	1469.98 g/mol
Water solubility	70 g/l
Maximum absorbance wavelength (λ_{max})	512 nm
Azo class	Diazo (-N=N-) bonds

Figures 5.23 and 5.24 present the percentage dye removal efficiency versus time curves, showing the decolourisation of Reactive Red 120 by TiO_2 and the various Er^{3+} and MWCNT functionalised nano-photocatalysts under simulated solar light. It was found that the $Er:TiO_2@MWCNT$ nanocomposites showed higher photocatalytic activity than the neat TiO_2 . It was also found that, over 240 minutes at 30-minute intervals, neat TiO_2 showed a 35.42% colour removal efficiency within 90 minutes, with the other photocatalysts removing less than 50% of the colour. However, $Er:TiO_2@MWCNT-w$ showed a 79.70% colour removal efficiency within 90 minutes and a consistently higher colour removal efficiency over the entire reaction time (Figure 5.23). The nanocomposites containing Er and MWCNTs show a marked improvement in the decolourisation of the Reactive Red 120. More so, the composite prepared by wet impregnation performed better (79.70% colour removal at 90 minutes) than those prepared via co-precipitation (58.18% colour removal at 90 minutes). This can be ascribed to the partial collapse of the MWCNTs upon calcination of the nanocomposite, where the MWCNT acts as a template for allowing the growth of the $Er:TiO_2$ crystals along the MWCNT, as well as increasing the interfacial charge transfer within the metal oxide surface, while increasing the photocatalyst surface area and capacity for dye adsorption.

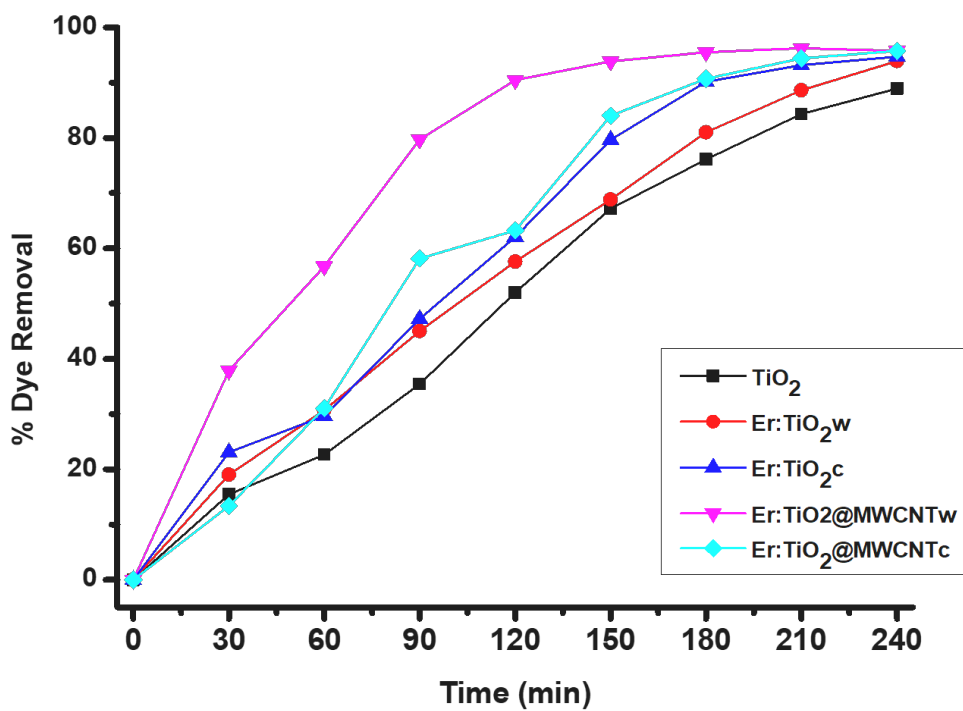


Figure 5.23: Percentage dye removal vs. time curves of TiO₂ and its Er³⁺ and MWCNT functionalised composites over a 240-minute period

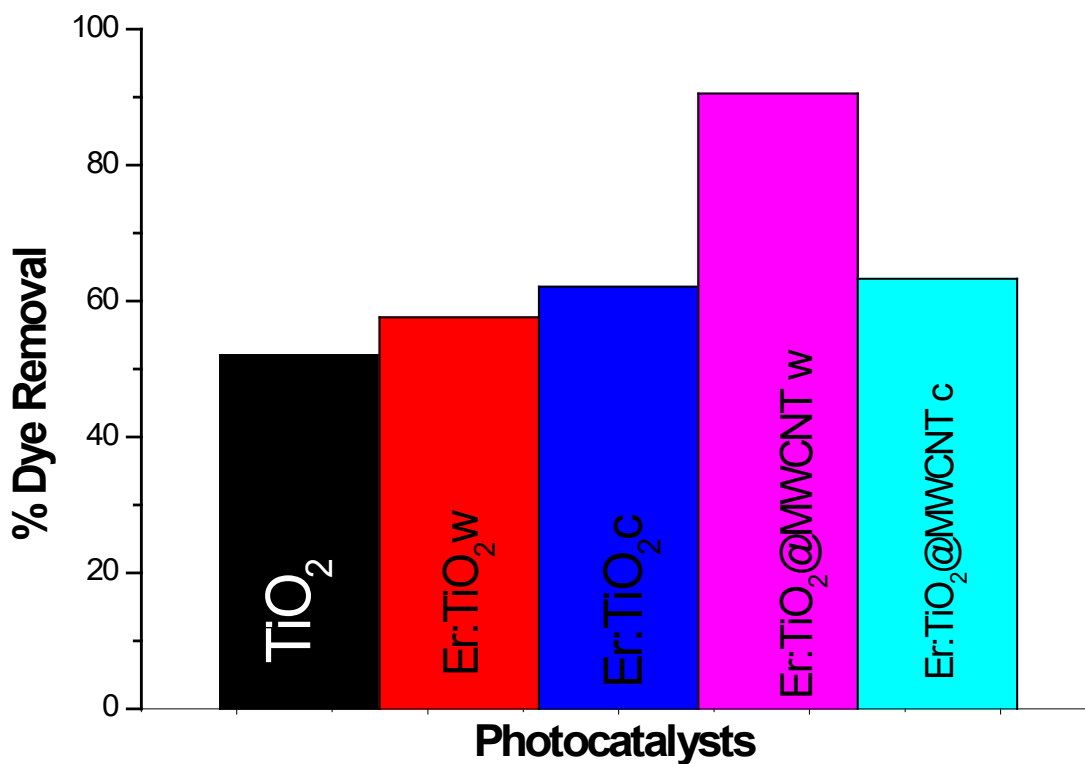


Figure 5.24: Percentage dye removal vs. time bar graph of TiO₂ and its Er³⁺ and MWCNT functionalised composites at 120 minutes' reaction time

This is supported by the amount of dye adsorbed (q_e) values in Table 5.3, where TiO₂ shows the lowest capacity for adsorbing the dye, and Er:TiO₂@MWCNT-w showing the highest capacity, coincident with its high BET surface area.

Table 5.3: Amount of Reactive Red 120 dye adsorbed and removed by the photocatalyst at 90 and 240 minutes

Sample	Amount of dye adsorbed (mg/g) (at 90 and 240 minutes)		Percentage dye removal (at 90 and 240 minutes)	
	90	240	90	240
TiO ₂	0.026	0.065	35.42	88.95
Er:TiO ₂ -w	0.032	0.067	45.04	93.91
Er:TiO ₂ -c	0.035	0.069	47.21	94.72
Er:TiO₂@MWCNT-w	0.058	0.070	79.70	95.76
Er:TiO ₂ @MWCNT-c	0.038	0.057	58.18	95.77

Mamba et al. (2015) conducted a study in which they synthesised gadolinium oxide (Gd₂O₃) nanoparticle-decorated MWCNT/titania (MWCNT-Gd/TiO₂) nanocomposites used for the photocatalytic degradation of Methylene Blue under simulated solar irradiation. Similar to this study, they found that neat TiO₂ nanopowder showed the lowest photoactivity compared to the MWCNT-Gd/TiO₂ nanocomposites. This was attributed to poor visible-light absorption by TiO₂ due to its wide band gap (~3.2 eV). The fabricated MWCNT-Gd/TiO₂ nanocomposites had an enhanced photoactivity compared to neat titania. The authors ascribe this to the incorporation of MWCNTs and Gd₂O₃. The MWCNTs extend the light absorption into the visible light region, improve electron-hole separation and increase the surface area of the nanocomposite, which it is essential for a higher photocatalytic activity, while the Gd₂O₃ is credited with acting as an electron transfer channel, thereby ensuring efficient charge

separation and delaying electron-hole recombination. The photocatalytic evaluation studies recorded maximum photocatalytic degradation efficiencies of 53.6% for neat TiO₂ and 85.8, 96.2 and 98.7% for MWCNT/TiO₂, 1MWCNT-Gd/TiO₂ and 3MWCNT-Gd/TiO₂, respectively. These percentage colour removal efficiencies were obtained after 300 minutes with a photocatalyst loading of 0.1 g mixed with 30 ppm, 150 ml Methylene Blue dye solution. In this study, the neat TiO₂ obtained 88.95% colour removal, while the Er:TiO₂-w and Er:TiO₂-c showed 93.91% and 94.72% colour removal efficiencies, while the Er:TiO₂@MWCNT-w and Er:TiO₂@MWCNT-c showed 95.76% and 95.77% maximum colour removal efficiencies, respectively. Comparatively, the Er₂O₃ and MWCNT-modified composites fabricated in the experiment showed superior performance to those synthesised by Mamba et al. (2015) since the obtained decolourisation efficiencies are higher than those reported in the experiment.

5.3 KINETICS AND PROPOSED PHOTOCATALYTIC ACTIVITY MECHANISM

5.3.1 General overview

The general process of decomposition of dyes occurs when CB electrons (e⁻) and VB holes (h⁺) are generated when TiO₂ is irradiated with photons of energy greater than its band gap energy (E_g , ~3.2 eV). The photo-formed electrons either reduce the dye or react with electron acceptors such as O₂ adsorbed on the Ti (III) surface or dissolved in water, reducing it to the superoxide radical anion O₂•⁻. The photogenerated holes can oxidise the dye to form charged dye radicals R⁺, or react with hydroxide (OH⁻) or H₂O oxidising them into OH• radicals. Together with other highly oxidant species, they are responsible for the TiO₂-photocatalysed decomposition of organic substances, such as azo dyes (Konstantinou and Albanis, 2004).

Alternative to photocatalytic oxidation is photosensitised oxidation by visible light irradiation. It is different from the reaction mechanism implicated under UV-light irradiation. In the photocatalytic oxidation mechanism, excitation of the adsorbed dye takes place by visible light to appropriate singlet or triplet states, followed by electron injection from the excited dye molecule onto the CB of the TiO₂ particles, whereas, in the photosensitised oxidation pathway, the dye is converted to the cationic dye radicals (Dye•⁺) that undergo degradation to yield products. The cationic dye radicals readily react with hydroxyl ions undergoing oxidation or interact with O₂•⁻, HO₂• or HO•⁻ species to generate intermediates that ultimately lead to CO₂. However, in instances where experiments are carried out

using simulated sunlight, it has been suggested that both the photo-oxidation and the photosensitising mechanisms occur during irradiation, and both TiO₂ and the light source are necessary for the reaction to occur. It remains unknown whether photocatalytic oxidation is superior to the photosensitising oxidation mechanism. However, the latter is expected to enhance the overall efficiency of the photodecomposition of the dye using solar light.

Having performed the photodegradation studies using the various composites, it was observed that Er:TiO₂@MWCNT-w was the best-performing composite over a 180-minute reaction time in terms of the colour removal efficiency (figures 5.23 and 5.24). It performed exceedingly better than the Er:TiO₂@MWCNT-c composite. Furthermore, for comparison purposes, Er:TiO₂@MWCNT-w was compared with neat TiO₂, Er:TiO₂-w and TiO₂@MWCNT. This allowed the researchers to evaluate the effect of Er³⁺ and MWCNTs on the nanocomposites' photocatalytic activity and propose a mechanism for the decolourisation of Reactive Red 120. Having plotted the concentration [RR120 mg/l] versus time graphs (Figure 5.25) for the photocatalyst composites, it was found that, from an observation of the degradation curves of Reactive Red 120, it can be deduced that the elimination of Reactive Red 120 fulfils the conditions established for a first-order homogeneous reaction kinetic model. Such a simplified model has previously been applied by researchers for the present system of simulated solar radiation (De Heredia et al., 2001).

Furthermore, the reason for using the present empirical models is so that one can carry out a simplified kinetic study of the process and thereby calculate the first-order kinetic rate constants. The parameters chosen for comparison are the kinetic constants, which are global parameters that include all phenomena involved in the studied process. However, because adsorption is an important factor in heterogeneous photocatalytic oxidation processes, the L-H model was used to analyse the photo-oxidation kinetics of Reactive Red 120 by the titania-based composites. The photodegradation reactions proceed as pseudo first-order reactions and follow the L-H kinetics model. The rate constants are presented in Table 5.4.

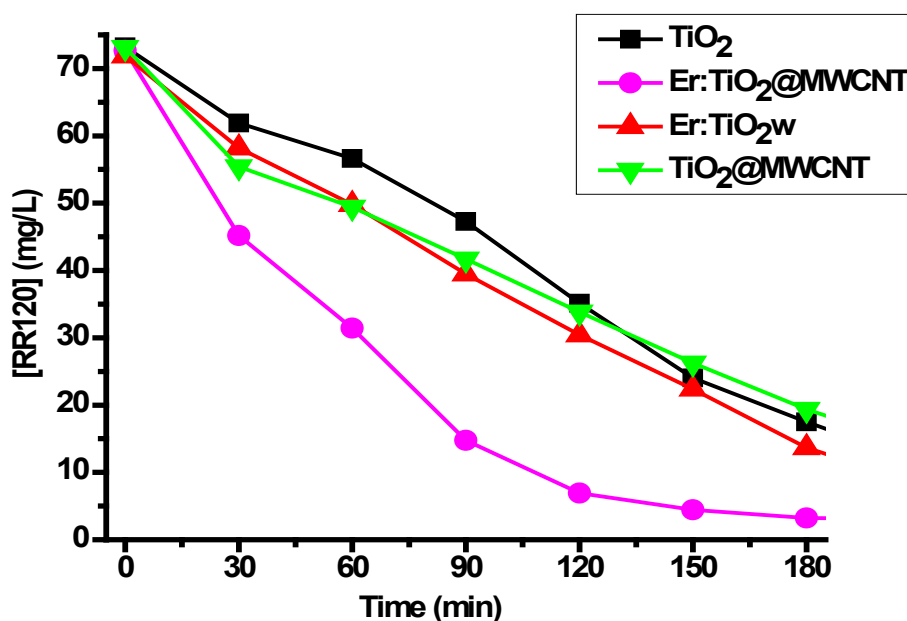


Figure 5.25: Reactive Red 120 decomposition vs. reaction time curves of TiO₂ and the Er³⁺ and MWCNT-modified composites over a 180-minute reaction time period

Table 5.4: Apparent reaction rate constant (k_{App}) for the various composites as estimated from the slope of the linear regression of the straight-line plots of $\ln(C_0/C_t)$ vs. time

Sample	Rate constant k_{App} (min ⁻¹)
TiO ₂	0.00559
Er:TiO ₂ w	0.00879
TiO ₂ @MWCNT	0.00697
Er:TiO ₂ @MWCNT w	0.01843

The Er:TiO₂@MWCNT-w has a higher reaction rate, as evinced by the estimated apparent pseudo first-order reaction rate constant $k_{App} \sim 18.43 \times 10^{-3} \text{ min}^{-1}$, which is nearly 3.5 times that of neat TiO₂ $k_{App} \sim 5.59 \times 10^{-3} \text{ min}^{-1}$, where the results were fitted to the integrated rate law equations to obtain the linear first-order reaction profiles. The results are presented in figures 5.26 and 5.27. The neat TiO₂, Er:TiO₂-w and TiO₂@MWCNT composites follow first-order reaction kinetics. This is seen in the results fitting the straight line obtained by linear regression as is the case for first-order reactions. Furthermore,

the straight line obtained upon linear regression has a slope that equals the apparent first-order rate constant k_{App} . The values are presented in Table 5.4.

The Er:TiO₂@MWCNT-w composite, however, has a [Reactive Red 120] concentration versus time profile with a markedly deeper curvature (Figure 5.26). When it is fitted to the first-order integrated rate law, it was found to follow the linear straight line, albeit $R^2 < 0.9$. Therefore, it appears to have higher order reaction kinetics, and does not follow the second-order reaction kinetic model (Figure 5.27). Thus, it follows pseudo first-order reaction kinetics.

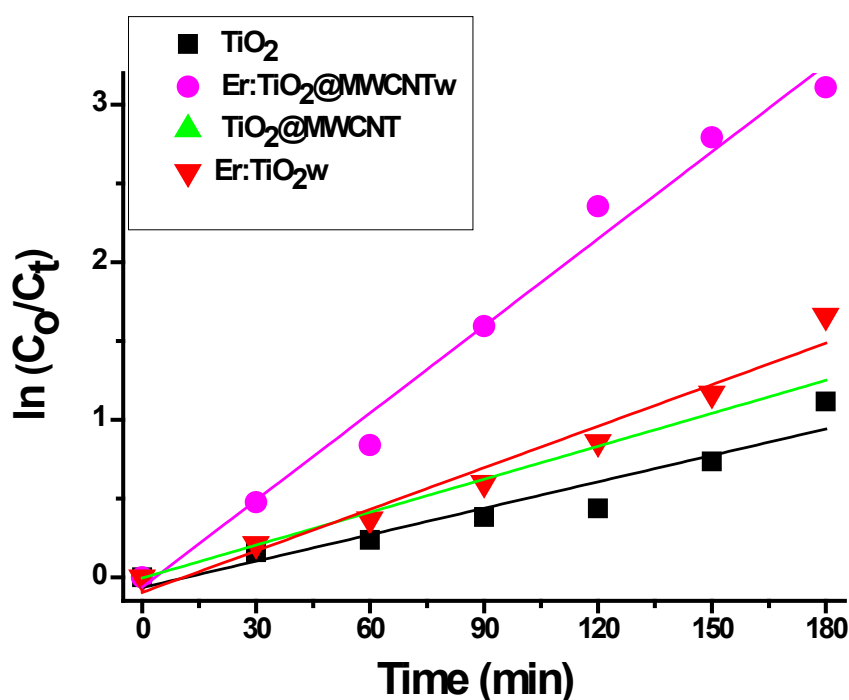


Figure 5.26: Integrated first-order plot of Reactive Red 120 decomposition vs. reaction time curves of TiO₂ and the Er³⁺ and MWCNT-modified composites presented over a 180-minute reaction time period

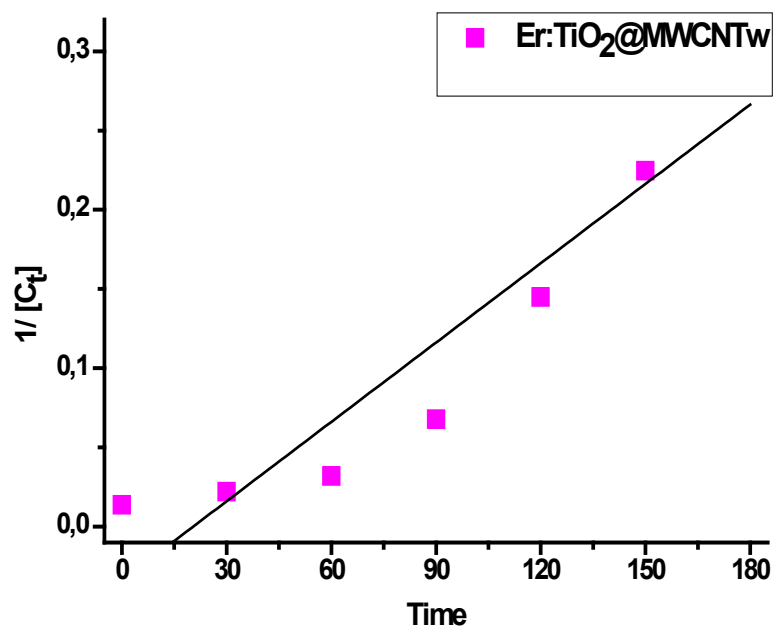


Figure 5.27: Integrated second-order plot of Reactive Red 120 decomposition vs. reaction time curves of an Er:TiO₂@MWCNT composite presented over a 180-minute reaction time period

In a study conducted by Mamba et al. (2015), the photocatalytic degradation rates of Methylene Blue using MWCNT-Gd/TiO₂ photocatalysts were found to follow first-order kinetics. The photocatalytic degradation rate for the best-performing photo-nanocomposite (3MWCNT-Gd/TiO₂) was $1.3 \times 10^{-2} \text{ min}^{-1}$. This was attributed to the improved interface between TiO₂ and MWCNTs as a result of the incorporation of the Gd₂O₃ nanoparticles.

Esplugas et al. (2002) reported pseudo first-order rate constants of $7.4 \times 10^{-2} \text{ min}^{-1}$ and $6.0 \times 10^{-2} \text{ min}^{-1}$ for 0.5 g/l neat commercial TiO₂ activated with UV irradiation at initial Reactive Red 120 concentrations of 60 mg/l and 80 mg/l, respectively.

These studies show higher pseudo first-order rate constants than those reported for the Er:TiO₂@MWCNT composites reported in the experiments. However, it is important to note that comparisons are tentative as there are numerous factors that affect the outcome of the results obtained, such as dopant loading to modify TiO₂ and synthesis methodology, as well as photocatalytic reaction parameters, such as target pollutant concentrations, photocatalyst concentrations and pH. For example,

in the study by Esplugas et al. (2002), the photocatalytic decomposition of Reactive Red 120 occurred in acidic medium (pH 3). This positively charged the TiO₂ surfaces and the repulsions between TiO₂ of the same charge prevented particle agglomeration, thus increasing the available surface-active sites for reaction. In addition, Reactive Red 120 has negatively charged sulphonate groups and the acidic solution favours adsorption of the dye onto the positively charged TiO₂ surfaces. In this study, the Reactive Red 120 solutions were determined to have a pH of approximately 6.6. At higher pH values, there is a potential risk of leaching Er³⁺ from the composite, as well as decreasing the adsorption of the azo dye onto the photocatalyst surface.

The researchers have attempted to elucidate the kinetics of the photocatalytic decomposition of Reactive Red 120, a diazo dye at the surface of Er and MWCNT-modified TiO₂ nanoparticles. The fitting of the data to the L-H rate forms is an oversimplification that has assumed that equilibrium adsorption was absolutely attained and has played a minor role during the photocatalysis process. The use of semilog plots of reactant concentration (C_t) vs. time ought to yield linear forms and hence the apparent rate constant (k_{app}). There are numerous factors to take into consideration when using integrated rate laws for modelling semi-conductor mediated heterogeneous photocatalytic reactions. In the case of a dye, for example photolysis, photocatalysis and photosensitisation play a role and may disguise the variability of the rate “constant” over time (Ollis, 2018).

In other words, there is a network of reactions that leads to a singular, simplified kinetic model: the L-H rate equation. However, this model arises from multiple reactions. Therefore, the model alone cannot reveal the multitude of mechanisms. This is due to the saturation of the dye on the substrate (photocatalyst surface), limitation of the oxygen supply, and the formation and therefore increase in concentration of additional by-products. The articulation of reaction rates using modelled rate expressions is difficult as it is impossible to estimate the exact value of the active catalyst surface area that participates in the photocatalytic reactions. This is, in part, because of unreliable knowledge of the depth of light penetration, or rather the percentage of light attenuated during the reaction. Therefore, it may not be entirely appropriate to approximate L-H kinetics to pseudo first-order kinetics.

5.3.2 Proposed mechanism

There is a complex synergy between Er_2O_3 , MWCNT and TiO_2 . The Er^{3+} functions as a photosensitiser, whereupon visible light illumination, the $4f-4f$ electrons are injected to the CB of TiO_2 . The $\text{Er}_2\text{O}_3/\text{Er}^{3+}$ forms (empty) multiple energy levels below the CB of TiO_2 , allowing for the electronic transitions of TiO_2 VB electrons to the (empty) sub-band gap energy levels of Er^{3+} . These transitions require less energy than the TiO_2 VB-to-CB (3.2 eV) transition and are induced by visible light.

These electrons, trapped by the Er^{3+} , can react with oxygen adsorbed on the surface of the nanocomposite to form superoxide ($\bullet\text{O}_2^-$) radicals and eventually a hydroxyl ($\bullet\text{OH}$) radical that can attack the Reactive Red 120. Moreover, the formation of these excited f -states below the CB of TiO_2 allows (surface) oxygen vacancies and surface defects for electron trapping, thus facilitating the separation of photo-formed electrons. Additionally, the results suggest that the formation of an excitation energy level beneath the titania CB from the binding of electrons and oxygen vacancies lowers the excitation energy of the Er^{3+} -modified TiO_2 , resulting in a heightened photo-response (Chai et al., 2014).

The effect of MWCNTs is multi-fold. They have a broad visible-light absorptivity and act as photosensitisers. They are also able to transfer excited electrons to the CB of TiO_2 upon visible-light illumination in the $\text{Er}:\text{TiO}_2@\text{MWCNT-c}$. In the $\text{Er}:\text{TiO}_2@\text{MWCNT-w}$ composite, the MWCNT introduced trace carbon doping into the TiO_2 lattice, which resulted in defects, such as oxygen vacancies and trivalent titanium, that increase the shallow trap states, leading to substantially enhanced optical absorption in the visible light region, while these defects induce disorder that facilitates separation and the transfer of photo-formed charge carriers, thus effectively delaying the recombination of electrons and holes. The MWCNTs improve the textural properties and thereby the visible-light sensitisation as they have a large surface area, pore volume and pore sizes that improve interfacial charge transfer and enhance visible-light absorption. When the MWCNTs absorb visible light and become excited, they transfer electrons to the TiO_2 CB and become positively charged. The MWCNTs can sequester electrons from the TiO_2 VB, leaving positive holes (h^+). The holes can oxidise water to form powerful and highly reactive hydroxyl radicals that can degrade Reactive Red 120.

5.4 SUMMARY

In summary, the TEM and SEM analyses showed that the synthesised MWCNTs contained catalyst particles. However, after being subjected to acid treatment, the Fe-Co@CaCO₃ catalyst and support were dissolved and removed, along with the amorphous graphitic carbon, without damaging the wall structure of the CNTs. The TiO₂ and Er:TiO₂ were highly crystalline, showing porous cubic and spherical nanoparticles. However, the metal oxides were highly aggregated. Subsequent to grafting onto MWCNTs, the semiconductor nanoparticles were less aggregated. Furthermore, XRD diffractograms showed that the synthesised nanocomposites were highly crystalline, showing single anatase phase TiO₂, while the incorporation of Er³⁺ and MWCNTs decreased the crystallite size. The XRD also suggested that the Er:TiO₂@MWCNT composite has been successfully blended into the CA-PCL polymer matrix. The BET adsorption-desorption isotherms showed that the nanocomposites had type IV and type V adsorption isotherms with H1 and H3 hysteresis loops indicative of their mesoporous nature, created by narrow and open-ended mesopores. More importantly, the incorporation of Er³⁺ and MWCNTs improved the textural properties when compared to neat TiO₂ by increasing the surface area and pore volume. This is seen in the increase in surface areas that ranged from 67.91 to 100.62 m²/g, with the highest BET surface area observed for the Er:TiO₂@MWCNT-w sample. The increased specific surface area as a result of the MWCNTs improved the adsorption ability of the composites. This further served to enhance the efficacy of the photocatalyst as the photocatalytic activity strongly depends on increased adsorption of the target molecule onto the substrate, This is illustrated where the best-performing photocatalyst shows the highest dye adsorption (q_t), in keeping with its large surface area. The Reactive Red 120 decolourisation experiments showed that Er:TiO₂@MWCNT was highly adsorbent and most effective for the photocatalytic decomposition of the dye solution, removing 79.90% of the dye in 90 minutes. The studies show rapid decolourisation of the model dye Reactive Red 120, where:



The concentration versus time profile for TiO₂ shows linear decay, implying first-order reaction rate kinetics. This implies that the ability of neat TiO₂ to decompose Reactive Red 120 depends on the concentration of the solution, whereas the nanocomposites Er:TiO₂@MWCNT show markedly curved

exponential decay reactant concentration curves and follow pseudo first-order reaction rate kinetics. Solar light-induced degradation of a complex diazo dye, Reactive Red 120, has been completely degraded by Er^{3+} and MWCNT-modified TiO_2 photoactive nanocomposites. The Reactive Red 120 dye was completely decomposed to a colourless product after 240 minutes by all photocatalysts. However, $\text{Er}:\text{TiO}_2@\text{MWCNT-w}$ showed the highest activity, with 79.70% colour removal efficiency after 90 minutes. Comparison of photocatalytic activity of the different semiconducting nanocomposites has shown that the TiO_2 in which Er^{3+} and MWCNTs were incorporated via the wet impregnation method is the most active photocatalyst in the degradation of Reactive Red 120 using sunlight as an energy source. This was attributed to the combined effect of Er^{3+} and MWCNTs, where the Er^{3+} -introduced sub-band gap states beneath the CB of TiO_2 , thereby reducing the band gap, and enabling visible-light activation of the composite.

The MWCNTs served as a co-adsorbent catalyst aid, thereby increasing dye-substrate interaction and increasing the surface area of the photocatalyst, as well as acting as a photosensitiser because MWCNTs inherently absorb photons over a broad range of the spectrum, as seen in the UV-Vis diffuse reflectance spectroscopy (DRS) spectra. Thus they can inject electrons into the TiO_2 CB. Embedding the photocatalyst onto the CA-PCL thin films allowed for an additional (~3%) adsorption of the dye and therefore concentration of Reactive Red 120 at the substrate surface interface as is required of an immobilising surface.

The $\text{Er}:\text{TiO}_2@\text{MWCNT}$ composites had higher photoactivity compared with the neat TiO_2 . This is ascribed to the synergy between the three parent compounds of the nanocomposite. Incorporating Er^{3+} and MWCNTs enhanced visible-light absorption and delayed electron-hole recombination, thereby increasing the quantum yield of TiO_2 and accelerating charge carrier migration to the catalyst surface to rapidly form oxidising radicals that decomposed the dye and thus improved the photocatalytic activity.

The Er and MWCNT-modified TiO_2 photo-nanocomposite fabricated in this study shows good potential for the decolourisation of azo dyes.

CHAPTER 6: CONCLUSIONS AND RECOMMENDATIONS

6.1 CONCLUSIONS

The main aim of this project was to develop a titania-based nanocomposite for the remediation of organic azo dyes. The nanomaterials were based on nanometric TiO₂ particles modified with Er₂O₃ and grafted onto MWCNTs.

The MWCNTs were successfully synthesised using the chemical vapour deposition method. The TiO₂, Er:TiO₂, TiO₂@MWCNT and Er:TiO₂@MWCNT composites were successfully synthesised using the sol-gel technique. The incorporation of Er³⁺ ions was varied, viz. wet impregnated into the pre-calcined TiO₂ and co-precipitation, where Er³⁺ was incorporated into the unhydrolysed metal alkoxide solution. The MWCNTs, TiO₂, Er:TiO₂, TiO₂@MWCNT and Er:TiO₂@MWCNT were characterised by microscopic, spectroscopic and physical techniques such as TEM, SEM, UV-Vis diffuse reflectance spectroscopy, XRD and N₂ BET adsorption-desorption isotherms.

The photocatalytic activity of the synthesised materials was evaluated by degrading Reactive Red 120 under simulated solar irradiation. The photodegradation studies show that the nanocomposites' ability to decolorise dye solutions is independent of the dye concentration. This is encouraging as it means that the nanocomposite is not prone to poisoning and could be recycled. Thus, the inclusion of Er and MWCNTs into TiO₂ has markedly improved the visible-light activity and ultimately its photocatalytic efficiency in visible light. The observed findings showed that the nano-photocatalysts have great potential for environmental protection applications, such as the decontamination of textile industrial effluents and wastewater. The green synthesis of the materials makes them appropriate for environmental remediation applications.

6.2 RECOMMENDATIONS

The facile nature of the synthesis methodology employed can be easily adapted to other rare earth metal dopants. Other techniques, such as microwave-assisted sol-gel could be employed to better control particle morphology. The Er:TiO₂@MWCNT-CAPCL composite has promise and needs to be explored further because of its demonstrated photocatalytic efficacy. Different varieties and

combinations of biodegradable polymers should be tested for the immobilisation of the photocatalyst. Starch, cellulose and its derivatives, and other natural polymers can be applied in various combinations of the materials to improve processability and properties. To overcome the inherent drawbacks of natural polymers, they are often modified in various ways. Cellulose is easily modified; therefore, it can be used as a starting material for further modification by techniques such as reactive processing to achieve the efficient grafting of a homogeneous structure of the polymer. This is an important consideration because miscibility of the polymers is critical for their robustness, as this will delay their degeneration upon prolonged UV-Vis light irradiation and exposure to highly oxidising radicals. Ultimately, optimising various parameters and upscaling them for a pilot plant-scale photoreactor may be an achievable outcome.

REFERENCES

- AKPAN UG and HAMEED BH (2009) Parameters affecting the photocatalytic degradation of dyes using TiO₂-based photocatalysts: A review. *Journal of Hazardous Materials* **170 (2–3)** 520–529.
- ALATON IA, BALCIOGLU IA and BAHNEMANN DW (2002) Advanced oxidation of a reactive dyebath effluent: Comparison of O₃, H₂O₂/UV-C and TiO₂/UV-A processes. *Water Research* **36 (5)** 1143–1154.
- ALEBOYEH A, ALEBOYEH H and MOUSSA Y (2003) Critical effect of hydrogen peroxide in photochemical oxidative decolorization of dyes: Acid Orange 8, Acid Blue 74 and Methyl Orange. *Dyes and Pigments* **57 (1)** 67–75.
- ALLEN RLM (1971) *Colour chemistry*, Springer, Bath, UK.
- ARSLAN S, EYVAZ M, GÜRBULAK E and YÜKSEL E (2016) A review of state-of-the-art technologies in dye-containing wastewater treatment – the textile industry case. In: *Textile wastewater treatment*, KÖRLÜ AE, IntechOpen, London, UK.
- ASGHAR A, RAMAN AAA and DAUD WMAW (2015) Advanced oxidation processes for *in-situ* production of hydrogen peroxide/hydroxyl radical for textile wastewater treatment: A review. *Journal of Cleaner Production* **87** 826–838.
- BAI H, ZHOU Y, WANG X and ZHANG L (2012) The permeability and mechanical properties of cellulose acetate membranes blended with polyethylene glycol 600 for treatment of municipal sewage. *Procedia Environmental Sciences* **16** 346–351.
- BANDARA J, KLEHM U and KIWI J (2007) Raschig rings-Fe₂O₃ composite photocatalyst activate in the degradation of 4-chlorophenol and Orange II under daylight irradiation. *Applied Catalysis B: Environmental* **76 (1–2)** 73–81.
- BARD AJ (1982) Design of semiconductor photoelectrochemical systems for solar energy conversion. *The Journal of Physical Chemistry* **86 (2)** 172–177.
- BHATIA D, SHARMA NR, SINGH J and KANWAR RS. (2017) Biological methods for textile dye removal from wastewater: A review. *Critical Reviews in Environmental Science and Technology* **47 (19)** 1836–1876.

- BOLTO BA, DIXON DR and GRAY SR (1996) Soluble organic polymers in water and wastewater treatment. In: *Chemistry for the protection of the environment*, PAWŁOWSKI L et al., 2nd ed., Springer, Boston, MA, USA.
- BOUSSOUARI B and BAITOUL M (2014) A comparative study of multi-walled carbon nanotubes purification techniques. *Journal of Materials Science and Engineering with Advanced Technology* **9 (1)** 1–15.
- BOYD LA and MBELU AM (2009) Guideline for the inspection of wastewater treatment works. In: *Wastewater treatment in South Africa: Field evaluation of the status and performance of wastewater treatment plants*, Water Research Commission, Pretoria, South Africa.
- BRIGDEN K, SANTILLO D and JOHNSTON P (2013) *Nonylphenol ethoxylates (NPEs) in textile products, and their release through laundering*. Greenpeace Research Laboratories, Exeter, UK.
- CARLIELL CM, BARCLAY S and BUCKLEY CA (1996) Treatment of exhausted reactive dyebath effluent using anaerobic digestion: Laboratory and full-scale trials. *Water SA* **22 (3)** 225–233.
- CARLIELL CM, BARCLAY SJ, NAIDOO N, BUCKLEY CA, MULHOLLAND DA and SENIOR E (1995) Microbial decolourisation of a reactive azo dye under anaerobic conditions. *Water SA* **21 (1)** 61–69.
- CEFIC (2012) *About titanium dioxide*, Titanium Dioxide Stewardship Council, Washington, DC, USA.
- CHADDHA A, DHANANI Q, MUROTANI R, NDIAYE F and KAMUKAMA R (2009) *Textiles and apparel cluster in South Africa*. Institute for Strategy and Competitiveness, Harvard Business School, Harvard, MA, USA.
- CHAI Y, LIN L, ZHANG K, ZHAO B and HE D (2014) Efficient visible-light photocatalysts from Gd–La codoped TiO₂ nanotubes. *Ceramics International* **40 (2)** 2691–2696.
- CHEREMISINOFF P (1997) *Handbook of engineering polymeric materials*, CRC Press, Boca Raton, FL, USA.
- CHEQUER FMD, DE OLIVEIRA DP, FERRAZ ERA, DE OLIVEIRA GAR, CARDOSO JCZ and ZANONI MVB (2013) *Textile dyes: Dyeing process and environmental impact*, IntechOpen, London, UK.
- CHOLLOM MN, RATHILAL S, PILLAY VL and ALFA D (2015) The applicability of nanofiltration for the treatment and reuse of textile reactive dye effluent. *Water SA* **41 (3)** 398–405.

- CLOETE TE, GERBER A and MARITZ LV (2010) *A first order inventory of water use and effluent production by SA industrial, mining and electricity generation sectors*, Water Research Commission, Pretoria, South Africa.
- CRINI G and BADOT P-M (2008) Application of chitosan, a natural aminopolysaccharide, for dye removal from aqueous solutions by adsorption processes using batch studies: A review of recent literature. *Progress in Polymer Science* **33 (4)** 399–447.
- DE HEREDIA JB, TORREGROSA J, DOMINGUEZ JR and PERES JA, (2001) Oxidation of p-hydroxybenzoic acid by UV radiation and by TiO₂/UV radiation: Comparison and modelling of reaction kinetic. *Journal of Hazardous Materials* **83 (3)** 255–264.
- DIETRICH HG and GOLKA K (2012) Bladder tumors and aromatic amines – historical milestones from Ludwig Rehn to Wilhelm Hueper. *Frontiers in Bioscience: Elite* **4 (1)** 279–288.
- DONNENFELD Z, CROOKES C and HEDDEN S (2018) *A delicate balance: Water scarcity in South Africa*, Institute for Security Studies, Pretoria, South Africa.
- ECKENFELDER, WW (2000) *Industrial water pollution control*, McGraw-Hill, New York, NY, USA.
- EDGE (2014) *Clothing, textiles and fashion*, eThekweni Policy Strategy Information and Research Department, eThekweni Economic Development and Investment Promotion Unit, KwaZulu-Natal, South Africa.
- EL-BAHY ZM, ISMAIL AA and MOHAMED RM (2009) Enhancement of titania by doping rare earth for photodegradation of organic dye (Direct Blue). *Journal of Hazardous Materials* **166 (1)** 138–143.
- ELZUBAIR A, ELIAS CN, SUAREZ JCM, LOPES HP and VIEIRA MVB (2006) The physical characterization of a thermoplastic polymer for endodontic obturation. *Journal of Dentistry* **34 (10)** 784–789.
- ESPLUGAS S, GIMÉNEZ J, CONTRERAS S, PASCUAL E and RODRÍGUEZ M (2002) Comparison of different advanced oxidation processes for phenol degradation. *Water Research* **36 (4)** 1034–1042.
- ETACHERI V, DI VALENTIN C, SCHNEIDER J, BAHNEMANN D and PILLAI SC (2015) Visible-light activation of TiO₂ photocatalysts: Advances in theory and experiments. *Journal of Photochemistry and Photobiology C: Photochemistry Reviews* **25** 1–29.

- EVOQUAWATER TECHNOLOGIES (n.d.) *Anaerobic vs. aerobic treatment: Weighing wastewater treatment options*. <https://www.evoqua.com/en/brands/adi-systems/Pages/Anaerobic-vs-Aerobic-Treatment.aspx>. (Accessed 17 April 2019).
- FABIYI ME and SKELTON RL (2000) Photocatalytic mineralisation of methylene blue using buoyant TiO₂-coated polystyrene beads. *Journal of Photochemistry and Photobiology A: Chemistry* **132 (1–2)** 121–128.
- FISHBEIN L (1984) Aromatic amine. In: *Anthropogenic compounds*, Springer, Berlin Heidelberg, Germany.
- FREITAS TKFS, OLIVEIRA, VM, DE SOUZA MTF, GERALDINO HCL, ALMEIDA VC, FÁVARO SL and GARCIA JC (2015) Optimization of coagulation-flocculation process for treatment of industrial textile wastewater using okra (*A. esculentus*) mucilage as natural coagulant. *Industrial Crops and Products* **76** 538–544.
- FUJISHIMA A and HONDA K (1972) Electrochemical photolysis of water at a semiconductor electrode. *Nature* **238 (5358)** 37–38.
- FUJISHIMA A, RAO TN and TRYK DA (2000) Titanium dioxide photocatalysis. *Journal of Photochemistry and Photobiology C: Photochemistry Reviews* **1 (1)** 1–21.
- GADIYAR C, BORUAH B, MASCARENHAS C and SHETTY VK (2013) Immobilized nano TiO₂ for photocatalysis of Acid Yellow-17 dye in fluidized bed reactor. In: *Proceedings of the National Conference on Women in Science and Engineerin (NCWSE 2013)*, Sri Dharmasthala Manjunatheshwara College of Engineering and Technology, Dharwad, India.
- GHALY AE, ANANTHASHANKAR R, ALHATTAB M and RAMAKRISHAN VV (2014) Production, characterization and treatment of textile effluents: A critical review. *Journal of Chemical Engineering Process Technology* **5 (1)** 1–19.
- GILPAVAS E, DOBROSZ-GÓMEZ I and GÓMEZ-GARCÍA M-Á (2019) Optimization and toxicity assessment of a combined electrocoagulation, H₂O₂/Fe²⁺/UV and activated carbon adsorption for textile wastewater treatment. *Science of the Total Environment* **651** 551–560.
- GORDON P and GREGORY P (1983) *Organic chemistry in colour*, Springer-Verlag, Berlin, Germany.
- GOSAVI VD and SHARMA S (2014) A general review on various wastewater treatment methods for textile wastewater. *Journal of Environmental Science, Computer Science and Engineering and Technology* **3 (1)** 29–39.

- GRATZEL M (2012) *Energy resources through photochemistry and catalysis*, Elsevier Science, Amsterdam, The Netherlands.
- GRIESS P (1858) Vorläufige Notiz über die Einwirkung von salpetriger Säure auf Amidinitro- und Aminotrophenylsäure. *Annalen der Chemie und Pharmacie* **106** 123.
- GROVES GR, Buckley CA and SIMPSON AE (1990) *A guide for the planning, design and implementation of wastewater treatment plants in the textile industry: Closed loop treatment/ recycle options for textile scouring, bleaching and mercerising effluents*, Water Research Commission, Pretoria, South Africa.
- GUIBAL E and ROUSSY J (2007) Coagulation and flocculation of dye-containing solutions using a biopolymer (Chitosan). *Reactive and Functional Polymers* **67 (1)** 33–42.
- HERNÁNDEZ-RAMÍREZ A and MEDINA-RAMIREZ I (2014) *Photocatalytic semiconductors: Synthesis, characterization, and environmental applications*, Springer, Berlin Heidelberg, Germany.
- HOEK EM, TARABARA VV, KOYUNCU I and GÜNEY K (2013) Membrane-based treatment of textile industry wastewaters. In: *Encyclopedia of membrane science and technology*, HOEK EM and TARABARA VV, Wiley, Hoboken, NJ, USA.
- HOLKAR CR, JADHAV AJ, PINJARI DV, MAHAMUNI NM and PANDIT AB (2016) A critical review on textile wastewater treatments: Possible approaches. *Journal of Environmental Management* **182** 351–366.
- HUANG CH (2011) *Rare earth coordination chemistry: Fundamentals and applications*, Wiley, Hoboken, NJ, USA.
- HUNGER K (2003) *Industrial dyes: Chemistry, properties, applications*, Wiley, Hoboken, NJ, USA.
- IQ BUSINESS and FP&M SETA (2014) *Clothing textiles footwear and leather sectors: A profile of the clothing, textiles, footwear and leather sub-sectors*, FP&M SETA, Pretoria, South Africa.
- JAUCH H, TRAUB-MERZ R and EBERT-STIFTUNG F (2006) *The future of the textile and clothing industry in sub-Saharan Africa*, Friedrich-Ebert-Stiftung, Division for International Development Cooperation, Africa Department.
- JIN X, XU J, WANG X, XIE Z, LIU Z, LIANG B, CHEN D and SHEN G (2014) Flexible TiO₂/cellulose acetate hybrid film as a recyclable photocatalyst. *RSC Advances* **4 (25)** 12640–12648.

- JOHANNESSON C (2016) Emerging textile production technologies: Sustainability and feasibility assessment and process LCA of supercritical CO₂ dyeing. In: *Energy and Environment*, Chalmers University, Goteborg, Sweden.
- KALRA SS, MOHAN S, SINHA A and SINGH G (2011) Advanced oxidation processes for treatment of textile and dye wastewater: A review. In: *Proceedings of the 2011 International Conference on Environmental Science and Development (ICESD 2011)*, Mumbai, India.
- KAMARUDDIN MA, YUSOFF MS, ABDUL-AZIZ H and AKINBILE CO (2013) Recent developments of textile wastewater treatment by adsorption process: A review. *International Journal of Scientific Research in Knowledge* **1 (4)** 60–73.
- KAZUHITO H, HIROSHI I and FUJUSHIMA A (2005) TiO₂ photocatalysis: A historical overview and future prospects. *Japanese Journal of Applied Physics* **44 (12)** 8269.
- KLÉBERT S, NAGY L, DOMJÁN A and PUKANSZKY, B (2009) Modification of cellulose acetate with oligomeric polycaprolactone by reactive processing: Efficiency, compatibility, and properties. *Journal of Applied Polymer Science* **113 (5)** 3255–3263.
- KONSTANTINOU IK and ALBANIS TA (2004) TiO₂-assisted photocatalytic degradation of azo dyes in aqueous solution: Kinetic and mechanistic investigations: A review. *Applied Catalysis B: Environmental* **49 (1)** 1–14.
- KRAEUTLER B and BARD AJ (1978) Heterogeneous photocatalytic synthesis of methane from acetic acid – new Kolbe reaction pathway. *Journal of the American Chemical Society* **100 (7)** 2239–2240.
- LEE CS, ROBINSON J and CHONG MF (2014) A review on application of flocculants in wastewater treatment. *Process Safety and Environmental Protection* **92 (6)** 489–508.
- LE ROES-HILL M, MUANDA C, ROHLAND J and DURRELL K (2017) Water and wastewater management in the textile industry. In: *NatSurv 13*, Water Research Commission, Pretoria, South Africa.
- LEWTAS J (2007) Air pollution combustion emissions: Characterization of causative agents and mechanisms associated with cancer, reproductive, and cardiovascular effects. *Mutation Research* **636** 95–133.
- LINSEBIGLER AL, LU G and YATES JT (1995) Photocatalysis on TiO₂ surfaces: Principles, mechanisms, and selected results. *Chemical Reviews* **95 (3)** 735–758.

- LUCAS M'S and PERES JA, (2006) Decolorization of the azo dye Reactive Black 5 by Fenton and photo-Fenton oxidation. *Dyes and Pigments* **71 (3)** 236–244.
- MAMBA G, MBIANDA XY and MISHRA AK (2015) Photocatalytic degradation of the diazo dye naphthol blue black in water using MWCNT/Gd, N, S-TiO₂ nanocomposites under simulated solar light. *Journal of Environmental Sciences* **33** 219–228.
- MARCUCCI M, CIARDELLI G, MATTEUCCI A, RANIERI L and RUSSO, M (2002) Experimental campaigns on textile wastewater for reuse by means of different membrane processes. *Desalination* **149 (1)** 137–143.
- MARMAGNE O and COSTE C (1996) Color removal from textile plant effluents. In: *American dyestuff reporter*, Degrémont SAS, Paris, France.
- MATTHIAS THOMMES KK, NEIMARK AV, OLIVIER JP, RODRIGUEZ-REINOSO F, ROUQUEROL J and SING KSW (2015) *Physisorption of gases, with special reference to the evaluation of surface area and pore size distribution*, IUPAC, Zhou Qifeng, China.
- MAYA JJ and SABU T (2012) Natural polymers: An overview. In: *Natural polymers, Volume 1: Composites*, The Royal Society of Chemistry, London, UK.
- MHLANGA SD, MONDAL KC, CARTER R, WITCOMB MJ and COVILLE NJ (2009) The effect of synthesis parameters on the catalytic synthesis of multiwalled carbon nanotubes using Fe-Co/CaCO₃ catalysts. *South African Journal of Chemistry* **62** 67–76.
- MIERZWA JC, RODRIGUES R and TEIXEIRA ACSC (2018) UV-hydrogen peroxide processes. In: *Advanced oxidation processes for waste water treatment*, AMETA SC and AMETA R, Academic Press, Cambridge, MA, USA.
- MISHRA A and BAJPAI M (2005) Flocculation behaviour of model textile wastewater treated with a food grade polysaccharide. *Journal of Hazardous Materials* **118 (1)** 213–217.
- MOHAJERANI M, MEHRVAR M and EIN-MOZAFFARI F (2009) An overview of the integration of advanced oxidation technologies and other processes for water and wastewater treatment. *International Journal of Engineering* **3 (2)** 120–146.
- MOODLEY P, ROOS JC, ROSSOUW N, HEATH R and COLEMAN T (2011) *Resource directed management of water quality: Planning level review of water quality in South Africa*, Directorate of Water Resource Planning Systems: Water Quality Planning, Department of Water Affairs and Golder and Associates, Pretoria, South Africa.

- MORRIS M, BARNES J and ESSELAAR J (2005) *An identification of strategic interventions at the provincial government level to secure the growth and development of the Western Cape clothing and textile industries*, Western Cape Provincial Government, Cape Town, South Africa.
- MULLER M, SCHREINER B, SMITH L, VAN KOPPEN B, SALLY H, ALIBER M, COUSINS B, TAPELA B, VAN DER MERWE-BOTHA M, KARAR E and PIETERSEN K (2009) Water security in South Africa. In: *Development Planning Division Working Paper Series*, PATERSON A, Development Bank of South Africa, Midrand, South Africa.
- NTULI F, IKHU-OMOREGBE D, KUIPA PK, MUZNDA E and BELAID M (2009) Characterization of effluent from textile wet finishing operations. In: *World Congress on Engineering and Computer Science*, Newswood Limited, San Francisco, CA, USA.
- OCTOBER L (1996) A study of Cape clothing industry. In: *Sectors, clusters and regions*, University of Cape Town, Cape Town, South Africa.
- OLLER I, MALATO S and SÁNCHEZ-PÉREZ JA (2011) Combination of advanced oxidation processes and biological treatments for wastewater decontamination – a review. *Science of the Total Environment* **409** (20) 4141–4166.
- ØLLGAARD H, FROST L, GALSTER J and HANSEN OC (1998) *Survey of azo-colorants in Denmark: Consumption, use, health and environmental aspects*, Danish Environmental Protection Agency, Denmark Ministry of Environment and Energy, Copenhagen, Denmark.
- OLLIS DF (2018) Kinetics of photocatalyzed reactions: Five lessons learned. *Frontiers in Chemistry* **6** 378–378.
- OSSWALD S, HAVEL M and GOGOTSI Y (2007) Monitoring oxidation of multiwalled carbon nanotubes by Raman spectroscopy. *Journal of Raman Spectroscopy* **38** (6) 728–736.
- PATEL H and VASHI RT (2010) Treatment of textile wastewater by adsorption and coagulation. *E-Journal of Chemistry* **7** (4) 1468–1476.
- PAZ Y (2010) Application of TiO₂ photocatalysis for air treatment: Patents' overview. *Applied Catalysis B: Environmental* **99** (3–4) 448–460.
- PELAEZ M, NOLAN NT, PILLAI SC, SEERY MK, FALARAS P, KONTO AG, DUNLOP PSM, HAMILTON JWW, BYRNE, JA, O'SHEA K, ENTEZARI MK and DIONYSIOU DD (2012) A review on the visible light active titanium dioxide photocatalysts for environmental applications. *Applied Catalysis B: Environmental* **125** 331–349.

- PINHEIRO HME, TOURAUD E and THOMAS O (2004) Aromatic amines from azo dye reduction: Status review with emphasis on direct UV spectrophotometric detection in textile industry wastewaters. *Dyes and Pigments* **61 (2)** 121–139.
- PRADO AGS, FARIA EA, DESOUZA JR and TORRES JD (2005) Ammonium complex of niobium as a precursor for the hydrothermal preparation of cellulose acetate/Nb₂O₅ photocatalyst. *Journal of Molecular Catalysis A: Chemical* **237 (1–2)** 115–119.
- PRINSLOO E (1996) The clothing industry in Durban. In: *Sectors, clusters and regions*, University of Cape Town, Cape Town, South Africa.
- RASHED MN (2013) Adsorption techniques for the removal of organic pollutants from water and wastewater. In: *Organic pollutants: Monitoring, risk and treatment*, RASHED MN, IntechOpen, London, UK.
- RAUF MA and ASHRAF SS (2009) Fundamental principles and application of heterogeneous photocatalytic degradation of dyes in solution. *Chemical Engineering Journal* **151 (1–3)** 10–18.
- RESZCZYŃSKA JG, SOBCZAK T, LISOWSKI JW, GAZDA WM, OHTANI B and ZALESKA A (2015) Visible light activity of rare earth metal doped (Er³⁺, Yb³⁺ or Er³⁺/Yb³⁺) titania photocatalysts. *Applied Catalysis B: Environmental* **163** 40–49.
- ROBERT D, KELLER V and KELLER N (2013) Immobilization of a semiconductor photocatalyst on solid supports: Methods, materials, and applications. In: *Photocatalysis and water purification*, Wiley, Hoboken, NJ, USA.
- ROBINSON T, CHANDRAN B and NIGAM P (2002) Removal of dyes from an artificial textile dye effluent by two agricultural waste residues, corncob and barley husk. *Environment International* **28 (1)** 29–33.
- ROBINSON T, MCMULLAN G, MARCHANT R and NIGAM P (2001) Remediation of dyes in textile effluent: A critical review on current treatment technologies with a proposed alternative. *Bioresource Technology* **77 (3)** 247–255.
- SALEH TA (2013) The role of carbon nanotubes in enhancement of photocatalysis. In: *Syntheses and applications of carbon nanotubes and their composites*, SUZUKI S, IntechOpen, London, UK.
- ŞEN S and DEMIRER G'N (2003) Anaerobic treatment of real textile wastewater with a fluidized bed reactor. *Water Research* **37 (8)** 1868–1878.

- SHAN AY, GHAZI TIM and RASHID SA (2010) Immobilisation of titanium dioxide onto supporting materials in heterogeneous photocatalysis: A review. *Applied Catalysis A: General* **389 (1–2)** 1–8.
- SHU H-Y and CHANG M-C (2005) Decolorization effects of six azo dyes by O₃, UV/O₃ and UV/H₂O₂ processes. *Dyes and Pigments* **65 (1)** 25–31.
- SINGH S, MAHALINGAM H and SINGH PK (2013) Polymer-supported titanium dioxide photocatalysts for environmental remediation: A review. *Applied Catalysis A: General* **462–463** 178–195.
- SÖKMEN M, TATLIDIL I, BREEN C, CLEGG F, BURUK CK, SIVLIM T and AKKAN S (2011) A new nano-TiO₂ immobilized biodegradable polymer with self-cleaning properties. *Journal of Hazardous Materials* **187 (1–3)** 199–205.
- SOLÍS M, SOLÍS A, PÉREZ HI, MANJARREZ N and FLORES M (2012) Microbial decolouration of azo dyes: A review. *Process Biochemistry* **47 (12)** 1723–1748.
- SPASIANO D, MAROTTA R, MALATO S, FERNANDEZ-IBANEZ P and SOMMA ID (2015) Solar photocatalysis: Materials, reactors, some commercial, and pre-industrialized applications. A comprehensive approach. *Applied Catalysis B: Environmental* **170–171** 90–123.
- ŠTENGL V, BAKARDJIEVA S and MURAFKA N (2009) Preparation and photocatalytic activity of rare earth doped TiO₂ nanoparticles, *Materials Chemistry and Physics*, **114 (1)** 217–226
- STEPHENSON RJ and DUFF SJB (1996) Coagulation and precipitation of a mechanical pulping effluent – I: Removal of carbon, colour and turbidity. *Water Research* **30 (4)** 781–792.
- SUN L-D, DONG H, ZHANG P-Z and YAN C-H (2015) Upconversion of rare earth nanomaterials. *Annual Review of Physical Chemistry* **66(1)** 619–642.
- TEH CM and MOHAMED AR (2011) Roles of titanium dioxide and ion-doped titanium dioxide on photocatalytic degradation of organic pollutants (phenolic compounds and dyes) in aqueous solutions: A review. *Journal of Alloys and Compounds* **509 (5)** 1648–1660.
- TERAMOTO N (2011) Synthetic green polymers from renewable monomers. In: *A handbook of applied biopolymer technology: Synthesis, degradation and applications*, The Royal Society of Chemistry, London, UK.
- TOBALDI DM, SEVER ŠKAPIN A, PULLAR RC, SEABRA MP and LABRINCHA JA, (2013) Titanium dioxide modified with transition metals and rare earth elements: Phase composition, optical properties, and photocatalytic activity. *Ceramics International* **39 (3)** 2619–2629.

- TRYBA B (2008) Immobilization of TiO₂ and Fe–C–TiO₂ photocatalysts on the cotton material for application in a flow photocatalytic reactor for decomposition of phenol in water. *Journal of Hazardous Materials* **151 (2–3)** 623–627.
- VANDEVIVERE PC, BIANCHI R and VERSTRAETE W (1998) Review: Treatment and reuse of wastewater from the textile wet-processing industry: Review of emerging technologies. *Journal of Chemical Technology and Biotechnology* **72 (4)** 289–302.
- VAN DER WESTHUIZEN C (2007) Trade and poverty: A case study of the South African clothing industry. *Studies in Economics and Econometrics* **31 (2)** 109–124.
- VAN ELDIK R and STOCHEL G (2011) Inorganic photochemistry. *Advances in Inorganic Photochemistry* **63**.
- VERMA AK, DASH RR and BHUNIA P (2012) A review on chemical coagulation/flocculation technologies for removal of colour from textile wastewaters. *Journal of Environmental Management* **93 (1)** 154–168.
- VERT M, DOI Y, HELLWICH K-H, HESS M, HODGE P, KUBISA P, RINAUDO M and SCHUÉ F (2012) Terminology for biorelated polymers and applications (IUPAC Recommendations 2012). *Pure and Applied Chemistry* **84 2** 377–410.
- WANG W, SERP P, KALCK P and FARIA JL (2005) Photocatalytic degradation of phenol on MWNT and titania composite catalysts prepared by a modified sol-gel method. *Applied Catalysis B: Environmental* **56 (4)** 305–312.
- WANG Z, XUE M, HUANG K and LIU Z (2011) Textile dyeing wastewater treatment, advances. In: *Treating textile effluent*, HAUSER PJ, IntechOpen, London, UK.
- WITTMAR A, THIERFELD H, KOCHER S and ULBRICHT M (2015) Routes towards catalytically active TiO₂ doped porous cellulose. *RSC Advances* **5 (45)** 35866–35873.
- XU J, ZHU Y, HUANG H, XIE Z, CHEN D and SHEN G (2011) Zinc-oleate complex as efficient precursor for 1-D ZnO nanostructures: Synthesis and properties. *CrystEngComm* **13 (7)** 2629–2635.
- XU Y-J, ZHUANG Y and FU X (2010) New insight for enhanced photocatalytic activity of TiO₂ by doping carbon nanotubes: A case study on degradation of Benzene and Methyl Orange. *The Journal of Physical Chemistry C* **114 (6)** 2669–2676.

- YAGHOUBI H, TAGHAVINIA N and ALAMDARI EK (2010) Self-cleaning TiO₂ coating on polycarbonate: Surface treatment, photocatalytic and nanomechanical properties. *Surface and Coatings Technology* **204 (9–10)** 1562–1568.
- YAMASHITA H and LI H (2016) *Nanostructured photocatalysts: Advanced functional materials*, Springer, Berlin Heidelberg, Germany.
- YAO Y, LI G, CISTON S, LUEPTOW RM and GRAY KA (2008) Photoreactive TiO₂/carbon nanotube composites: Synthesis and reactivity. *Environmental Science and Technology* **42 (13)** 4952–4957.
- YU Y, YU JC, CHAN C-Y, CHE Y-K, ZHAO J-C, DING L, GE W-K and WONG P-K (2005) Enhancement of adsorption and photocatalytic activity of TiO₂ by using carbon nanotubes for the treatment of azo dye. *Applied Catalysis B: Environmental* **61 (1–2)** 1–11.
- ZAHRIM AY, TIZAOUI C and HILAL N (2010) Evaluation of several commercial synthetic polymers as flocculant aids for removal of highly concentrated CI Acid Black 210 dye. *Journal of Hazardous Materials* **182(1)** 624–630.
- ZANGENEH H, ZINATIZADEH AAL, HABIBI M, AKIA M and HASNAIN ISA M (2015) Photocatalytic oxidation of organic dyes and pollutants in wastewater using different modified titanium dioxides: A comparative review. *Journal of Industrial and Engineering Chemistry* **26** 1–36.
- ZHOU Z, PENG X and SUN R (2016) Electrospun cellulose acetate supported Ag@AgCl composites with facet-dependent photocatalytic properties on degradation of organic dyes under visible-light irradiation. *Carbohydrate Polymers* **136** 322–328.
- ZHU YR, LI GC, ZHANG QP and TANG C (2012) The photocatalytic degradation of Methylene Blue wastewater with nanoscale ferric oxide as catalyst. In: *Advanced materials research*, Trans Tech Publications, Zürich, Switzerland.
- ZOLLINGER H (1987) *Color chemistry: Syntheses, properties and applications of organic dyes and pigments*, 1st ed., VCH Publishers, New York, NY, USA.

APPENDICES

(I) CAPACITY BUILDING

Ms Diseko Boikanyo is currently working on her PhD project entitled “Bioinorganic nanocomposite for the photocatalytic degradation azo dyes”. She is focusing on the development of smart nanocomposites for the remediation of organic dyes used in the textile industry. The nanomaterials were based on nanosized TiO₂ particles modified with erbium oxide, grafted onto MWCNTs and immobilised onto a biodegradable, blended cellulose acetate polycaprolactone thin film. The MWCNTs functioned as both a co-adsorbent and a charge carrier, while the polymeric matrix functioned to immobilise and support the photocatalyst. The nanocomposite was used in the decolourisation of Reactive Red 120, a model azo dye.

Mr Kgaugelo Mabape is currently working on his PhD project entitled “Synergetic removal of organic and inorganic wastewater pollutants using polymer functionalised photocatalytic mesoporous nanomaterial”. His project deals with the physicochemical properties of photocatalytic polymer-zeolite nanocomposites to make them a plausible wastewater treatment nanomaterial. He also aims to develop a cost-effective, organic group of functionalised, polymer-zeolite nanocomposites embedded with TiO₂ nanoparticles that can sufficiently remove both inorganic trace metals and degrade a range of organic pharmaceutical products from complex real wastewater.

Ms Rudzani Muthivhi is currently working on her PhD project entitled “Photodegradation of azo dyes using nanocomposites and polymeric nanofibres under visible light irradiation”. She is focusing on the synthesis of Ag and Co nanoparticles, followed by incorporating them onto the doped TiO₂ and g-C₃N₄ to form nanocomposites. The stability and reusability of the nanocomposites and nanofibres can be done towards the azo dyes and in real waste water.

(II) PUBLICATIONS

- “Modulation of optoelectronic properties of TiO₂ using Er³⁺ and MWCNT”, Diseko Boikanyo, Ajay Kumar Mishra, Shivani B Mishra, Sabelo D Mhlanga, *Advanced Materials*, Submitted January 2019.
- “Biopolymers: A natural support for photocatalysts applied to pollution remediation”, Diseko Boikanyo, Ajay Kumar Mishra, Shivani B Mishra, Sabelo D Mhlanga. *Nanotechnology in environmental science*. Editor: Chaudhery Mustansar Hussain and Ajay Kumar Mishra, Chapter 20, pp. 649-684, Wiley-VCH Publishers, USA, 2018. **ISBN: 978-3-527-34294-5**.
- “Carbon-supported photocatalysts for organic dye photodegradation”, Diseko Boikanyo, Ajay Kumar Mishra, Shivani B Mishra, Sabelo D Mhlanga. *New polymer nanocomposites for environmental remediation*. Editor: Chaudhery Mustansar Hussain and Ajay Kumar Mishra, Chapter 20, pp. 649-684, Elsevier Publishers, UK, 2018. **ISBN: 978-0-12-811033-1**.

(III) CONFERENCES

- D Boikanyo, SB Mishra, SD Mhlanga, AK Mishra, “Synthesis and structure property relationship of Er³⁺-MWCNT modified TiO₂”, 3rd International South African-Taiwan Workshop, August 2018, Johannesburg, South Africa.
- D Boikanyo, SB Mishra, SD Mhlanga, AK Mishra, “Erbium-modified titania decorated MWCNT nanocomposite: A visible light-driven photocatalyst for the decolourisation of Reactive Red 120”, International Conference on Structural Nanocomposites (NANOSTRUC 2018), May 2018, Berlin, Germany.
- D Boikanyo, SB Mishra, SD Mhlanga, AK Mishra, “Erbium-modified titania decorated onto MWCNT nanocomposite: The effect of synthesis techniques on structural and optical properties”, 7th International Conference on Nanoscience and Nanotechnology (NANOAFRICA 2018), April 2018, Durban, South Africa.
- D Boikanyo, SB Mishra, SD Mhlanga, AK Mishra, “Evaluation of the visible light activity of rare earth metal-modified titania/ MWCNT composite”, 2nd International South African-Taiwan Workshop, July 2017, Johannesburg, South Africa.